

**The effect of various experimental parameters on glow peaks  
and TL kinetics of some dosimetric materials**

**PhD Thesis  
in  
Physics Engineering  
University of Gaziantep**

**Supervisor**

**Assoc. Prof. Dr. A. NECMEDDİN YAZICI**

**Co-Supervisor**

**Assist. Prof. Dr. R.Güler YILDIRIM**

**by**

**VURAL EMİR KAFADAR**

**July 2009**

UNIVERSITY OF GAZİANTEP  
GRADUATE SCHOOL OF  
NATURAL & APPLIED SCIENCES  
Department of Engineering Physics

Name of the thesis: The effect of various experimental parameters on glow curves and  
TL kinetics of some dosimetric materials

Name of the student: Vural Emir Kafadar  
Exam Date: 21.07.2009

Approval of the Graduate School of Natural and Applied Sciences

Prof.Dr. Ramazan KOÇ  
Director

I certify that this thesis satisfies all the requirements as a thesis for the degree of Master of  
Science / Doctor of Philosophy.

Prof.Dr. Ramazan KOÇ  
Head of Department

This is to certify that we have read this thesis and that in our opinion it is fully adequate, in  
scope and quality, as a thesis for the degree of Master of Science / Doctor of Philosophy.

Assist. Prof. Dr. R. Güler YILDIRIM  
Co- Supervisor

Assoc.Prof.Dr.A. Necmeddin YAZICI  
Supervisor

Examining Committee Members

Prof.Dr. Nurdoğan CAN

\_\_\_\_\_

Prof.Dr. Zihni ÖZTÜRK

\_\_\_\_\_

Assoc. Prof. Dr. Necmeddin YAZICI

\_\_\_\_\_

Assoc. Prof. Dr. Turgay KARALI

\_\_\_\_\_

Assoc. Prof. Dr. Metin BEDİR

\_\_\_\_\_

## ABSTRACT

### THE EFFECT OF VARIOUS EXPERIMENTAL PARAMETERS ON GLOW PEAKS AND TL KINETICS OF SOME DOSIMETRIC MATERIALS

KAFADAR, V. Emir

Ph.D. in Physics Eng.

Supervisor: Assoc. Prof. Dr. A. Necmeddin YAZICI

Co-Supervisor: Asist. Prof. Dr. R. Güler YILDIRIM

July 2009, 138 pages

Either natural fluoride which contains, depending on its origin, a wide variety of different impurities acting as activators, or synthetic  $\text{CaF}_2$  as a host lattice with artificial dopants such as Tm, Dy, and Mn have been used as dosimeter. The samples used in this study were  $\text{CaF}_2:\text{Dy}$  (TLD-200),  $\text{CaF}_2:\text{Tm}$  (TLD-300) and  $\text{CaF}_2:\text{Mn}$  (TLD- 400) crystal chips obtained from Harshaw Chemical Company, Ohio, USA. In this study we have investigated the effect of heating rate on the dose response and linearities of these samples by evaluating their supra / super linearity indexes,  $f(D)$  and  $g(D)$  respectively. Also the fading characteristics of the samples both in the dark and under tungsten filament lamp and the effect of heating rate on shape of the glow curves and total peak areas of the glow curves have been investigated in detail.

Lithium triborate, ( $\text{LiB}_3\text{O}_5$ , LBO), is one of the most known lithium borates. It is a newly developed nonlinear optical crystal. In this work, the trapping parameters of Al- doped  $\text{LiB}_3\text{O}_5$ , synthesized in Middle East Technical University, were evaluated by using different experimental methods, namely; the additive dose repeated initial rise, variable heating rate, peak shape, isothermal decay, three points methods and the computerized glow curve deconvolution method.

Keywords: TLD-200, TLD-300, TLD- 400, LBO,  $f(D)$  and  $g(D)$

## ÖZ

### ÇEŞİTLİ DENEYSEL PARAMETRELERİN BAZI DOZİMETRİK MALZEMELERİN IŞILDAMA EĞRİSİ VE TL KİNETİK DEĞERLERİNE ETKİSİNİN ARAŞTIRILMASI

KAFADAR, V. Emir

Doktora Tezi, Fizik Müh. Bölümü

Tez Yöneticisi: Doç. Dr. A. Necmeddin YAZICI

Tez Yöneticisi Yardımcısı: Yrd. Doç. R. Güler YILDIRIM

Temmuz 2009, 138 sayfa

Doğal florit, içerisindeki safsızlığın mineralin alındığı bölgeye göre değişmesiyle beraber, sentetik olarak Dy, Tm ve Mn aktivatörleri ile katkılandırılarak termoluminesans dozimetre olarak kullanılmaktadır. Bu çalışmada Harshaw firmasından alınmış olan  $\text{CaF}_2\text{:Dy}$  (TLD-200),  $\text{CaF}_2\text{:Tm}$  (TLD-300) ve  $\text{CaF}_2\text{:Mn}$  (TLD- 400) kristalleri kullanılmış ve bu kristallerin doz tepkileri ve doğrusallıkları  $f(D)$  ve  $g(D)$  fonksiyonları elde edilerek incelenmiştir. Aynı zamanda bu kristallerin karanlık ortamda ve tungsten lambası altındaki termal sönümleri ve ısıtma sıcaklığı oranının ışıldama eğrilerinin şekline, toplam pik alanına etkisi de detaylı olarak araştırılmıştır.

Lityum triborat, ( $\text{LiB}_3\text{O}_5$ , LBO), son zamanlarda geliştirilmiş önemli bir teknolojik madde olup, aynı zamanda etkin bir termoluminesans malzeme olarak kullanılabileceği ortaya çıkmıştır. Bu kristalin temel ışıldama eğrisine (P3) ait kinetik parameter değerleri, doz tepkisi, ilk yükselme, değişken ısıtma sıcaklığı oranı, pik şekli, izotermal ışımaya bozunma, üç nokta ve bilgisayarlı pik ayrıştırma gibi çeşitli metodlar kullanılarak hesaplanmıştır.

Anahtar Kelimeler: TLD-200, TLD-300, TLD- 400, LBO,  $f(D)$ ,  $g(D)$

## ACKNOWLEDGEMENT

During the writing of this thesis, the author received many helps from people to whom he would like to thank.

First of all I would like to thank my supervisor Assoc. Prof. Dr. A. Necmeddin YAZICI for all his help and advice during this thesis. I am truly grateful for the encouragement and consideration of him. It is now my privilege to thank him.

Secondly, I wish to thank to my co-supervisor Assist. Prof. Dr. R. Güler YILDIRIM. I have benefited from the aid and advice of her during the writing and preparation of this thesis.

I am deeply grateful to my wife Feyza Nur KAFADAR for her constant and loving support to my work.

I would like to thank my gratitude to my family for their support at every stage of my life.

I also want to thank my roommate Dr. Hüseyin TOKTAMIŞ for his kind help and friendship. Also Dr. Tolga DEPCI from METU, for the synthesis of  $\text{LiB}_3\text{O}_5$  crystal.

I and my supervisor are grateful for financial support from the Research Fund of Gaziantep University. We are grateful to Dr.A.J.J.Bos and Dr.T.M.Piters from Interfaculty Reactor Institute, The Netherlands, for providing the CGCD program.

<b>CONTENTS</b>	page
<b>ABSTRACT</b> .....	ii
<b>ÖZET</b> .....	iii
<b>ACKNOWLEDGEMENT</b> .....	iv
<b>CONTENTS</b> .....	v
<b>LIST OF FIGURES</b> .....	viii
<b>LIST OF TABLES</b> .....	xviii
<b>CHAPTER 1: INTRODUCTION</b> .....	1
<b>CHAPTER 2: MODELS AND ANALYSIS OF THERMALLY STIMULATED PROCES</b> .....	5
2.1 Models for Thermoluminescence.....	5
2.1.1 <i>Randall- Wikins model (First Order Kinetics)</i> .....	7
2.1.2 <i>Garlick-Gibson model (Second Order Kinetics)</i> .....	14
2.1.3 <i>May-Partridge model (General Order Kinetics)</i> .....	18
2.1.4 <i>Advanced models</i> .....	20
2.2 Thermoluminescence Analysis.....	23
2.3 Method of Analysis.....	24
2.3.1 <i>Initial Rise Method</i> .....	24
2.3.2 <i>Heating Rate Method</i> .....	26
2.3.3 <i>Peak Shape Methods</i> .....	27
2.3.4 <i>CGCD Method</i> .....	30

2.3.5 Isothermal Decay Method.....	32
2.3.6 Three Points Method (TPM).....	33
<b>CHAPTER 3: CHARACTERIZATION OF NONLINEARITIES IN THE DOSE DEPENDENCE OF TL.....</b>	<b>36</b>
3.1 General Considerations.....	36
3.1.1 Superlinearity.....	36
3.1.2 Supralinearity.....	38
3.2 Further Discussions of Supralinearity.....	39
3.2.1 Trap Creation Models.....	39
3.2.2 Sensitization.....	40
3.2.3 Competing Trap Models.....	40
3.2.4 Centre Conversion Models.....	41
3.3 Heating Rate Effect.....	42
3.4 Thermal Annealing.....	46
3.5 Thermal Fading.....	48
<b>CHAPTER 4: EXPERIMENTAL PROCEDURE.....</b>	<b>50</b>
4.1 Materials.....	50
4.2 Experimental Procedure and Equipments.....	50
4.3 Synthesis of Lithium Triborate (LBO).....	54

<b>CHAPTER 5: EXPERIMENTAL RESULTS.....</b>	<b>55</b>
5.1 The effect of heating rate on the dose response of CaF <sub>2</sub> : Dy (TLD-200).....	55
5.2 The effect of heating rate on the dose response of CaF <sub>2</sub> : Tm (TLD-300).....	74
5.3 The effect of heating rate on the dose response of CaF <sub>2</sub> : Mn (TLD-400).....	94
5.4 The thermoluminescence properties of Lithium triborat (LiB <sub>3</sub> O <sub>5</sub> : Al) after β- irradiation.....	110
<b>CHAPTER 6: CONCLUSION.....</b>	<b>128</b>
<b>REFERENCES.....</b>	<b>133</b>



## LIST OF FIGURES

<b>Figure No</b>		<b>Page</b>
Figure 2.1	Energy band model showing the electronic transitions in a TL material according to a simple two-level model (a) generation of electrons and holes; (b) electron and hole trapping; (c) electron release due to thermal stimulation; (d) recombination. (•) shows electrons, (◦) shows holes. Level T is an electron trap, level R is a recombination centre, $E_f$ is Fermi level	8
Figure 2.2	Properties of the R–W first-order TL equation, showing: (a) variation with $n_0$ , the concentration of trapped charge carriers after irradiation; (b) the variation with $E$ , the activation energy; (c) the variation with $s$ , the escape frequency; (d) the variation with $\beta$ , the heating rate. Parameter values: $n_0=1 \text{ m}^{-3}$ ; $E=1 \text{ eV}$ ; $s=1 \times 10^{12} \text{ s}^{-1}$ , $\beta=1 \text{ K/s}$ of which one parameter is varied while the others are kept constant	14
Figure 2.3	Properties of the Garlick–Gibson second-order TL equation, showing: (a) variation with $n_0$ , the concentration of trapped charge carriers after irradiation; (b) the variation with $E$ , the activation energy; (c) the variation with $s/N$ ; (d) the variation with $\beta$ , the heating rate. Parameter values: $n_0=1 \text{ m}^{-3}$ ; $E=1 \text{ eV}$ ; $s/N=1 \times 10^{12} \text{ s}^{-1} \text{ m}^3$ , $\beta=1 \text{ K/s}$ of which one parameter is varied while the others are kept constant	16
Figure 2.4	Comparison of first-order ( $b=1$ ), second-order ( $b=2$ ) and intermediate-order ( $b=1.3$ and $1.6$ ) TL peaks, with $E=1 \text{ eV}$ , $s=1 \times 10^{12} \text{ s}^{-1}$ , $n_0=N=1 \text{ m}^{-3}$ and $\beta=1 \text{ K/s}$	20

Figure 2.5	Advanced models describing the thermally stimulated release of trapped charged carriers including: (a) a shallow trap (ST), a deep electron trap (DET), and a active trap (AT); (b) two active traps and two recombination centres; (c) localised transitions; (d) defect interaction (trapping centre interacts with another defect)	22
Figure 2.6	The characteristics points on a TL glow-peak, which define the peak-shape parameters	28
Figure 2.7	Geometrical factor, $\mu_g$ , (shape parameter) as a function of the given order	28
Figure 2.8	An isolated TL glow peak. The parameters $I_x$ , $I_y$ , $I_z$ , $T_x$ , $T_y$ , and $T_z$ are as defined in the text	34
Figure 3.1	Superlinearity of the 260 K peak in two samples semiconducting diamond. $I_{max}$ is the height of the 260 K peak and the dotted line shows the line of linearity	37
Figure 3.2	TL output vs. dose in LiF	38
Figure 3.3	Energy levels involved in the competition during excitation. $m$ is concentration of recombination centers, $N_1$ and $N_2$ are concentrations of active and contrations of active and competing traps, of which $n_1$ and $n_2$ , respectively, are occupied. $n_c$ is instantaneous concentration of electrons in the conduction band, $A_1$ , $A_2$ and $A_m$ are the retrapping, competing trapping and recombination probabilities, respectively	41
Figure 3.4	Energy levels involved in the competition during heating (read-out). $m$ is concentration of holes in centers, $N_1$ and $N_2$ are concentrations of active TL traps and competing traps, respectively (levels 1 and 2); $n_1$ and $n_2$ are concentration of electrons in these traps, respectively. $A_1$ , $A_2$ are trapping probabilities into 1 and 2 respectively; $A_m$ is the recombination probability; and $n_c$ is concentration of free electrons in the conduction band	41

Figure 3.5	Change of the peak shape and shift in the peak position as a function of the heating rate. From (a) to (h) = 2, 8, 20, 30,40, 50, 57, 71°C/s	45
Figure 3.6	TL response of Al <sub>2</sub> O <sub>3</sub> as a function of heating rate. The response has been normalized to the one obtained with the lowest heating rate	46
Figure 4.1	Basic block diagram of TL reader	52
Figure 4.2	Typical time temperature profile (TTP)	52
Figure 4.3	Experimental equipments (a) <sup>90</sup> Sr- <sup>90</sup> Y β-source (b) 9010 Optical Dating System (c) Harshaw TLD System 3500	53
Figure 5.1a	A typical glow curve of TLD-200 measured after an annealing procedure of 500 ± 1 °C for 1 hour by irradiation at room temperature from exposed to beta rays from 0.04 Gy up to 72 Gy and readout at a linear heating rate of β = 1 °C/s	57
Figure 5.1b	A typical glow curve of TLD-200 measured after an annealing procedure of 500 ± 1 °C for 1 hour by irradiation at room temperature from exposed to beta rays from 144 Gy up to 34.5 kGy and readout at a linear heating rate of β = 1 °C/s	58
Figure 5.2	The growth of the height of the peaks from TLD-200 as a function of dose at a linear heating rate of β = 1 °C/s	60

Figure 5.3	The dose response function $f(D)$ vs $D$ of TLD-200 ( $\beta=1$ °C/s)	61
Figure 5.4	The dose response function $f(D)$ vs $D$ of the LTPs and HTPs of TLD-200 ( $\beta=1$ °C/s)	62
Figure 5.5	The superlinearity function $g(D)$ vs $D$ of TLD-200 (a) LTPs, (b) HTPs ( $\beta=1$ °C/s)	63
Figure 5.6a	A typical glow curve of TLD-200 measured after an annealing procedure of $500 \pm 1$ °C for 1 hour by irradiation at room temperature from exposed to betarays from 0.04 Gy up to 72 Gy and readout at a linear heating rate of $\beta = 10$ °C/s	65
Figure 5.6b	A typical glow curve of TLD-200 measured after an annealing procedure of $500 \pm 1$ °C for 1 hour by irradiation at room temperature from exposed to betarays from 144 Gy up to 34.5 kGy and readout at a linear heating rate of $\beta = 10$ °C/s	66
Figure 5.7	The growth of the height of the peaks from TLD-200 as a function of dose at a linear heating rate of $\beta = 10$ °C/s	67
Figure 5.8	The dose response function $f(D)$ vs $D$ of TLD-200 ( $\beta=10$ °C/s)	68
Figure 5.9	The dose response function $f(D)$ vs $D$ of the LTPs and HTPs of TLD-200 ( $\beta=10$ °C/s)	69
Figure 5.10	The superlinearity function $g(D)$ vs $D$ of TLD-200 ( $\beta=10$ °C/s)	70

Figure 5.11	The glow curves of TLD-200 crystals irradiated with $^{90}\text{Sr}$ - $^{90}\text{Y}$ beta source at linear heating rates between 1 °C/s and 30 °C/s (D=12 Gy)	71
Figure 5.12	The normalized total TL peak area of TLD-200 crystals irradiated with $^{90}\text{Sr}$ - $^{90}\text{Y}$ beta source at linear heating rates between 1 °C/s and 30 °C/s (D=12 Gy)	72
Figure 5.13	A set of TL glow curves for TLD-200 crystal measured after different storage times at room temperature (a) in the dark, (b) under light. All glow curves were read out at 1 °C / s after the samples were exposed to an irradiation of 12 Gy	73
Figure 5.14	The normalized TL intensity of the glow curves after planned storage time periods both in the dark and under light	74
Figure 5.15	The CGCD analyzed glow curves of Tm-doped $\text{CaF}_2$ measured after 12 Gy irradiation by beta ray at room temperature after an annealing procedure of 1 hour at 400 °C	76
Figure 5.16a	A typical glow curve of TLD-300 measured after an annealing procedure of $400 \pm 1$ °C for 1 hour by irradiation at room temperature from exposed to beta rays from 0.04 Gy up to 72 Gy and readout at a linear heating rate of $\beta = 1$ °C/s	77
Figure 5.16b	A typical glow curve of TLD-300 measured after an annealing procedure of $400 \pm 1$ °C for 1 hour by irradiation at room temperature from exposed to beta rays from 144 Gy up to 14 kGy and readout at a linear heating rate of $\beta = 1$ °C/s	78
Figure 5.17	The growth of the height of the peaks from TLD-300 as a function of dose at a linear heating rate of $\beta = 1$ °C/s	79

Figure 5.18	The dose response function $f(D)$ vs $D$ of TLD-300 ( $\beta=1$ °C/s)	80
Figure 5.19	The dose response function $f(D)$ vs $D$ of TLD-300 ( $\beta=1$ °C/s)	81
Figure 5.20	The superlinearity function $g(D)$ vs $D$ of TLD-300 ( $\beta=1$ °C/s)	82
Figure 5.21a	A typical glow curve of TLD-300 measured after an annealing procedure of $400 \pm 1$ °C for 1 hour by irradiation at room temperature from exposed to beta rays from 0.04 Gy up to 72 Gy and readout at a linear heating rate of $\beta = 10$ °C/s	84
Figure 5.21b	A typical glow curve of TLD-300 measured after an annealing procedure of $400 \pm 1$ °C for 1 hour by irradiation at room temperature from exposed to beta rays from 144 Gy up to 14 kGy and readout at a linear heating rate of $\beta = 10$ °C/s	85
Figure 5.22	The growth of the height of the peaks from TLD-300 as a function of dose at a linear heating rate of $\beta = 10$ °C/s	86
Figure 5.23	The dose response function $f(D)$ vs $D$ of TLD-300 (a) P1, P2, P3 (b) P4, P5, P6 ( $\beta=10$ °C/s)	87
Figure 5.24	The dose response functions (a) $f(D)$ and (b) $g(D)$ vs $D$ of TLD-300 ( $\beta=10$ °C/s)	89
Figure 5.25	The glow curves of TLD-300 crystals irradiated with $^{90}\text{Sr}$ - $^{90}\text{Y}$ beta source at linear heating rates between 1 °C/s and 30 °C/s ( $D=12$ Gy)	90
Figure 5.26	The normalized total TL peak area of TLD-300 crystals irradiated with $^{90}\text{Sr}$ - $^{90}\text{Y}$ beta source at linear heating rates between 1 °C/s and 30 °C/s ( $D=12$ Gy)	91

Figure 5.27a	A set of TL glow curves for TLD-300 crystal measured after different storage times at room temperature and normalized TL intensity for dark fading. All glow curves were read out at 1 °C / s after exposing to an irradiation of 72 Gy	92
Figure 5.27b	A set of TL glow curves for TLD-300 crystal measured after different storage times at room temperature and normalized TL intensity for optical fading. All glow curves were read out at 1 °C / s after exposing to an irradiation of 72 Gy	93
Figure 5.28	The CGCD analyzed glow curves of Mn-doped CaF <sub>2</sub> measured after 12 Gy irradiation by beta ray at room temperature after an annealing procedure of 30 min. at 400 °C	96
Figure 5.29a	A typical glow curve of TLD-400 measured after an annealing procedure of 400 ± 1 °C for 30 min by irradiation at room temperature from exposed to beta rays from 0.04 Gy up to 72 Gy and readout at a linear heating rate of β = 1 °C/s	97
Figure 5.29b	A typical glow curve of TLD-400 measured after an annealing procedure of 400 ± 1 °C for 30 min by irradiation at room temperature from exposed to beta rays from 144 Gy up to 14 kGy and readout at a linear heating rate of β = 1 °C/s	98
Figure 5.30	The growth of the peak areas of glow peaks of TLD-400 as a function of applied dose (β=1 °C/s)	99
Figure 5.31	The dose response function f(D) vs D of TLD-400 (β=1 °C/s)	99
Figure 5.32	The dose response function f(D) vs D of TLD-400. (β=1 °C/s)	100

Figure 5.33	The superlinearity function $g(D)$ vs $D$ of the total peak area of the TL peaks from TLD- 400 at linear heating rates of $1\text{ }^{\circ}\text{C}\cdot\text{s}^{-1}$	101
Figure 5.34a	A typical glow curve of TLD-400 measured after an annealing procedure of $400 \pm 1\text{ }^{\circ}\text{C}$ for 30 m. by irradiation at room temperature from exposed to beta rays from 0.04 Gy up to 72 Gy and readout at a linear heating rate of $\beta = 10\text{ }^{\circ}\text{C}/\text{s}$	102
Figure 5.34b	A typical glow curve of TLD-400 measured after an annealing procedure of $400 \pm 1\text{ }^{\circ}\text{C}$ for 30 min by irradiation at room temperature from exposed to beta rays from 144 Gy up to 14 kGy and readout at a linear heating rate of $\beta = 10\text{ }^{\circ}\text{C}/\text{s}$	103
Figure 5.35	The growth of the peak areas of glow peaks of TLD-400 as a function of applied dose ( $\beta=10\text{ }^{\circ}\text{C}/\text{s}$ )	104
Figure 5.36	The dose response function $f(D)$ vs $D$ of TLD-400 ( $\beta=10\text{ }^{\circ}\text{C}/\text{s}$ )	104
Figure 5.37	The dose response function $f(D)$ vs $D$ of TLD-400 ( $\beta=10\text{ }^{\circ}\text{C}/\text{s}$ )	105
Figure 5.38	The dose response function $g(D)$ vs $D$ of TLD-400 ( $\beta=10^{\circ}\text{C}/\text{s}$ )	106
Figure 5.39	The glow curves of TLD-400 crystals irradiated with $^{90}\text{Sr}$ - $^{90}\text{Y}$ beta source at lineear heating rates between $1\text{ }^{\circ}\text{C}/\text{s}$ and $30\text{ }^{\circ}\text{C}/\text{s}$ ( $D=12\text{ Gy}$ )	107
Figure 5.40	The normalized TL peak area of TLD-300 crystals irradiated with $^{90}\text{Sr}$ - $^{90}\text{Y}$ beta source at lineear heating rates between $1\text{ }^{\circ}\text{C}/\text{s}$ and $30\text{ }^{\circ}\text{C}/\text{s}$ ( $D=12\text{ Gy}$ )	108



Figure 5.41	A set of TL glow curves for TLD-400 crystal measured after different storage times at room temperature (a) in the dark, (b) optical fading. All glow curves were read out at 1 °C / s after exposing to an irradiation of 36 Gy	109
Figure 5.42	Normalized TL intensity for dark and optical fading for TLD-400	110
Figure 5.43	The glow curve of Al-doped LiB <sub>3</sub> O <sub>5</sub> measured after various radiation exposed dose levels ( $\beta=1$ °C/s)	114
Figure 5.44	Normalized isothermal decay curves of peak 3 at 190, 195, 200, 205, 210±1 °C for the radiation dose of 12 Gy	118
Figure 5.45	Plots of $I^{b-1}$ versus decay time for peak 3	119
Figure 5.46	Some of the selected glow curves of Al-doped LiB <sub>3</sub> O <sub>5</sub> measured at various heating rates for 1, 3, and 5 °C/s. All glow curves were measured after $\beta$ irradiation of 12 Gy	120
Figure 5.47	Some of the selected glow curves of Al-doped LiB <sub>3</sub> O <sub>5</sub> after different T <sub>stop</sub> temperatures at a linear heating rate $\beta=1$ °C/s. Dose levels are always adjusted to 12 Gy	123
Figure 5.48	The activation energy (E <sub>a</sub> ) resulting from the RIR method after T <sub>m</sub> (E <sub>a</sub> )-T <sub>stop</sub> procedure	124
Figure 5.49	T <sub>1</sub> -T <sub>stop</sub> , T <sub>m</sub> - T <sub>stop</sub> , T <sub>2</sub> - T <sub>stop</sub> , and I <sub>m</sub> - T <sub>stop</sub> plot for the thermoluminescent dosimetric glow peak of Al-doped LiB <sub>3</sub> O <sub>5</sub>	124

Figure 5.50 The geometric factor  $\mu_g$ ,  $T_2-T_1$  and  $T_2-T_m$  as a result of  $T_{stop}$  determined from the  $T_m-T_{stop}$  procedure. (b) The activation energy ( $E_a$ ) resulting from the PS method after the  $T_m-T_{stop}$  procedure 125

Figure 5.51 The CGCD analyzed glow curves of Al-doped  $LiB_3O_5$  measured after 0.6 Gy irradiation by beta ray at room temperature 127

## LIST OF TABLES

Table No		Page
Table 2.1	Numerical values of the coefficients comparing in Eq. (2.52)	30
Table 5.1	The constants used in the superlinearity function	62
Table 5.2	The constants used in the superlinearity function	69
Table 5.3	Numerical values of the coefficients comparing in Eq. (5.14)	115
Table 5.4	The values of the activation energy $E_a$ (eV) and frequency factor $s$ ( $s^{-1}$ ) of main dosimetric peak of -Al doped $LiB_3O_5$ determined by the modified PS method of Gartia et al. [93]	116
Table 5.5	The values of the activation energy $E_a$ (eV) and frequency factor $s$ ( $s^{-1}$ ) of main dosimetric peak of Al- doped $LiB_3O_5$ determined by the Chen's PS,RIR, VHR, and TP methods	125
Table 5.6	The values of the activation energy $E_a$ (eV) and frequency factor $s$ ( $s^{-1}$ ) of main dosimetric peak 3 of -Al doped $LiB_3O_5$ determined by CGCD method.	127

## INTRODUCTION

Thermoluminescence is the physical phenomenon in which a solid sample absorbs energy while irradiated at a given temperature, and releases this energy in the form of light while heating the sample. The emitted light is recorded as intensity vs. temperature in the shape of one or more TL peaks. Under favourable conditions, the emitted TL light intensity is proportional to the absorbed dose, and thus, using an appropriate calibration, one can evaluate the applied dose in the given radiation field. The TL signal may be the intensity at the maximum or the area under the TL glow peak, which are usually nearly proportional to each other. In regular dosimetric applications, one can choose an appropriate material with reproducible results in repeated measurements, linear dose dependence for the kind of radiation in question as well as dose-rate independence and long time stability [1].

The phenomenon thermoluminescence (TL) has been known for a long time. The first application of this phenomenon for dosimetric purposes was from Daniel et al. [2]. Since then much research has been carried out for a better understanding and improvement of the material characteristics as well as to develop new TL materials. Nowadays, thermoluminescence dosimetry (TLD) is a well-established dosimetric technique with applications in areas such as personnel, environmental and clinical dosimetry. TLD is based on materials which (after exposure to ionizing radiation) emit light while they are heated. The impurities in the TL material give rise to localized energy levels within the forbidden energy band gap and that these are crucial to the TL process.

TL should not be confused with the light spontaneously emitted from a substance when it is heated to incandescence. At higher temperatures (say in excess of 200 °C) a solid emits (infra) red radiation of which the intensity increases with increasing temperature. This is thermal or black body radiation. TL, however, is the thermally stimulated emission of light following the previous absorption of energy from radiation. According to this phenomenon, the three essential ingredients necessary for the production of TL can be deduced. Firstly, the material must be an

insulator or semiconductor–metals do not exhibit luminescent properties. Secondly, the material must have at some time absorbed energy during exposure to ionizing radiation. Thirdly, the luminescence emission is triggered by heating the material [3]. A thermoluminescent material is thus a material that absorbs some energy which is stored during exposure to ionizing radiation. When the material is heated, the stored energy is released in the form of visible light. In fact that TL does not refer to thermal *excitation*, but to *stimulation* of luminescence in a sample which was excited in a different way. TL material cannot emit light again by simply cooling the sample and reheating it another time. It should first be re-exposed to ionizing radiation before it produces light again. The storage capacity of a TL material makes it suitable for dosimetric applications.

The main features required for making a material a good TLD (TL dosimeter) candidate are [4]:

- Wide interval in which the luminescence intensity is linear with absorbed dose. In most materials, the linear interval is limited by superlinearity and saturation (decay) of the TL intensity at large doses. The useful range is determined by the linear dose dependence.
- Low dependence of the TL response on the energy of the incident radiation. If necessary, the energy dependence can be partially compensated by metallic filters.
- High sensitivity, i.e., a high TL signal per unit absorbed dose. High sensitivity is important for use in personal and medical dosimetry, as well as in environmental radiation monitoring.
- Low fading, i.e., the ability to store dosimetric information for a long time.
- Simple TL curve (with one isolated peak). If several peaks are present, the dosimeter heating protocol is complicated.
- The luminescence spectrum should match the maximum spectral sensitivity of the photomultiplier.
- The TL dosimetric material should be mechanically strong, chemically inert, and radiation resistant

Normally, the shape of the glow curve will be of one or more peaks of emitted light, some of which may be overlapping. The shape of the glow curve depends on the light sensitive device, and in particular, on its spectral response. Moreover, even with a given device, the glow curve may look different if different filters are inserted between the sample and the detector. Also, the shape of the TL glow curve depends on the heating rate used [5]. Since doses are evaluated as fast as possible in personnel monitoring, reader systems having fast heating rates are employed to read out the largest number of TLD cards in the shortest possible time with high intensity. Therefore, in TL dosimetric investigations, the routine personnel and environmental dosimetry uses heating rates higher than  $10\text{ }^{\circ}\text{C s}^{-1}$  to record the TL signals within a short time. It is well known that the dosimetric characteristics of many TL materials are influenced by changes in location, size and shape of the glow curves due to changes in the heating rate [6].

Another important feature of glow curves is their dependence on the excitation dose. In the applications in dosimetry and archaeological dating of ceramic samples, a linear dependence on the dose in broad ranges is highly desirable, but this is by no means always found to be in case. Typically, at high doses, the dose dependence curve approaches some saturation value. At low doses, linear dose dependence is quite prevalent, however superlinear (or supralinear) dependence as of the lowest doses sometimes occurs. In some cases (though quite rarely), one has to consider the dependence upon dose rate as well [5]. Nonlinearities often occur in the dose dependence of thermoluminescence (TL). These include sublinearity, usually when there is an approach to saturation in the dose dependence, as well as supralinearity, also termed superlinearity in the literature. Different researchers in the field have viewed the effect of supralinearity / superlinearity from two somewhat different points of view. One point of view has to do with the rate of change with dose of the dose dependence function. The other approach is related more to the applications of TL in dosimetry and archaeological and geological dating, and basically has to do with the correction to be made in extrapolation in cases where supra (super) linearity occurs following an initial linear dose range or prior to such a linear range. The term supralinearity index,  $f(D)$ , is used in cases where the feature of interest is the deviation from linearity, namely, when the correction in the extrapolation is the main issue. The term superlinearity index,  $g(D)$ , in the dose

ranges where the growth is more than linear and when extrapolation is not the main issue [7].

In this Ph.D thesis the effects of various experimental factors on the glow curves and TL intensities of CaF<sub>2</sub>: Dy (TLD-200), CaF<sub>2</sub>: Tm (TLD-300), CaF<sub>2</sub>: Mn (TLD-400) crystals were investigated using the dose response functions  $f(D)$  and  $g(D)$  and also, the trap parameters of Al-doped LiB<sub>3</sub>O<sub>5</sub> (LBO) crystal were found using different experimental methods.

This thesis consists of six chapters. Chapter 2 explains the thermoluminescence phenomena, its mathematical expressions and some important models for thermoluminescence and also the methods to evaluate the kinetic parameters responsible for the TL emission.

In chapter 3, characterization of nonlinearities in the dose dependence of TL has been explained. Also, the dose response functions; supralinearity index,  $f(D)$  and superlinearity index,  $g(D)$  have been explained and related mathematical expressions have been introduced. The experimental equipments and their specifications, the experimental procedures and the samples used in this thesis have been given in chapter 4.

All the experimental results were given in chapter 5. This chapter contains mainly two parts. In the first part, the linearity and dose response behaviors of Dy doped CaF<sub>2</sub> (TLD-200), Tm doped CaF<sub>2</sub> (TLD-300) and Mn doped CaF<sub>2</sub> (TLD-400) crystals were investigated at two different linear heating rates of 1 °C/s and 10 °C/s by using the dose response functions,  $f(D)$  and  $g(D)$ . And also their fading characteristics, both in the dark and under tungsten filament lamp and the effect of heating rate on shape of the glow curves and total peak areas of the glow curves have been investigated in detail. In the second part of chapter 5, the kinetic parameters of the main dosimetric peak, P3, of Al-doped LiB<sub>3</sub>O<sub>5</sub> were evaluated by using different experimental methods, namely; the additive dose (AD), T<sub>m</sub>(E<sub>a</sub>)-T<sub>stop</sub>, repeated initial rise (RIR), variable heating rate (VHR), peak shape (PS), isothermal decay (ID), three points methods (TPM) along with the deconvolution method (CGCD). Finally, in chapter 6, all the experimental results concluded and discussed with support of the literature.

## CHAPTER 2

### MODELS AND ANALYSIS OF THERMALLY STIMULATED PROCESS

#### 2.1 Models for Thermoluminescence

The energy band theory of solids explains the observed TL properties. In an ideal semiconductor or insulator crystalline most of the electrons reside in the valence band. The next highest band that the electrons can occupy is the conduction band, separated from the valence band by the so-called forbidden band gap. The energy difference between the valence band and conduction band is  $E_g$ . However, whenever structural defects occur in a crystal, or if there are impurities within the lattice, there is a possibility for electrons to possess energies which are forbidden in the perfect crystal.

From a theoretical point of view, TL is directly connected to the band structure of solids and particularly to the effects of impurities and lattice irregularities. These can be described as centers that may occur when ions of either signs move away from their original sites, thus leaving vacancy states, able to interact with free charge carriers and to trap them; alternatively, ions can diffuse in interstitial positions and break locally the ideal lattice geometry; finally, impurity ions can perturb the lattice order, because of their sizes and valences, generally different from their neighbor ones. Moreover, these extrinsic defects can interact with the intrinsic ones, and eventually either of them can aggregate in more complex configuration. From an atomic standpoint a defect can be described by means of the sign and number of charge carriers it may interact with, and the eventual existence of excited states; to such a description, a characteristic energy for each center corresponds: this may be defined as the amount of energy able, when supplied, to set the trapped charges free, thus destroying the center and restoring a situation of local order.



It is feasible therefore to describe the band structure in term of valance and conduction bands, parted from each by forbidden gap in which the defects are represented as sites localized at different depths, below the conduction band, where free charge carriers of either sign may be trapped.

Therefore, the mapping of the forbidden gap reveals quite a complex configuration, and the experimental TL emission study can provide a satisfactory tool to get detailed information on its most meaningful parameters. These are, for each site, the characteristic energy ( $E$ ), a frequency factor ( $s$ ), connected to the transition frequency and a kinetic order ( $b$ ) synthezing the quality of the involved phenomena. The kinetic order ranges between 1 and 2. The former value corresponds to a situation where a charge (electron) is supplied energy to raise in the conduction band and, consequently, to fall to a center where it undergoes recombination with hole; the latter one stands for a situation where this phenomenon has the same probability of retrapping. Intermediate cases are likely to occur as well as contributions from non- radiative events ( $b=0$ ).

The mathematical models based upon these definitions are consisting of convenient differential equations systems, yielding for each case, the evolution of charged carrier populations, the analytical forms of which are to be checked by means of suitable experimental data. It is therefore evident how the involved parameters are to be conveniently adjusted until a fair aggrement between theory and practise is attained. The most promising tool is the observation and recording of TL emission, under several experimental conditions, as a function of temperature which the TL sample is heated to, or of heating up time. For a constant heating rate, these two observations are equivalent. The plot shape depends on the physical and chemical properties of the material and on the kind of the treatment it is submitted to. However it is always a single- or- multi- peaks structure, as may be expected from the general equations, and a correspondence can be pointed out between a peak and an electron trap level. This explained by considering how, at a certain temperature, the amount of thermal energy supplied reaches, for a given level, the threshold necessary to raise the relative trapped charges in the conduction band from where they can give rise to radiative recombination events. For this purpose, other centers, able to trap positive charge carriers, are involved, and they are likely to be connected to the quality of the emitted light. The analytical form for a single peak, which the

overall curve is a superposition of, can fully described by means of some geometrical parameters as the peak position, its left and right widths, the ratio between the overall width, the height. This last one is dependent on the heating rate and increases, for given experimental conditions, with the increasing of it. These geometrical parameters can be shown to correspond to the main physical ones: the mathematical expressions can be evaluated by a convenient analytical manipulation of the involved equations. It is also to be remarked that the experimental uncertainties, obtained by means of the glow-curve plot, allow for an estimate of the physical errors related to them, and their evaluations can point out a well defined method as the fittest one [8].

### 2.1.1 Randall - Wilkins model (First Order Kinetics)

In 1945, Randall and Wilkins [9] extensively used a mathematical representation for each peak in a glow curve, starting from studies on the phosphorescence. Their mathematical treatment was based on the energy band model and yields the well-known first order expression. The following figure, Fig. 2.1, shows the simple model used for theoretical treatment. Between the delocalized bands, conduction band, CB, and valance band, VB, two localized levels (metastable states) are considered, one acting as a trap,  $T$ , and the other acting as a recombination center,  $R$ . The distance between the trap  $T$  and the bottom of the CB is called the activation energy or trap depth,  $E$ . This energy is the energy required to liberate a charge, i.e., an electron, which is trapped in  $T$  [9].

The absorption of radiant energy with  $h\nu > E_g$  results in ionisation of valence electrons, producing energetic electrons and holes which will, after thermalization, produce free electrons in the conduction band and free holes in the valence band (transition a). The free charge carriers recombine with each other or become trapped. In the case of direct recombination an amount of energy will be released which may excite a luminescent centre. The luminescent centre relaxes (returns to the ground state) under the emission of light. However, in semiconductors and insulators a certain percentage of the charge carriers is trapped: the electrons at  $T$  and the holes at  $R$  (transition b).

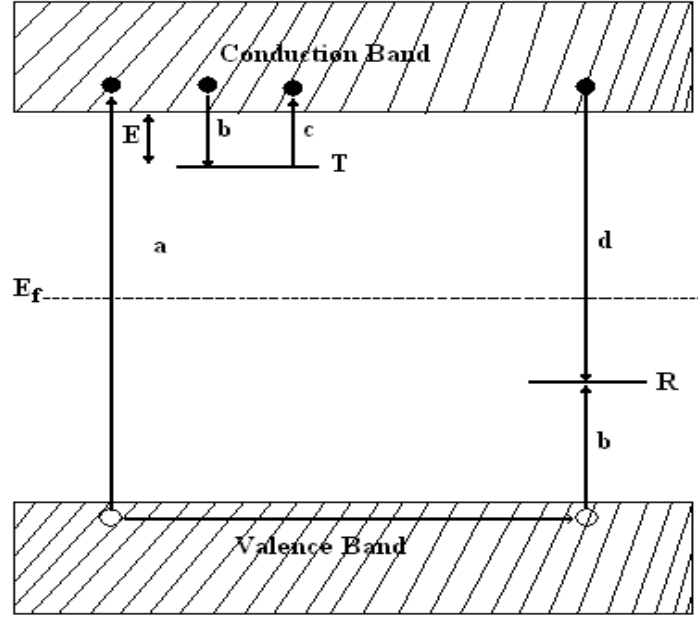


Figure 2.1 Energy band model showing the electronic transitions in a TL material according to a simple two-level model (a) generation of electrons and holes; (b) electron and hole trapping; (c) electron release due to thermal stimulation; (d) recombination. (•) shows electrons, (◦) shows holes. Level  $T$  is an electron trap, level  $R$  is a recombination centre,  $E_f$  is Fermi level. [3]

The probability,  $p$ , per unit of time, that a trapped electron will escape from a trap, or the probability rate of escape per second, is given by the Arrhenius equation, having considered that the electron in the trap have a Maxwellian distribution of thermal energies

$$p = s \exp\left\{-\frac{E}{kT}\right\} \quad (2.1)$$

where  $p$  is the probability per unit time,  $s$  is the frequency factor,  $k$  is the Boltzmann's constant,  $E$  is called the trap depth (eV) or activation energy, the energy needed to release an electron from the trap into the conduction band,  $T$  is the absolute temperature (K) [5].

The intensity of TL  $I(t)$  in photons per second at any time  $t$  during heating is proportional to the rate of recombination of holes and electrons at  $R$ . If  $m$  ( $\text{m}^{-3}$ ) is the concentration of holes trapped at  $R$  the TL intensity can be written as

$$I(t) = -\frac{dm}{dt} \quad (2.2)$$

Here we assume that each recombination produces a photon and that all produced photons are detected. The rate of recombination will be proportional to the concentration of free electrons in the conduction band  $n_c$  and the concentration of holes  $m$ ,

$$I(t) = -\frac{dm}{dt} = n_c mA \quad (2.3a)$$

with the constant  $A$  the recombination probability expressed in units of volume per unit time which is assumed to be independent of the temperature.

The rate of change of the concentration of trapped electrons  $n$  is equal to the rate of thermal release minus the rate of retrapping,

$$-\frac{dn}{dt} = np - n_c(N - n)A_r \quad (2.3b)$$

with  $N$  the concentration of electron traps and  $A_r$  the probability of retrapping ( $\text{m}^3/\text{s}$ ). Likewise the rate concentration of free electrons is equal to the rate of thermal release minus the rate of retrapping and the rate of recombination,

$$\frac{dn_c}{dt} = np - n_c(N - n)A_r - n_c mA \quad (2.3c)$$

Eqs.(2.3a)-(2.3c) described the charge carrier traffic in the case of release of a trapped electron from a single-electron trap and recombination in a single centre. For TL produced by the release of holes the rate equations are similar to Eqs.(2.3a)-(2.3c). These equations form the basis of many analyses of TL phenomena. There is no general analytical solution. To develop an analytical expression some simplifying assumptions must be made. An important assumption is at any time

$$\left| \frac{dn_c}{dt} \right| \ll \left| \frac{dn}{dt} \right|, \quad \left| \frac{dn_c}{dt} \right| \ll \left| \frac{dm}{dt} \right| \quad (2.4)$$

This assumption is called by Chen and McKeever [5] the quasiequilibrium assumption since it requires that the free electron concentration in the conduction band is quasistationary. The trapped electrons and holes are produced in pairs during the irradiation. Charge neutrality dictates therefore

$$n_c + n = m \quad (2.5)$$

which for  $n_c \gg 0$  means that  $n \approx m$  and

$$I(t) = -\frac{dm}{dt} \approx -\frac{dn}{dt} \quad (2.6)$$

Since  $dn_c/dt \approx 0$  one gets from (2.3a) and (2.3b):

$$I(t) = \frac{mAn_s \exp\left\{-\frac{E}{kT}\right\}}{(N-n)A_r + mA} \quad (2.7)$$

Even (2.7) cannot be solved analytically without additional simplifying assumptions. Randall and Wilkins [10] assumed negligible retrapping during the heating stage, i.e. they assumed  $mA \gg (N-n)A_r$ . Under this assumption Eq.(2.7) can be written

$$I(t) = -\frac{dn}{dt} = sn \exp\left\{-\frac{E}{kT}\right\} \quad (2.8)$$

This differential equation describes the charge transport in the lattice as a first-order process and the glow peaks calculated from this equation are called first-order glow peaks. Solving the differential equation (2.8) yields

$$I(t) = -\frac{dn}{dt} = n_0 s \exp\left\{-\frac{E}{kT}\right\} \exp\left\{-s \int_0^t \exp\left\{-\frac{E}{kT(t')}\right\} dt'\right\} \quad (2.9)$$

where  $n_0$  is the total number of trapped electrons at time  $t=0$ . Usually the temperature is raised as a linear function of time according to

$$T(t) = T_0 + \beta t \quad (2.10)$$

with  $\beta$  the constant heating rate and  $T_0$  the temperature at  $t=0$ . This gives for the intensity as function of temperature

$$I(T) = -\frac{1}{\beta} \frac{dn}{dt} = n_0 \frac{s}{\beta} \exp\left\{-\frac{E}{kT}\right\} \exp\left\{-\frac{s}{\beta} \int_{T_0}^T \exp\left\{-\frac{E}{kT'}\right\} dT'\right\} \quad (2.11)$$

This is the well-known Randall–Wilkins first-order expression of a single glow peak. The peak has a characteristic asymmetric shape being wider on the low temperature side than on the high temperature side. On the low temperature side, i.e. in the initial rise of the glow peak, the intensity is dominated by the first exponential ( $\exp(-E/kT)$ ). Thus, if  $I$  is plotted as function of  $1/T$ , a straight line is expected in the initial rise temperature range, with the slope of  $-E/k$ , from which the activation energy  $E$  is readily found.

The properties of the Randall–Wilkins equation are illustrated in Fig.2.2. In Fig.2.2 (a) it is shown how  $I(T)$  varies if  $n_0$  varies from  $n_0=0.25 \text{ m}^{-3}$  till  $n_0=2 \text{ m}^{-3}$  while  $E=1 \text{ eV}$ ,  $s=1.0 \times 10^{12} \text{ s}^{-1}$  and  $\beta=1 \text{ K/s}$  are kept constant.

It can be noted that the temperature at the peak maximum,  $T_m$ , stays fixed. This is a characteristic of all first-order TL curves. The condition for the maximum can be found by setting  $dI/dt=0$  (or, somewhat easier from  $d \ln I(T)/dt=0$ ). From this condition one gets

$$\frac{\beta E}{kT_m^2} = s \exp\left\{-\frac{E}{kT_m}\right\} \quad (2.12)$$

In this equation  $n_0$  does not appear which shows that  $T_m$  does not depend on  $n_0$ . From Fig.2.2 (a) it can be further seen that not only the peak height at the maximum but each point of the curve is proportional to  $n_0$ . In the application in dosimetry  $n_0$  is the parameter of paramount importance since this parameter is proportional to the absorbed dose. It is simple to see that the area under the glow peak is equal to  $n_0$  since

$$\int_0^{\infty} I(t) dt = -\int_0^{\infty} \frac{dn}{dt} dt = -\int_{n_0}^{n_{\infty}} dn = n_0 - n_{\infty} \quad (2.13)$$

and  $n_\infty$  is zero for  $t \rightarrow \infty$ . In Fig. 2.2 (b) the activation energy  $E$  has been varied from 0.8 to 1.2 eV. As  $E$  increases the peak shifts to higher temperatures with a decrease in the height and an increase in the width keeping the area (i.e.  $n_0$ ) constant.

Similar changes can be noticed as  $s$  is varied (see Fig.2.2(c)) but now in the opposite way: as  $s$  increases the peak shifts to lower temperatures with an increase of the height and a decrease in width. In Fig. 2.2 (d) the heating rate has been varied. As  $\beta$  increases the peak shifts to higher temperatures while the height decreases and the width increases just as in the case of decreasing  $s$ . This can be expected since  $s$  and  $\beta$  appear as a ratio  $s/\beta$  in Eq.(2.11). It is worthwhile to note that of the four parameters the activation energy  $E$  and the frequency factor  $s$  are the main physical parameters. They are called the trapping parameters and are fixed by the properties of the trapping centre. The other two parameters can be chosen by the experimenter by choosing a certain dose ( $n_0$ ) and by read-out of the signal at a certain heating rate  $\beta$ . Investigation of a new TL material will therefore start with studying the glow peak behaviour under variation of the absorbed dose and the heating rate.

The evaluation of Eqn.(2.11) is hampered by the fact that the integral on the right-hand side is not elementary in the case of linear heating. Chen [11] has shown how the integral can be approximated by asymptotic series. In practical applications it is convenient to describe the glow peak in terms of parameters which are easy to derive experimentally, namely the intensity of peak at the maximum  $I_m$  and the temperature at the maximum  $T_m$ . The integral comparing in Eqn. (2.11) cannot be solved in an analytical form, but using successive integration by parts, in a second-order approximation (integral approximation) it becomes

$$\int_{T_0}^T \exp\left(-\frac{E}{kT'}\right) dT' = \frac{kT^2}{E} \left(1 - \frac{2kT}{E}\right) \exp\left(-\frac{E}{kT}\right) \quad (2.14)$$

Hence, Eqn. (2.14) becomes

$$I(T) = sn_0 \exp\left(-\frac{E}{kT} \exp\left[-\frac{skT^2}{\beta E} \left(1 - \frac{2kT}{E}\right) \exp\left(-\frac{E}{kT}\right)\right]\right) \quad (2.15)$$

From which the condition at the maximum is given as in Eqn.(2.12) or

$$s = \frac{\beta E}{kT_m^2} \exp\left\{-\frac{E}{kT_m}\right\} \quad (2.16)$$

Inserting Eqn.(2.16) into Eqn.(2.15) one obtains

$$I_m = \frac{n_0 \beta E}{kT_m^2} \exp\left[-\left(1 - \frac{2kT_m}{E}\right)\right] \quad (2.17a)$$

or better

$$I_m = \frac{n_0 \beta E}{kT_m^2} \exp[-(1 - \Delta_m)] \quad (2.17b)$$

Equation (2.17b) can be rewritten as

$$\frac{n_0 \beta E}{kT_m^2} = I_m \exp[-(1 - \Delta_m)] \quad (2.18)$$

Inserting Eqn.(2.12) into Eqn.(2.11), Kitis et al. [12] have shown that Eqn. (2.11) can be quite accurately approximated by

$$I(T) = I_m \exp\left[1 + \frac{E}{kT} \frac{T - T_m}{T_m} - \frac{T^2}{T_m^2} \exp\left\{\frac{E}{kT} \frac{T - T_m}{T_m}\right\} (1 - \Delta) - \Delta_m\right] \quad (2.19)$$

with  $\Delta = 2kT/E$  and  $\Delta_m = 2kT_m/E$ .



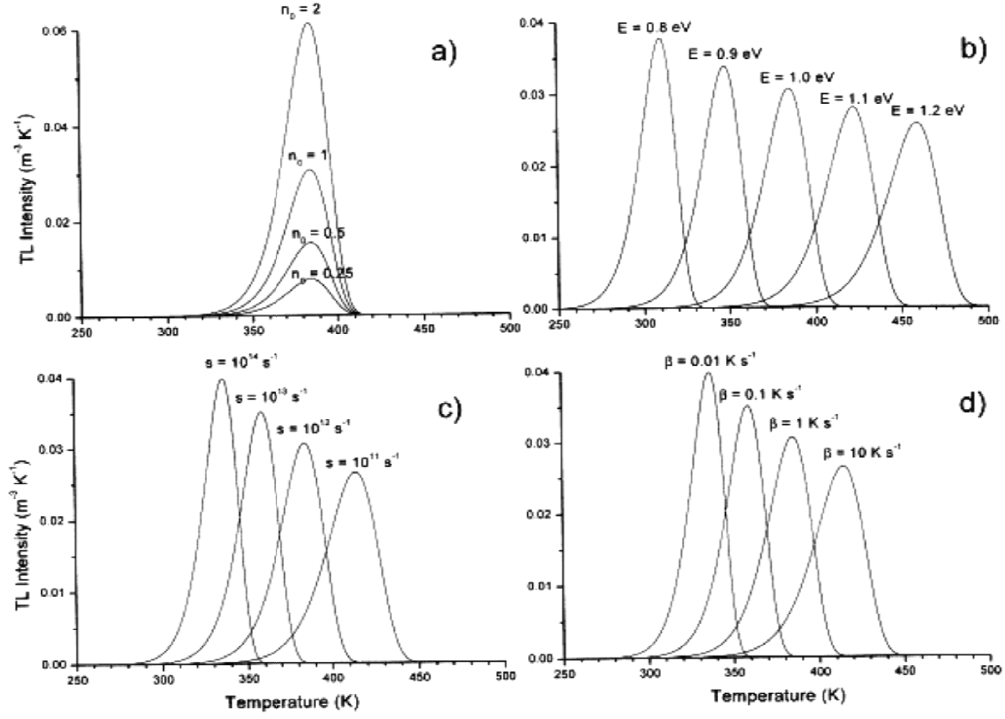


Figure 2.2 Properties of the R–W first-order TL equation, showing: (a) variation with  $n_0$ , the concentration of trapped charge carriers after irradiation; (b) the variation with  $E$ , the activation energy; (c) the variation with  $s$ , the escape frequency; (d) the variation with  $\beta$ , the heating rate. Parameter values:  $n_0=1 \text{ m}^{-3}$ ;  $E=1 \text{ eV}$ ;  $s=1 \times 10^{12} \text{ s}^{-1}$ ,  $\beta=1 \text{ K/s}$  of which one parameter is varied while the others are kept constant. [5]

### 2.1.2 Garlick- Gibson model (Second Order Kinetics)

In 1948 Garlick and Gibson [13], in their studies on phosphorescence, considered the case when a free charge carrier has probability of either being trapped or recombining within a recombination center. The term second order kinetics is used to describe a situation in which retrapping is present i.e.  $mA \ll (N-n)A_r$

They assumed that the escaping electron from the trap has equal probability of either being retrapped or of recombining with hole in a recombination centre. Further they assume that the trap is far from saturation, i.e.  $N \gg n$  and  $n=m$ . With these assumptions, Eqn. (2.7) becomes

$$I(t) = -\frac{dn}{dt} = s \frac{A}{NA_r} n^2 \exp\left\{-\frac{E}{kT}\right\} \quad (2.20)$$

We see that now  $dn/dt$  is proportional to  $n^2$  which means a second-order reaction. With the additional assumption of equal probabilities of recombination and retrapping,  $A=A_r$ , integration of Eqn.(2.20) gives

$$I(T) = \frac{n_0^2}{N} \frac{s}{\beta} \exp\left\{-\frac{E}{kT}\right\} \left[ 1 + \frac{n_0 s}{N\beta} \int_{T_0}^T \exp\left\{-\frac{E}{kT'}\right\} dT' \right]^{-2} \quad (2.21)$$

This is the Garlick–Gibson TL equation for second-order kinetics. The main feature of this curve is that it is nearly symmetric, with the high temperature half of the curve slightly broader than the low temperature half. This can be understood from the consideration of the fact that in a second-order reaction significant concentrations of released electrons are retrapped before they recombine, in this way giving rise to a delay in the luminescence emission and spreading out of the emission over a wider temperature range. The initial concentration  $n_0$  appears here not merely as a multiplicative constant as in the first-order case, so that its variation at different dose levels change the shape of the whole curve. This is illustrated in Fig.2.3 (a). It is seen that  $T_m$  decreases as  $n_0$  increases. It can be derived [14] that the temperature shift can be approximated by

$$T_1 - T_2 \approx T_1 T_2 \frac{k}{E} \ln f \quad (2.22)$$

where  $T_1$  is the temperature of maximum intensity at a certain dose and  $T_2$  the temperature of maximum intensity at  $f$  times higher dose. With the parameter values of Fig.2.3 (a) the shift is 25 K. When  $E=1$  eV,  $T_1=400$  K and the absorbed dose is increased by a factor 1000, which is easy to realise experimentally, a temperature shift of 77 K can be expected. From Eqn. (2.22) it follows further that for a given increase of the dose the shallower the trap, i.e., the smaller  $E$ , the larger the peak shift. Fig. 2.3(b) illustrates the variation in size and position of a second-order peak as function of  $E$ , in Fig.2.3(c) as function of  $s/N$ , and in Fig.2.3 (d) as function of the heating rate. The area under the curve is, as in the case of first-order kinetics, proportional to the initial concentration  $n_0$  but the peak height is no longer directly proportional to the peak area, although the deviation is small.

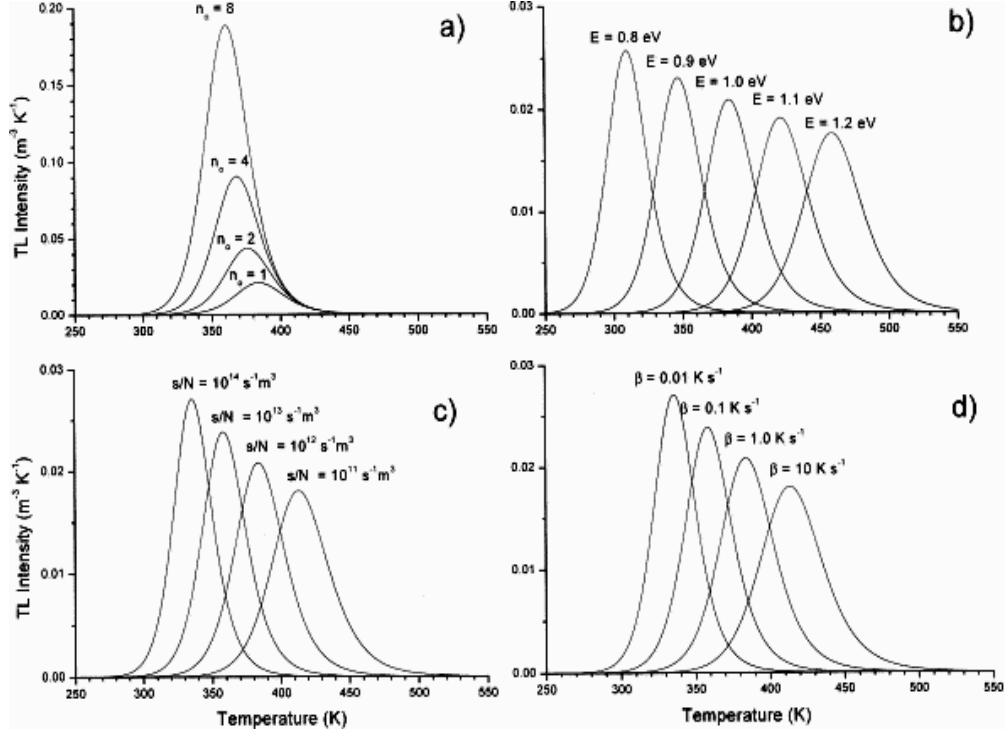


Figure 2.3 Properties of the Garlick–Gibson second-order TL equation, showing: (a) variation with  $n_0$ , the concentration of trapped charge carriers after irradiation; (b) the variation with  $E$ , the activation energy; (c) the variation with  $s/N$ ; (d) the variation with  $\beta$ , the heating rate. Parameter values:  $n_0=1$  m<sup>-3</sup>;  $E=1$  eV;  $s/N=1 \times 10^{12}$  s<sup>-1</sup> m<sup>3</sup>,  $\beta=1$  K/s of which one parameter is varied while the others are kept constant. [5]

Note that, similarly to the first-order case, the term dominating the temperature dependence in the initial rise is  $\exp(-E/kT)$ . So the 'initial rise method' for the determination of the trap depth can be applied here as well.

Inserting the integral approximation given by Eqn.(2.14) in Eqn.(2.18), one gets

$$I(T) = sn_0 \exp\left\{-\frac{E}{kT}\right\} \left[ \frac{skT^2}{\beta E} (1 - \Delta) \exp\left(-\frac{E}{kT}\right) + 1 \right]^{-2} \quad (2.23)$$

from which the condition at the maximum is given by

$$s = \frac{\beta E}{kT_m^2} \frac{1}{1 + \Delta_m} \exp\left(\frac{E}{kT_m}\right) \quad (2.24)$$

or in another form

$$s \exp\left(-\frac{E}{kT_m}\right) = \frac{\beta E}{kT_m^2} \frac{1}{1 + \Delta_m} \quad (2.25)$$

Furthermore, Eqn.(2.23) can be rewritten for the peak at the maximum:

$$I_m = sn_0 \exp\left\{-\frac{E}{kT}\right\} \left[ \frac{skT_m^2}{\beta E} (1 - \Delta_m) \exp\left(-\frac{E}{kT}\right) + 1 \right]^{-2} \quad (2.26)$$

The insertion of Eqn.(2.24) into Eqn.(2.23) gives the following expression for  $I(T)$

$$I(T) = \frac{n_0 \beta E}{kT_m^2} \frac{1}{1 + \Delta_m} \exp\left[\frac{E}{kT} \left(\frac{T - T_m}{T_m}\right)\right] \times \left( \frac{T^2}{T_m^2} \frac{1 - \Delta}{1 + \Delta_m} \exp\left[\frac{E}{kT} \left(\frac{T - T_m}{T_m}\right)\right] + 1 \right)^{-2} \quad (2.27)$$

Inserting Eqn.(2.25) into Eqn.(2.26) we get a more simplified expression for  $I_m$ :

$$I_m = \frac{n_0 \beta E}{kT_m^2} \frac{1}{1 + \Delta_m} \left(\frac{2}{1 + \Delta_m}\right)^2 \quad (2.28)$$

which can be rewritten as

$$\frac{n_0 \beta E}{kT_m^2} \frac{1}{1 + \Delta_m} = I_m \left(\frac{2}{1 + \Delta_m}\right)^2 \quad (2.29)$$

Eqn.(2.28) is now inserted into Eqn.(2.27) for getting the final expression for the TL intensity:

$$I(T) = 4I_m \exp\left(\frac{E}{kT} \frac{T - T_m}{T_m}\right) \times \left[ \frac{T^2}{T_m^2} (1 - \Delta) \exp\left\{\frac{E}{kT} \frac{T - T_m}{T_m}\right\} + 1 + \Delta_m \right]^{-2} \quad (2.30)$$

with  $\Delta$  and  $\Delta_m$  the same meaning as in Eqn.(2.19).

### 2.1.3 May – Partridge model (General Order Kinetics)

When the conditions of first or second order kinetics are not satisfied, one obtains the so called general order kinetics which deals with intermediate cases. May and Partridge (1964) [15] wrote an empirical expression for taking into account experimental situations which indicated intermediate kinetic process. They started with the assumption that the energy level of traps is single, as already assumed for the first and second orders.

For general – order kinetics

$$I(t) = -\frac{dn}{dt} = n^b s' \exp\left\{-\frac{E}{kT}\right\} \quad (2.31)$$

where  $s'$  has the dimension of  $m^{3(b-1)} s^{-1}$  and  $b$  is defined as the general-order parameter and is not necessarily 1 or 2. Integration of Eqn.(2.31) for  $b \neq 1$  yields

$$I(T) = sn_0 \exp\left\{-\frac{E}{kT}\right\} \left[1 + \frac{s(b-1)}{\beta} \int_{T_0}^T \exp\left\{-\frac{E}{kT'}\right\} dT'\right]^{\frac{b}{b-1}} \quad (2.32)$$

where now  $s'' = s'n_0^{b-1}$  with unit  $s^{-1}$ . Eqn.(2.32) includes the second-order case ( $b=2$ ) and reduces to Eqn.(2.11) when  $b \rightarrow 1$ . It should be noted that according to Eqn. (2.31) the dimension of  $s'$  should be  $m^{3(b-1)} s^{-1}$  that means that the dimension changes with the order  $b$  which makes it difficult to interpret physically.

It transforms in the following equation using the approximation in Eqn.(2.14):

$$I(T) = sn_0 \exp\left\{-\frac{E}{kT}\right\} \left[\frac{(b-1)skT^2}{\beta E} (1 - \Delta) \exp\left(-\frac{E}{kT}\right) + 1\right]^{b/(b-1)} \quad (2.33)$$

The intensity at the peak maximum is then given by

$$I_m = sn_0 \exp\left\{-\frac{E}{kT_m}\right\} \left[\frac{(b-1)skT_m^2}{\beta E} (1 - \Delta_m) \exp\left(-\frac{E}{kT_m}\right) + 1\right]^{b/(b-1)} \quad (2.34)$$

The maximum condition, obtained from Eqn.(2.33), is

$$\frac{\beta E}{kT_m^2} = Z_m s \exp\left(-\frac{E}{kT_m}\right) \quad (2.35)$$

with

$$Z_m = 1 + (b-1)\Delta_m \quad (2.36)$$

Eqn.(2.35) can be rewritten in two different ways:

$$s = \frac{\beta E}{kT_m^2} \frac{1}{Z_m} \exp\left(-\frac{E}{kT_m}\right) \quad (2.37)$$

or

$$s \exp\left(-\frac{E}{kT_m}\right) = \frac{\beta E}{kT_m^2 Z_m} \quad (2.38)$$

Inserting Eqn.(2.37) into Eqn.(2.33) we obtain the following expression for the intensity:

$$I(T) = \frac{n_0 \beta E}{kT_m^2 Z_m} \exp\left\{-\frac{E}{kT} \frac{T-T_m}{T_m}\right\} x \left[ \frac{(b-1) T^2}{Z_m T_m^2} (1-\Delta_m) \exp\left(-\frac{E}{kT} \frac{T-T_m}{T_m}\right) + 1 \right]^{b/(b-1)} \quad (2.39)$$

Inserting Eqn.(2.39) into Eqn.(2.33) we get, after arrangement, the expression for the intensity at the maximum:

$$I_m = \frac{n_0 \beta E}{kT_m^2 Z_m} \left(\frac{b}{Z_m}\right)^{\frac{b}{b-1}} \quad (2.40)$$

from which

$$\frac{n_0 \beta E}{kT_m^2 Z_m} = I_m \left(\frac{b}{Z_m}\right)^{-\frac{b}{b-1}} \quad (2.41)$$

Insertion of Eqn.(2.41) into Eqn.(2.39) gives the final equation for the TL intensity:

$$I(T) = I_m (b)^{\frac{b}{b-1}} \exp\left\{\frac{E}{kT} - \frac{T-T_m}{T_m}\right\} \times \left[ (b-1)(1-\Delta) \frac{T^2}{T_m^2} \exp\left(\frac{E}{kT} - \frac{T-T_m}{T_m}\right) + Z_m \right]^{\frac{b}{b-1}} \quad (2.42)$$

Still, the general-order case is useful since intermediate cases can be dealt with and it smoothly goes to first- and second-orders when  $b \rightarrow 1$  and  $b \rightarrow 2$ , respectively (see Fig.2.5).

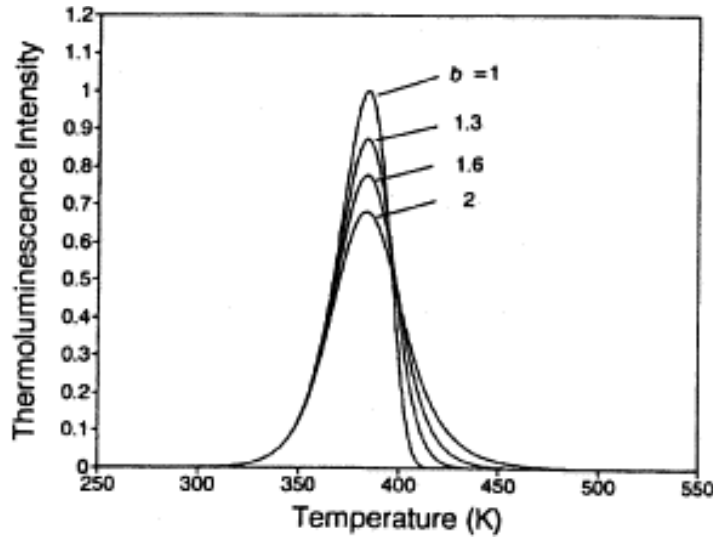


Figure 2.4 Comparison of first-order ( $b=1$ ), second-order ( $b=2$ ) and intermediate-order ( $b=1.3$  and  $1.6$ ) TL peaks, with  $E=1$  eV,  $s=1 \times 10^{12} \text{ s}^{-1}$ ,  $n_0=N=1 \text{ m}^{-3}$  and  $\beta=1 \text{ K/s}$ . [11]

#### 2.1.4 Advanced models

The one trap–one centre model shows all the characteristics of the phenomenon TL and explains the behaviour of the glow peak shape under variation of the dose and heating rate. However, there is no existing TL material known that accurately is described by the simple model. This does not mean that the simple model has no meaning. On the contrary, it can help us in the interpretation of many

features which can be considered as variations of the one trap–one centre model. There is no room to discuss all the advanced (more realistic) models in detail. The reader is referred to the text book of Chen and McKeever [5] for a deeper and quantitative treatment. Here, only some models are very briefly mentioned in order to get some idea about the complexity of the phenomenon in a real TL material.

In general, a real TL material will show more than one single electron trap. Not all the traps will be active in the temperature range in which the specimen is heated. A thermally disconnected trap is one which can be filled with electrons during irradiation but which has a trap depth which is much greater than the active trap such that when the specimen is heated only electrons trapped in the active trap (AT) and the shallow trap (ST) (see Fig.2.5(a)) are freed. Electrons trapped in the deeper levels are unaffected and thus this deep electron trap (indicted in Fig.2.5 (a) with DET) is said to be thermally disconnected. But its existence has a bearing on the trapping filling and eventually on the shape of the glow peak [16].

In Section 2.1.1 it was assumed that the trapped electrons are released during heating while the trapped holes are stable in the recombination centre. A description in which the holes are released and recombine at a centre where the electrons are stable during heating is mathematically identical. However, the situation will change if both electrons and holes are released from their traps at the same time at the same temperature interval and the holes are being thermally released from the same centres as are acting as recombination sites for the thermally released electrons and vice versa (see Fig.2.5 (b)). In this case Eqn. (2.2) is no longer valid. New differential equations should be drafted. Analysis of this complicated kinetic model reveals a TL glow curve which retains the simple Randall–Wilkins (Eqn.(2.11)) or Garlick–Gibson (Eqn.(2.16)) shape, depending upon the chosen values of the parameters. However, the  $E$  and  $s$  values used in Eqn.(2.11) and Eqn.(2.16) in order to obtain a fit on this complicated kinetic model need further interpretation.

Another process which might happen is a recombination without a transition of the electron into the conduction band (Fig.2.6(c)) Here the electron is thermally stimulated into an excited state from which a transition into the recombination centre is allowed. This means that the trap has to be in the proximity of a centre.



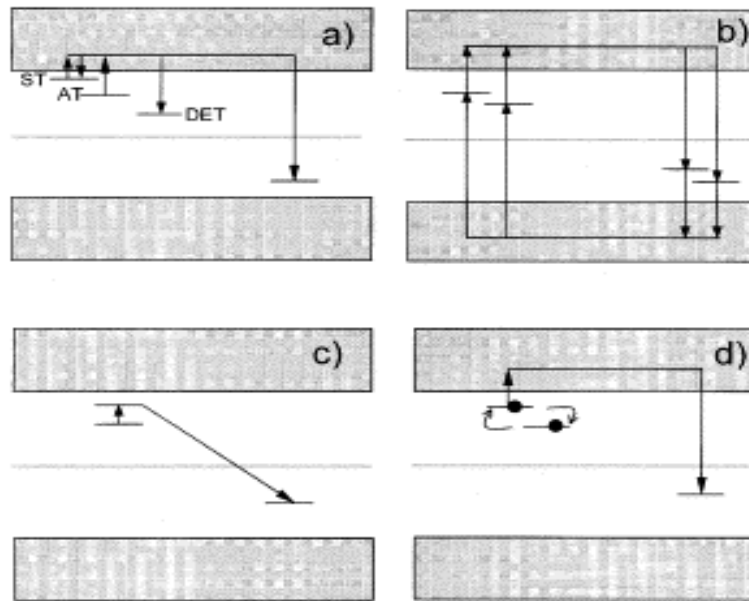


Figure 2.5 Advanced models describing the thermally stimulated release of trapped charged carriers including: (a) a shallow trap (ST), a deep electron trap (DET), and a active trap (AT); (b) two active traps and two recombination centres; (c) localised transitions; (d) defect interaction (trapping centre interacts with another defect). [11]

The transition probability may strongly depend on the distance between the two centres. Under certain assumptions an expression for the TL intensity can be derived [16] which has the same form as Eqn. (2.11) but with  $s$  replaced by a quantity related to the probability for recombination. This means that these localised transitions are governed by first-order kinetics.

Finally, we will mention the possibility that the defect which has trapped the electron is not stable but is involved in a reaction with another defect (Fig.2.6(d)). The result may be that at low temperature the trap depth is changing while the trapped electron concentration is stable. At higher temperatures electrons are involved in two processes: the escape to the conduction band and the defect reaction. Piters and Bos [17] have defect reactions incorporated into the rate equations and glow curves simulated. It appears that the simulated glow curves can be very well fitted by Eqn. (2.11). It is clear that (again) the fitting parameters do not have the simple meaning of trap depth and escape frequency.

## 2.2 Thermoluminescence Analysis

One of the prime objectives of a thermoluminescence experiment is to extract data from an experimental glow-curve, or a series of glow-curves, and to use these data to calculate values for the various parameters associated with the charge transfer process in the material under study. These parameters include the trap depth ( $E$ ), the frequency factor ( $s$ ), the capture cross-sections and the densities of the various traps and recombination centres taking part in the thermoluminescence emission. Of course, arriving at values for these parameters does not necessarily mean that we fully understand them, or that we are knowledgeable about the defect model with which they are associated.

The most popular procedure begins by selecting the rate equations appropriate to a particular model and continues by introducing simplifying assumptions into these equations in order to arrive at an analytical expression which describes the variation in thermoluminescence intensity with temperature, in terms of the desired parameters. From these equations even simpler expressions are produced which relate the parameters directly to the data.

However, this procedure firstly requires an assumption as to which model is used to describe the thermoluminescence production; and secondly, by introducing further assumptions into play which inevitably limit the generality, and possibly the validity, of the results obtained. Invariably, the model which is most often chosen for analysis is the simple two-level model, sometimes with addition of a third level (i.e., thermally disconnected traps). However, more often than not, no tests are carried out (a) check the validity of the simple model, and (b) confirm that the approximations place severe restrictions on the kinetics of the thermoluminescence emission. Fortunately, this is becoming recognized as an important factor in thermoluminescence analysis and many experiments are making great efforts to try to be certain about the order of kinetics approximations (such as the constancy of the electron distribution in the conduction band) remain unverified, and the chosen energy level model stays unconfirmed. The reason for this lack of verification is quite straightforward - it is experimentally very difficult to do [18].

## 2.3 Methods of Analysis

Since the pionerring work of Randall & Wilkins and Garlick & Gibson there has been a plethora of published papers dealing with methods by which the trapping parameters (mainly  $E$  and  $s$ ) can be obtained from a glow-curve. Some utilize simple formulae; others consist of elaborate curve- fitting procedures. The determination of trapping parameters from thermoluminescence glow curves has been a subject of interest for half a century. There are various methods for evaluating the trapping parameters from the glow curves [9-10, 16, 19-20]. When one glow peak is highly isolated from the others, the experimental methods such as initial rise, variable heating rates, isothermally decay, and peak shape methods are suitable methods to determine these parameters.

### 2.3.1 Initial Rise Method

This method stems from the recognition by Garlick&Gibson (1948) that the initial rise part of a thermoluminescence curve is exponentially dependent on temperature according to

$$I(T) = C \exp(-E / kT) \quad (2.43)$$

where the constant  $C$  includes all the dependencies on the other parameters and occupancies,  $E$  is the activation energy (eV),  $k$  is the Boltzmann`s constant (eV/K<sup>-1</sup>) and  $T$  is the temperature (K).

This expression can be understood by examination of any equations (2.8), (2.20) or (2.31) or in which it can be seen that if the temperature to which the specimen is heated is low enough for  $n$  to be approximately constant (i.e., for very little detrapping to have taken place) then equation 2.43 naturally emerges, independent of kinetics. Clearly then, if a plot  $\ln(I)$  versus  $1/T$  is made over this initial region, then a straight line of slope  $-E/k$  is obtained, from which the activation energy  $E$  is easily found. This procedure is commonly termed the initial rise method [18]. Hence it is possible to evaluate  $E$  without any knowledge of the frequency factor  $s$  by means of equation

$$E = -kd(\ln(I))/d(1/T) \quad (2.44)$$

The important requirement in this analysis is that  $n$  remains approximately constant. Only upon an increase in temperature beyond a critical value,  $T_c$ , does this assumption become invalid. The initial rise technique can only be used when the glow peak is well defined and clearly separated from the other peaks. To overcome this problem in a glow curve, several methods of peak separation have been devised. Possibly the most popular of these separation procedures is the so-called “thermal cleaning” technique. In this method the specimen is heated to a temperature just beyond the maximum of the first peak in the glow curve, thereby substantially emptying the traps responsible for this peak. The sample is then rapidly cooled and reheated to a temperature just beyond the maximum of the next peak, and so on throughout the whole glow curve. Thus, by removing in stages the lower temperature peaks, an essentially clean initial part of the next peak in the series is obtained. With closely overlapping peaks, however, there is always the danger that the preceding peak will not have been completely removed [18]. In this case, cleaning cycles to produce a method of analysis which enables the trap energy distribution to be determined and, at the same time, checks that the important ingredient of the initial rise analysis (namely, that  $n$  is approximately constant) is satisfied. If the temperature is raised by only a few degrees there will be very little change in  $n$  during the cooling as well, then there will be little difference in intensity between the heating and cooling cycles. The whole thermoluminescent may be excited by repeatedly heating and cooling the sample in small cycles, but many times, and, from the slope of the heating and cooling curves, the average depth of the traps being emptied during each temperature cycle may be determined. Obviously, the smaller the temperature rise on each heating, the closer the two slopes will be and so more precise will be the calculated value of  $E$ .

Once the value of  $E$  was determined, the frequency factor ( $s$ ) was obtained from the equation

$$\frac{\beta E}{kT_m} = s \exp\left(-\frac{E}{kT}\right) \quad (2.45)$$

where  $T_m$  is the temperature at the maximum intensity.

### 2.3.2 Heating Rate Method

Another important method is various heating rates for the determination of activation energies. Changing the heating function or even changing the heating rate while keeping the heating function linear, alters the shape of the TL peak and, in particular, the maximum temperature  $T_m$ . If a sample is heated at two different linear heating rates  $\beta_1$  and  $\beta_2$  the peak temperatures will be different. Equation (2.45) can therefore, be written for each heating rate and dividing the equation for  $\beta_1$  (and  $T_{m1}$ ) by the equation for  $\beta_2$  (and  $T_{m2}$ ) and rearranging, one gets an explicit equation for the calculation of  $E$

$$E = k \frac{T_{m1} T_{m2}}{T_{m1} - T_{m2}} \ln \left[ \left( \frac{\beta_1}{\beta_2} \right) \left( \frac{T_{m2}}{T_{m1}} \right)^2 \right] \quad (2.46)$$

The major advantage of the heating rate method is that it only requires data to be taken at a peak maximum ( $T_m, I_m$ ) which, in case of a large peak surrounded by smaller satellites, can be reasonably accurately determined from the glow curve. Furthermore the calculation of  $E$  is not affected by problems due to thermal quenching, as with the initial rise method. However, when it is the activation energies of the smaller peaks that need to be determined, it becomes a difficult technique to use. For first-order curves, thermal cleaning might separate the peaks enough to determine  $T_m$  (but not  $I_m$  which has been affected by the cleaning process). With second-order kinetics even  $T_m$  is unreliable because the peaks will move due to the reduction in trapped charge during cleaning. Similar arguments apply when two (or more) peaks so closely overlapping that they appear as one composite peak [18].

Another important point that has to be taken into consideration to avoid large errors in the kinetic parameters determined by variable heating rate method is the temperature lag (TLA) between the heating element and the thermoluminescent sample during the TL readout in readers using contact heating. To avoid this problem, a simple method has been recently proposed by Kitis and Tuyn [21] to correct the TLA and to determine the exact peak temperatures after different heating rates by using the following equation:

$$T_m^j = T_m^i - C \ln \left( \frac{\beta_i}{\beta_j} \right) \quad (2.47)$$

where  $T_m^j$  and  $T_m^i$  are the maximum temperatures of a glow peak with heating rates  $\beta_j$  and  $\beta_i$ , respectively, and  $C$  is a constant, which is initially evaluated by using two very low heating rates where TLA can be considered as negligible. In preference, the low heating rates should be chosen below  $1 \text{ }^\circ\text{C s}^{-1}$  to calculate the constant  $C$ .

When various heating rates for the first-order kinetics are used, the following expression is obtained:

$$\ln \left( \frac{T_m^2}{\beta} \right) = \left( \frac{E}{k} \right) \left( \frac{1}{T_m} \right) + \text{constant} \quad (2.48)$$

A plot of  $\ln (T_m^2/\beta)$  versus  $(1/T_m)$  should yield a straight line with a slope  $E/k$ , then  $E$  is found. Additionally, extrapolating to  $1/T_m = 0$ , a value for  $\ln(sk/E)$  is obtained from which  $s$  can be calculated by inserting the value of  $E/k$  found from the slope.

This method of various heating rates is applicable for general-order kinetics which includes the second-order case. For the general order case, one can plot  $\ln \left[ I_m^{b-1} (T_m^2 / \beta)^b \right]$  versus  $1/T_m$ , whose slope is equal to  $E/k$

### 2.3.3 Peak Shape Methods

In contrast to partial or whole peak analyses, methods based on the shape of the peak utilize just two or three points from the glow-curve. Usually, these are the maximum of the peak  $T_m$  and either, or both, the low-and high-temperature half height at  $T_1$  and  $T_2$ . Evaluation of  $E$  from the shape of the peak utilising parameters such as  $T_m$ , full width at half-maximum  $\omega = T_2 - T_1$ , half width on the high temperature side of the maximum  $\delta = T_2 - T_m$ , half width on the low-temperature side of the maximum  $\tau = T_m - T_1$ , and  $\mu_g = \delta/\omega$  called the shape parameter. Figure 2.6 shows characteristics of a single glow-peak, in which the peak shape method is based.

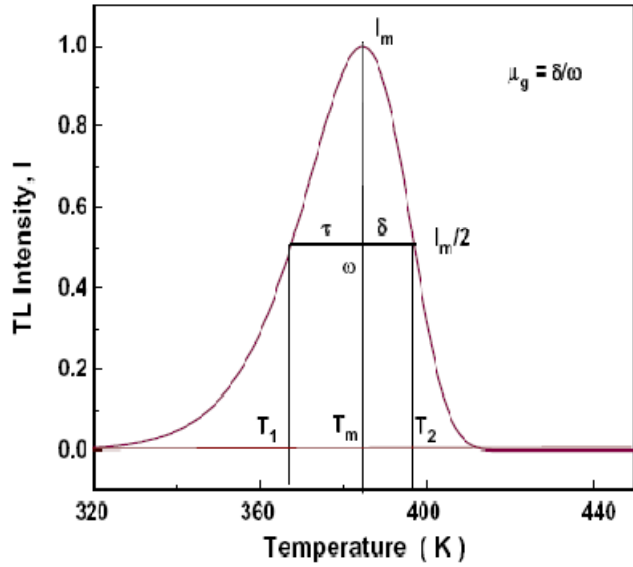


Figure 2.6 The characteristics points on a TL glow-peak, which define the peak-shape parameters. [22]

The order of kinetics  $b$  can be estimated by means of shape parameters. Chen [19] found that  $\mu_g$  is not sensitive to changes in  $E$  and  $s$ , but it changes with the order of kinetics  $b$ . It has been shown that the ranges of  $\mu_g$  varies from 0.42 for  $b=1$  to 0.52 for  $b=2$  in case of linear heating (Figure 2.7).

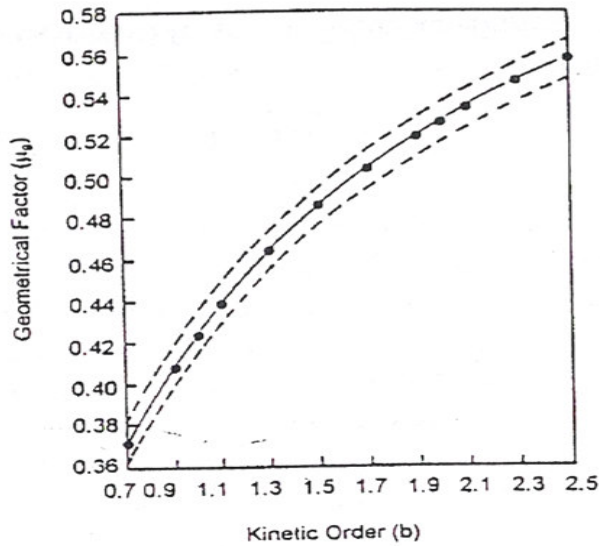


Figure 2.7 Geometrical factor,  $\mu_g$ , (shape parameter) as a function of the given order. [7]

The first peak shape method was developed by Grossweiner [23]; later Chen [19] modified Halperin and Braner's equations [24] for calculating  $E$  values;

$$\begin{aligned}
 E_{\tau} &= [1.51 + 3(\mu_g - 0.42)] \frac{kT_m^2}{\tau} - [1.58 + 4.2(\mu_g - 0.42)] 2kT_m \\
 E_{\delta} &= [0.976 + 7.3(\mu_g - 0.42)] \frac{kT_m^2}{\delta} \\
 E_{\omega} &= [2.52 + 10.2(\mu_g - 0.42)] \frac{kT_m^2}{\omega} - 2kT_m
 \end{aligned} \tag{2.49}$$

After determination of the activation energy and the order of kinetics, using the following expressions the frequency factor  $s$ , it must be noted that this parameter called as pre-exponential factor in the general order kinetic, can be estimated for first and general order kinetics respectively.

$$\begin{aligned}
 s &= \frac{\beta E}{kT_m^2} \exp\left[\frac{E}{kT_m}\right] \\
 s &= \frac{\beta E}{kT_m^2} \left[ \exp\left(-\frac{E}{kT_m}\right) \left(1 + (b-1) \frac{2kT_m}{E}\right) \right]^{\frac{b}{b-1}}
 \end{aligned} \tag{2.50}$$

In addition to Chen peak shape method the kinetic parameters have also determined by using Gartia, Singh & Mazumdar [25] peak shape method which requires the prior knowledge of the kinetics order. The method uses any three points of a peak. According to this method, it is possible to calculate the activation energy as follows

$$E_a = \frac{CkT_m^2}{|T_x - T_y|} + DkT_m \tag{2.51}$$

where  $|T_x - T_y| = \tau, \delta, \omega$ . The coefficients  $C$  and  $D$  are found using the method of least squares for different order of kinetics  $b$  in the range from 0.7 to 2.5 and for  $x = 1/2, 2/3, 4/5$ . For a particular value of  $x$  the coefficients results to be dependent on  $b$  and then can be expressed as a quadratic function of  $b$  itself. So that, the previous equation can be rewritten as

$$E_a = \frac{(C_0 + C_1 + C_2 b^2) kT_m^2}{|T_x - T_y|} + (D_0 + D_1 b + D_2 b^2) kT_m \tag{2.52}$$



Table 2.1 gives the coefficients for different values of  $x$ . The results obtained by using expression for  $x=1/2$  are more accurate than those of Chen. Furthermore, it is pointed out that  $E_\tau, E_\delta$  and  $E_\omega$  are in excellent agreement among themselves, whereas the Chen's values for  $E_\delta$  and  $E_\omega$  yield poor results [25].

Table 2.1 Numerical values of the coefficients comparing in Eq. (2.52)

Ratio	Parameter	$C_0$	$C_1$	$C_2$	$D_0$	$D_1$	$D_2$
1/2	$\tau$	1.019	0.504	-0.066	-1.059	-1.217	0.109
	$\delta$	0.105	0.926	-0.048	0.154	-0.205	-0.128
	$\omega$	1.124	1.427	-0.113	-0.902	-0.346	-0.061
2/3	$\tau$	0.684	0.426	-0.055	-0.720	-1.21	0.098
	$\delta$	0.146	0.683	-0.048	0.184	-0.432	-0.094
	$\omega$	0.830	1.108	-0.103	-0.529	-0.607	-0.029
4/5	$\tau$	0.449	0.342	-0.043	-0.0480	-1.184	0.085
	$\delta$	0.153	0.487	-0.041	0.180	-0.606	-0.062
	$\omega$	0.602	0.829	-0.084	-0.293	-0.777	-0.006

### 2.3.4 CGCD Method

Instead of employing simple formulae to derive values for the parameters  $E$ ,  $s$  and  $b$ , methods of computerized curve fitting have been used on several occasions with apparent success. The procedure is to establish the approximate positions of the most prominent peaks in the glow-curve and to estimate initial values of  $E$ ,  $s$ , and  $b$  by using one of the analytical methods discussed so far. A theoretical curve is then computed using the general-order equation for  $b \neq 1$ , or the first-order equation for  $b=1$ . The computed curve is then compared with the actual experimental curve and a root mean square (RMS) deviation between the two is calculated. The procedure continues by sequentially changing the  $E$ ,  $s$ , and  $b$  values until a minimum value of

the RMS deviation is obtained. This method has the advantage over experimental methods in that they can be used in largely overlapping-peak glow curves without resorting to heat treatment [18]. The program was developed at the Reactor Institute at Delft, The Netherlands [26]. This program is capable of simultaneously deconvoluting as many as nine glow peaks from glow curve. Two different models were used in the computer program. In the first model, the glow curve is approximated from first order TL kinetic by the expression,

$$I(T) = n_0 s \exp\left(-\frac{E}{kT}\right) \exp\left[\left(-\frac{s kT^2}{\beta E} \exp\left(-\frac{E}{kT}\right) * (0.9920 - 1.620 \frac{kT}{E_a})\right)\right] \quad (2.53)$$

In the second model the glow curve is approximated with general order TL kinetics by using the expression,

$$I(T) = n_0 s \exp\left(-\frac{E}{kT}\right) \left[1 + \left(-\frac{(b-1)s kT^2}{\beta E} \exp\left(-\frac{E}{kT}\right) * (0.9920 - 1.620 \frac{kT}{E_a})\right)\right]^{\frac{b}{b-1}} \quad (2.54)$$

where  $n_0$  ( $\text{m}^{-3}$ ) is the concentration of trapped electrons at  $t=0$ ,  $s$  ( $\text{s}^{-1}$ ) is the frequency factor for first-order and the pre-exponential factor for the general-order,  $E$  (eV) the activation energy,  $T$  (K) the absolute temperature,  $k$  ( $\text{eVK}^{-1}$ ) Boltzmann's constant,  $\beta$  ( $^{\circ}\text{Cs}^{-1}$ ) heating rate and  $b$  the kinetic order.

The summation of overall peaks and background contribution can lead to composite glow curve formula as shown below

$$I(T) = \sum_{i=1}^n I_i(T) + a + b \exp(T) \quad (2.55)$$

where  $I(T)$  is the fitted total glow curve,  $a$  allows for the electronic noise contribution to the planchet and dosimeters infrared contribution to the background.

Starting from the above equation (2.55), the least square minimisation procedure and also FOM (Figure of Merit) was used to judge the fitting results as to whether they are good or not. i.e.

$$FOM = \sum_{i=1}^n \frac{|N_i(T) - I(T)|}{A} = \sum_{i=1}^n \frac{|\Delta N_i|}{A} \quad (2.56)$$

where  $N_i(T)$  is the  $i$ -th experimental points (total  $n=200$  data points),  $I(T)$  is the  $i$ -th fitted points, and  $A$  is the integrated area of the fitted glow curve.

From many experiences [27-28], it can be said that if the values of the FOM are between 0.0% and 2.5% the fit is good, 2.5 % and 3.5% the fit is fair, and  $> 3.5\%$  it is bad fit. To have a graphic representation of the agreement between the experimental and fitted glow curves, the computer program also plots the function,

$$X(T) = \frac{N_i(T) - I_i(T)}{\sqrt{I_i(T)}} \quad (2.57)$$

which is a normal variable with an expected value 0 and  $\sigma=1$  where  $\sigma^2(T)=I_i(T)$ .

### 2.3.5 Isothermal Decay Method

In the methods of analysis discussed so far  $E$  is calculated from the form or shape, or position of the glow peak which itself is produced during a non-isothermal rise in sample temperature. Quite a different method of analysis has been devised in which the sample temperature is kept constant and the luminescence intensity is followed as a function of time. This method of analysis, therefore, deals with phosphorescence rather than thermoluminescence, but raising the temperature at which the phosphorescence decay is being monitored, the deep traps which take part in thermoluminescence can be sampled and their trap depths determined [18].

Generally, in the isothermal decay method, the following equation is solved for constant  $T$  for the first order kinetics

$$I(T) = -c \frac{dn}{dt} = c \frac{n_0}{\tau} \exp\left(-\frac{t}{\tau}\right) \quad (2.58)$$

where  $n_0$  is the initial value of  $n$  and  $\tau = s^{-1} \exp\left(\frac{E}{kT}\right)$ .

The above equation shows that at a constant temperature  $T$ , the light emission will decay exponentially with time  $t$  and a plot of  $\ln(I)$  against  $t$  will give a straight line with a slope  $m = s \exp\left(-\frac{E}{kT}\right)$ . In order to find  $E$  and  $s$ , the experiments are carried out at two different constant temperatures  $T_1$  and  $T_2$ , resulting in two different

slopes  $m_1$  and  $m_2$ . Thus the activation energy can be determined by using the following equation

$$E = \frac{k}{\left(\frac{1}{T_2} - \frac{1}{T_1}\right)} \ln\left(\frac{m_1}{m_2}\right) \quad (2.59)$$

The isothermal decay method is not applicable to higher order kinetics. In 1979; a method has been proposed by Kathuria and Sunta [29] to calculate the order of kinetics from the isothermal decay of thermoluminescence. According to this method; if the decaying intensity from the sample is held at a constant temperature, the plot of  $I^{\left(\frac{1}{b}-1\right)}$  versus  $t$  gives a straight line, when the proper value of  $b$  is chosen. Therefore, various  $b$  values are tried and the correct one is that giving a straight line.

### 2.3.6 Three Points Method (TPM)

Recently, Rasheedy [30] has improved the three points analysis method (TPM) for separating a composite TL glow curve into its individual components of glow peaks and to evaluate the trap parameters of these peaks. According to this method, the order of kinetics  $b$  is given by,

$$b = \frac{T_y[T_x - T_z] \ln(y) - T_z[T_x - T_y] \ln(z)}{T_y[T_x - T_z] \ln[A_x / A_y] - T_z[T_x - T_y] \ln[A_x / A_z]} \quad (2.60)$$

where  $A_x$ ,  $A_y$  and  $A_z$  are the areas under the glow peak from the temperatures  $T_x$  to  $T_f$ ,  $T_y$  to  $T_f$  and  $T_z$  to  $T_f$ , respectively as shown in figure 2.8. The values of  $y$  and  $z$  are given by  $y=(I_x/I_y)$  and  $z=(I_x/I_z)$ .

The characteristic point of this equation is that any set of three data points in a TL glow curve can yield the kinetics order  $b$  of the glow peak. Thereafter,  $E$  (eV), then  $s$  ( $s^{-1}$ ) and  $n_0$  ( $cm^{-3}$ ) of this peak are determined, successively.

The activation energy  $E_a$  is given either by

$$E_a = \{\ln y - b \ln[A_x / A_y]\} \left\{ \frac{kT_x T_y}{T_x - T_y} \right\} \quad (2.61)$$

or by

$$E_a = \{ \ln z - b \ln [ A_x / A_z ] \} \left\{ \frac{kT_x T_z}{T_x - T_z} \right\} \quad (2.62)$$

Also, the frequency factor  $s$  in the case of first-order is given by

$$s = (\beta E_a / kT_m^2) \exp(E_a / kT_m), \quad (2.63)$$

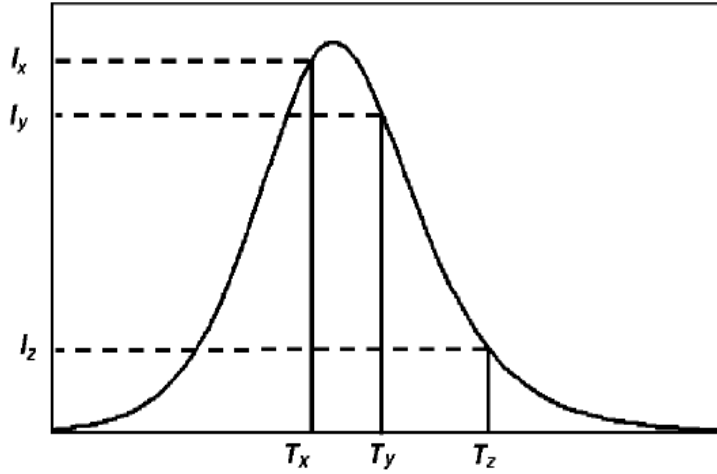


Figure 2.8 An isolated TL glow peak. The parameters  $I_x$ ,  $I_y$ ,  $I_z$ ,  $T_x$ ,  $T_y$ , and  $T_z$  are as defined in the text [30]

However, the pre-exponential factor  $s''$  in the case of general-order glow peaks is given by

$$s'' = \frac{\beta E_a \exp(E / kT_m)}{[bkT_m^2] - (b-1)E_a \Phi \exp(E_a / kT_m)}, \quad (2.64)$$

where

$$\Phi = \int_{T_o}^{T_m} \exp(-E_a / kT') dT' \quad (2.65)$$

Finally the relative value of  $n_o$  is given by

$$n_o = \frac{I_m \exp(E_a / kT_m)}{s''} \left[ \frac{bkT_m^2 s''}{\beta E_a \exp(kT_m)} \right]^{\frac{b}{b-1}} \quad (2.66)$$

## CHAPTER 3

### CHARACTERIZATION OF NONLINEARITIES IN THE DOSE DEPENDENCE OF TL

#### 3.1. General Considerations

The dose can be defined as the accumulated amount of irradiation incident on the sample during the excitation period at low temperature, or the total amount absorbed prior to the heating. In most cases, there is no direct way to relate the released TL to the amount of radiation exposure in absolute units and, therefore, a proportionality factor will always be included or implied in the considerations of response to dose. In addition, no variations in the absorption of the irradiation are usually observed during the excitation, and therefore, we can alternatively speak of incident and absorbed doses, and only another proportionality factor is to be added. As long as the applied radiation intensity (or dose rate),  $X$ , measured either in incident photons or particles per units of time and area, is kept constant, the dose is given by the product  $Xt$  where  $t$  is the time of excitation. In cases where the applied dose varies during the excitation like  $X(t)$ , the total dose is given by  $\int_0^t X(\tau).d\tau$ . In

the application of TL for the measurement of the dose of irradiation and for archaeological and geological dating, one usually hopes that, at least in certain dose ranges, the measured effect would be proportional to the applied dose. This is indeed so for certain materials and in certain dose ranges. In many other materials or dose ranges, however, different degrees of nonlinearities of different sorts are observed. These are very important to comprehend, both from the applications point of view and the theoretical aspects of understanding the process taking place in the thermoluminescent material during its excitation and heating.

Nonlinearities often occur in the dose dependence of thermoluminescence (TL). These include sublinearity, usually when there is an approach to saturation in the dose dependence, as well as supralinearity, also termed superlinearity in the literature. Different researches in the field have viewed the effect of supralinearity/superlinearity from two somewhat different points of view. One point of the view has to do with the rate of change with dose of the dose dependence function. The other approach is related more to the application of TL in dosimetry and archaeological and geological dating, and basically has to do with the correction to be made in extrapolation in cases where supra (super) linearity occurs following an initial linear dose range or prior to such a linear range. The term “supralinearity index”,  $f(D)$ , is used in cases where the feature of interest is the deviation from linearity, namely when the correction in extrapolation is the main issue. The term “superlinearity index”,  $g(D)$ , in the dose ranges where the growth is more than linear and when extrapolation is not the main issue.

A number of ways for the classification of the nonlinear dose dependence effects are to be considered. One can distinguish between *sublinear* and *superlinear* (or *supralinear*) behaviour. One can discuss the difference between various models explaining the nonlinear effects, e.g. models related to processes taking place during the excitation stage and those occurring during the heating phase [4]. Nonlinear growth of TL as a function of the absorbed dose, mainly in LiF (TLD-100), has been discussed by Cameron et al. [33]. In their study the term *supralinearity* was utilized. The characteristic behaviour, as shown in figure 3.2 is that of an initial linear dependence on the dose, followed by a more than linear range after which, an approach to saturation is observed.

### 3.1.1 Superlinearity

The term “superlinearity” is reserved to refer to the increase in the derivative of the dose dependence function (Figure 3.1). The measured TL signal by  $S(D)$ , be it either the maximum intensity or the total area under the peak, as a function of the dose  $D$ .

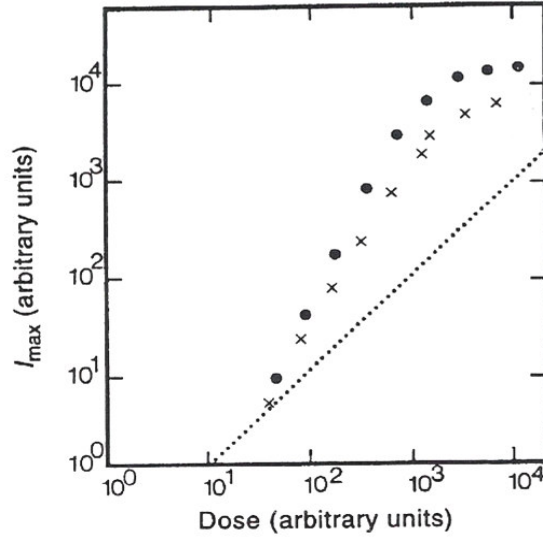


Figure 3.1 Superlinearity of the 260 K peak in two samples semiconducting diamond.  $I_{\max}$  is the height of the 260 K peak and the dotted line shows the line of linearity. [7]

The derivative of this function at any point  $D$  is  $dS/dD$  (i.e.  $S'(D)$ ), and an increase of the derivative at a certain point is expressed by stating that  $d^2S/dD^2$  (i.e.  $S''(D)$ ) is positive. Thus,  $d^2S/dD^2 > 0$  represents ranges of superlinearity;  $d^2S/dD^2 < 0$  characterizes ranges of sublinearity, and of course,  $d^2S/dD^2 = 0$  signifies a range (or point) of linearity. The difficulty with this definition is that it is merely qualitative since it has to do with the sign of the second derivative only. Moreover, one of the detecting superlinearity is by plotting the results on a log-log scale. In this presentation of function  $S \propto D^k$ , slope is  $k$  and is a direct measure of the degree of superlinearity (or sublinearity). Chen and McKeever [5], defined the *superlinearity index*,  $g(D)$ , which is a dimensionless quantity, as

$$g(D) = \left[ \frac{DS''(D)}{S'(D)} \right] + 1 \quad (3.1)$$

As long as if one dealing with a range of an increasing dose dependence ( $(D) > 0$ , which is nearly always true), it is obvious that the condition  $g(D) > 1$  indicates superlinearity since  $S''(D) > 0$ . Moreover,  $g(D) = 1$  means a range (or point) of linearity and  $g(D) < 1$  signifies sublinearity. It is readily seen that  $DS''(D)/S'(D)$  is a dimensionless number, which makes  $g(D)$  a dimensionless function, and makes legal



the addition of unity. It is quite obvious that taking  $S(D) = \alpha D^k$  results in  $g(D) = k$ , as initially requested [5].

### 3.1.2. Supralinearity

A number material has the characteristic property namely, an initial linear range which is followed by a nonlinear (i.e. superlinear) region before saturation effects set in (Figure 3.2).

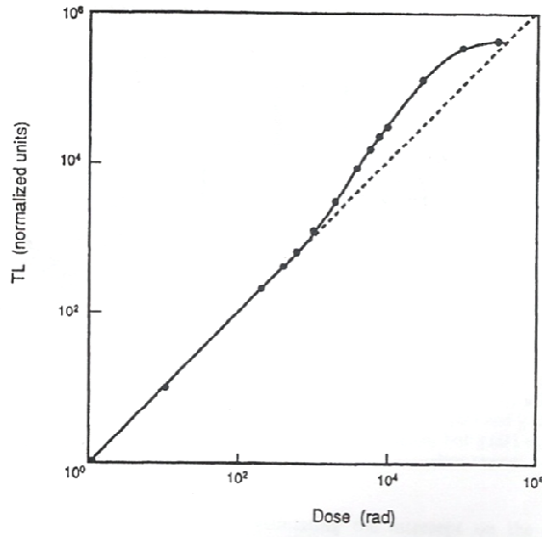


Figure 3.2 TL output vs. dose in LiF [7]

The term “supralinearity” has presented by many authors as response per unit of dose, normalized to a dose in the initial linear range. Some authors, such as Horowitz [31], and Mische and McKeever [32], quantified this property by defining the dimensionless function termed *supralinearity index* or *dose response function* as;

$$f(D) = \left[ \frac{S(D)/D}{S(D_1)/D_1} \right] \quad (3.2)$$

Here,  $D_1$  is a normalization dose in the initial linear range. But this definition is applicable only if such a linear range exists at the low dose range.

Chen and McKeever [5] modified a definition of  $f(D)$ :

$$f(D) = \left[ \frac{S(D) - S_0}{D} \right] / \left[ \frac{S(D_1) - S_0}{D_1} \right] \quad (3.3)$$

Where  $S_0$  is the intercept on the TL intensity axis of the extrapolation of the linear region. The advantage of the new definition is that it can be applied to the two cases in which a broad linear range occurs either preceded by or followed by a range of nonlinearity. Thus, in cases in which the superlinear region precedes the linear range, it is impossible to define  $f(D)$  according to equation 3.2 and equation 3.3 may be used. A negative value of  $S_0$  yields  $f(D) > 1$  in the low dose region, i.e., that part of the dose dependence in which the TL intensity is greater than that inferred from a backwards extrapolation of the linear range.

### **3.2 Further Discussions of Supralinearity**

#### **3.2.1 Trap Creation Models**

One obvious candidate for the cause of supralinear growth is that of trap creation during irradiation. This model was suggested originally by Cameron [33] and colleagues for supralinearity in LiF and in this material it requires that the freshly created traps are the same as those originally present, an unlikely event. A later suggestion was that luminescence centres are being created by the irradiation, but again this requires that the new centres are the same as the original ones because no change in the emission spectrum is noted from the phosphor [37]. However, although trap or luminescence centre creation is an unlikely explanation for the supralinear growth in LiF, it may be applicable to other materials (e.g., quartz) [38] and must be generally considered as a possible cause of supralinearity in thermoluminescence phosphors.

It is clear from the above discussions on supralinearity that this phenomenon has several plausible explanations, each of which can produce typical supralinear growth curves. Not all of them can equally predict all of the supralinear properties [36]; however, each of the mechanisms discussed have, on various occasions, been forwarded to explain supralinearity in LiF and with the present level of knowledge it is impossible to decide between them and to determine which mechanism is operative in any one sample. In fact, several mechanisms may be making a contribution to the effect – for example, in LiF competition during irradiation (and heating) could be working alongside the multi-stage reaction model involving interstitial trapping. It is probable that a definitive statement on the cause of supralinearity will never be made for any material.

### 3.2.2 Sensitization

The sensitivity of a thermoluminescence phosphor is measured by the intensity of the luminescence emission per unit of absorbed dose of radiation per unit weight. Thus, if two phosphors of equal weight are irradiated with exactly the same dose then the specimen which gives the more intense thermoluminescence emission on heating is said to be the more sensitive. An important effect which is commonly observed in many thermoluminescent materials is the increase in the sensitivity of the phosphor (more particularly, of a given thermoluminescence peak) following the absorption of radiation. This process, known as sensitization, is important in the field of radiation dosimetry using thermoluminescence where the enhancement of sensitivity is a desirable feature. The mechanism of sensitization is closely related to the phenomenon of supralinearity and often the models which have been invoked to explain certain features of the other [18].

### 3.2.3 Competing Trap Models

The competing trap model has been extensively discussed as a means of providing increased sensitivity following irradiation. An often quoted sensitization procedure for LiF is to irradiate the specimen to a dose of approximately  $10^3$  Gy and to follow this by an anneal of 300 °C for one hour [33]. This has the effect of filling the deep traps (i.e. >300 °C), most specifically peak 5. Thus, on subsequent irradiation, peak 5 can be filled without the competitive interference of the deeper traps. This procedure increases the sensitivity several fold. Peak 7 is also said to be sensitized in a similar fashion and here peak 10 is said to be related to the competing trap [34].

Clearly, if the initial radiation causes damage to the competitor, then on subsequent irradiation there will be fewer competitors available, resulting in more charge being trapped at the centre of interest, per unit dose, giving rise to an increase in sensitivity [35]. The radiation may cause a decrease in the concentration of killer centres an increase in the concentration of luminescence centres or an increase in the concentration of traps. All of these phenomena could give rise to increased sensitivity and all have been proposed, in one form or another, by different research groups to explain sensitization in a variety of materials. Figures 3.3 and 3.4 show competition mechanisms during excitation and during heating process.

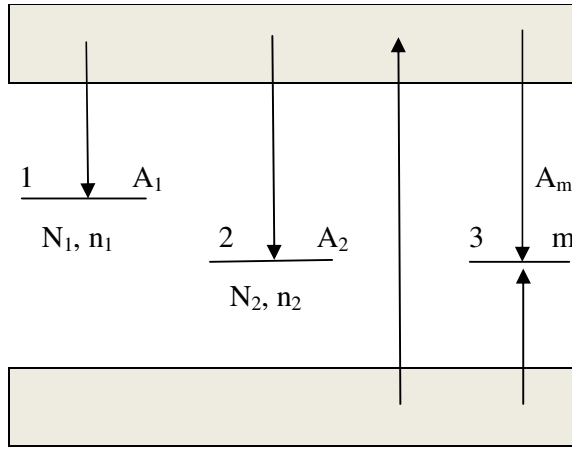


Figure 3.3 Energy levels involved in the competition during excitation.  $m$  is concentration of recombination centers,  $N_1$  and  $N_2$  are concentrations of active and competing traps, of which  $n_1$  and  $n_2$ , respectively, are occupied.  $n_c$  is instantaneous concentration of electrons in the conduction band,  $A_1$ ,  $A_2$  and  $A_m$  are the retrapping, competing trapping and recombination probabilities, respectively. [7]

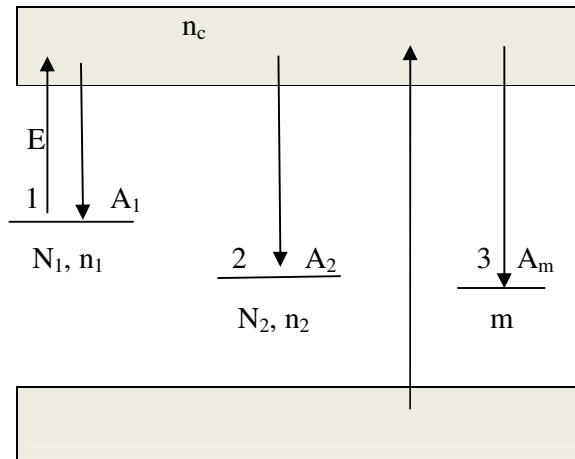


Figure 3.4 Energy levels involved in the competition during heating (read-out).  $m$  is concentration of holes in centers,  $N_1$  and  $N_2$  are concentrations of active TL traps and competing traps, respectively (levels 1 and 2);  $n_1$  and  $n_2$  are concentration of electrons in these traps, respectively.  $A_1$ ,  $A_2$  are trapping probabilities into 1 and 2 respectively;  $A_m$  is the recombination probability; and  $n_c$  is concentration of free electrons in the conduction band. [7]

### 3.2.4 Centre Conversion Models

Many different kinds of radiation-induced defect centre conversion mechanism have been proposed to explain sensitization effects. It is fair to say that all of these mechanisms have been developed with a view to describing the sensitization observed in LiF and, therefore, are rather specialized. It is also fair to

say that each relies heavily on the model for thermoluminescence in this material which has been the source of an enormous literature over the years. For example, Nink&Kos [39] use the two-step Z-centre conversion model to explain the sensitization of peak 5 in LiF. Here  $Z_3$  – centres are converted to  $Z_2$  – centres by the trapping of electrons thus leading to a higher concentration of  $Z_2$  – centres than would normally be present in the unsensitized material. Chandara et al. [37] suggest that a similar kind of trap conversion mechanism may be taking place between peak 10 and peak 7 defects, leading to the sensitization of peak 7. In a series of papers, Jain [40-41] proposed that the radiation causes the break-up of a complex centre and converts it to both trapping centres and luminescence centres. The increase of luminescence centres causes an increase in the luminescence sensitivity of all the luminescence peaks. Sagastibelza & Alveraz Rivas [42] suggest a complex trap conversion mechanism for sensitization in LiF. In their model, peak 2 defects convert to peak 5 under irradiation. Heavier irradiation results in the conversion of peak 5 defects responsible for higher temperature peaks by increased interstitial trapping. A similar interconversion relationship would also be appropriate if the peak 2 defects were impurity-vacancy pairs and if peak 5 defects were trimer clusters of these pairs. This is so because the radiation has been observed to induce clustering of pairs into trimers [43]. However, without a detailed knowledge of the defects involved in the production of thermoluminescence it is extremely difficult to decide between the various mechanisms and the occurrence of more than one mechanism cannot be dismissed.

### **3.3. Heating Rate Effect**

In the thermoluminescence (TL), the glow curve is affected by some experimental parameters. Heating rate is one of the most important experimental variables, which changes the glow curve shape [44]. In addition to the conventionally used heating rate in TL readers, very high ones had been reportedly achieved by laser heating [45]. In the TL dosimetry, the absorbed dose and TL intensity are affected by changes in heating rate [46-47]. Many investigations have been carried out by scientists in order to understand that how the TL glow curve changes under the different heating rate [47-50]. Taylor and Lilley [47] pointed out that changes in intensity, caused by the change of heating rate, may have a bearing on the determination of the trapping parameters  $E$  (trap depth) and  $s$  (frequency factor). As a result of many studies, a decrease in TL intensity was observed with increasing

heating rate [50]. This phenomenon has been explained to be due to thermal quenching, whose efficiency increases as temperature increases. Thermal quenching of the luminescence is the phenomenon in which the luminescence efficiency decreases as the temperature increases.

In order to account for thermal quenching, the luminescence efficiency expression in equation 3.4 can be used [50]

$$\eta = [1 + c \exp(-W/kT)]^{-1} \quad (3.4)$$

where  $W$  is the activation energy of luminescence efficiency due to the thermal quenching,  $k$  is the Boltzmann constant. Just like it was assumed by Spooner and Franklin [50], if it is assumed that at the temperatures at which the two peaks to be studied occur the 1 in the denominator can be neglected, and the Napierian logarithm of the integrated TL intensity can be written as

$$\text{Ln (integrated TL)} = (W/k)T_m^{-1} + F \quad (3.5)$$

The second term on the right, here by denoted by  $F$ , has been discussed by Spooner and Franklin [50] and is constant with heating rate. Hence the slope of the plot of  $\text{Ln(integrated TL)}$  against  $1/T_m$  gives  $W/k$ . Where  $T_m$  is the maximum peak temperature.

The temperature of a TL peak shifts to higher values as the heating rate increases. Thus at low heating rates the TL peak may appear in a range where thermal quenching is minimal, whereas at higher heating rates the peak temperature may be such that thermal quenching is strong [51]. Also, Berkane- Krachai et al. [52] have studied that heating rate effect on TL response and showed that the TL response decreases when heating rate increases and this reduction of TL sensitivity is well described using a Mott- Seitz theory.

During experiment, the measured temperature may be different from the sample temperature caused by a small temperature lag due to the thermal contact of the heater and the sample. Therefore, there is a linear ramp in the sample with a

temperature lag and so that the  $T_m$  read from the glow curve will be systematically lower than its actual value. Consequently, the sample thickness has an important influence on the temperature gradient and temperature lag especially at higher heating rates [53].

Because the great importance of the heating rate in any kind of thermoluminescent measurements, it is better to report here the most relevant observations on this experimental parameter. Kelly and co-workers [54] discussed about the validity of the TL kinetic theories when high heating rates are involved: they found that heating rates up to 105 °C/s do not invalidate the Shockley-Read statistics on which kinetic theories are based. Gorbics et al. [55] reported studies on thermal quenching of TL by varying the heating rate between 0.07 and about 11 °C/s. They found the following results:

- the maximum glow-peak temperature,  $T_m$ , is shifted to higher temperatures as the heating rate increases.
- the TL intensity, measured by both integrating and peak height methods, decreases as the heating rate increases.

Other papers, not specifically dedicated to the effect of heating rate on the TL intensity, report experimentally results not always in agreement among them. The heating rate effect on TL glow-peaks has been largely discussed by G.Kitis [56] who considers the heating rate as a dynamic parameter rather than a simple experimental setup variable. His study has been carried out on single, well separated glow peaks, considering the following experimental characteristics: i.e.,  $T_m$ , full width at half maximum (FWHM), peak intensity and peak integral. The first thing to be considered is a possible delay between the temperature monitored by the thermocouple, fixed on the heating planchet, and the sample. Furthermore, the possibility of temperature gradients within the measured sample must be considered too. To avoid, totally or partially, these effects, special care has to be taken: i.e. the use of powder instead of solid samples diminishes greatly the gradient effects within the sample as well as between the heating planchet and the sample. To ensure a good thermal contact between the heating strip and the powder sample, the following rules have to be taken into account:

- dimensions of powder grains in the range of 80 - 140  $\mu\text{m}$
- use no more than 4 mg in weight of powder
- fix the powder on the heating element with silicon oil. However, a certain gradient between sample and heating strip is emerging when high heating rates are used.

From figure 3.5 one can observe the behavior of the shape of the experimental glow-curves for the 110 °C glow-peak of quartz, obtained using various heating rates between 2 °C/s and 70 °C/s. As the heating rate increases, the peak height decreases and the peak temperature shifts towards high values of temperature.

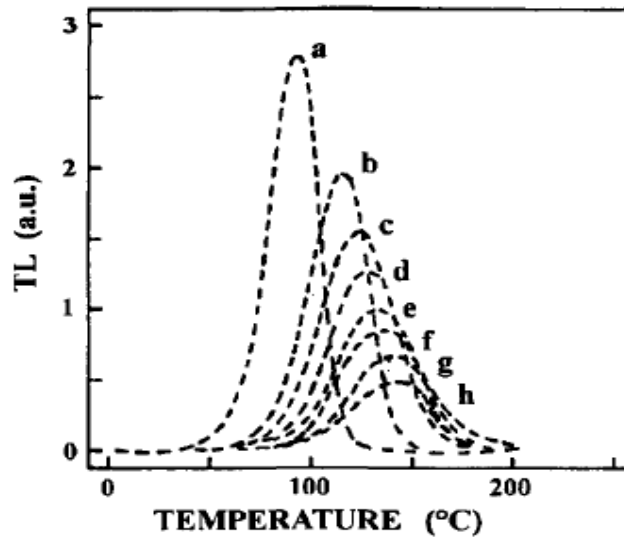


Figure 3.5 Change of the peak shape and shift in the peak position as a function of the heating rate. From (a) to (h) = 2, 8, 20, 30, 40, 50, 57, 71 °C/s [56].

More other important data are also reported in the same paper [4]. One of these is concerning the evolution of the integral and the peak height as a function of the heating rate. Figure 3.6 shows the TL response of  $\text{Al}_2\text{O}_3$  normalized to the response at the lower heating rate (0.6 °C/s) as a function of heating rate for both integral (•) and peak height (A).



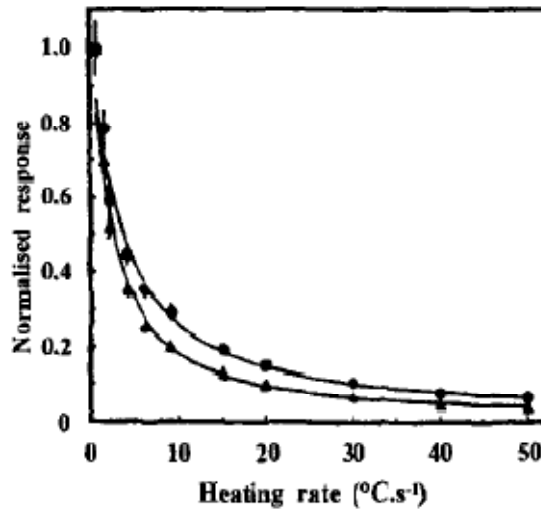


Figure 3.6 TL response of  $\text{Al}_2\text{O}_3$  as a function of heating rate. The response has been normalized to the one obtained with the lowest heating rate .[57]

### 3.4. Thermal Annealing

Annealing is the thermal treatment needs to erase any irradiation memory from the dosimetric material. Some thermoluminescent material required a complex annealing procedure.  $\text{LiF:Mg,Ti}$  is one of them. It requires a high temperature anneal, followed by a low temperature anneal. Generally speaking the high temperature anneal is required to clear the dosimetric traps of residual signal which may cause unwanted background during subsequent use of the dosimeters. The low temperature anneal is required to stabilize and aggregate low temperature traps in order to enhance the sensitivity of the main dosimetry traps and to reduce losses of radiation-induced signal due to thermal or optical fading during use. The combination of these two anneals is termed standard anneal. For lithium fluoride the standard annealing consists of a high temperature anneal at  $400^\circ\text{C}$  during 1 hour followed by a low temperature thermal treatment for 20 hours at  $80^\circ\text{C}$ . In some laboratories, annealing at  $100^\circ\text{C}$  for 2 hours has been used instead of the longer anneal at  $80^\circ\text{C}$ .

The TL properties exhibited by a phosphor strongly depend upon the kind of thermal annealing experienced by it prior to the irradiation. It is also true, in general, that more defects are produced at higher temperatures of annealing. The number of defects also depends on the cooling rate employed to cool the phosphor to the ambient temperature. Once the best annealing procedure has been determined, i.e. the

highest TL response with the lowest standard deviation, the same procedure must always be followed for reproducible results in TL applications [58,59].

Before using a thermoluminescent material for dosimetric purposes, it has to be prepared. To prepare a TL material means to erase from it all the information due to any previous irradiation, i.e., to restore in it the initial conditions of the crystal as they were before irradiation. The preparation also has the purpose of stabilizing the trap structure. In order to prepare a thermoluminescent material for use, it is needed to perform a thermal treatment, usually called annealing [58-59], carried out in oven or/and furnace, which consists of heating up the TL samples to a predetermined temperature, keeping them at that temperature for a predetermined period of time and then cooling down the samples to room temperature. It has to be stressed that the thermal history of the thermoluminescent dosimeters is crucial for the performance of any TLD system. There is a large number of thermoluminescent materials, however the annealing procedures are quite similar. Just a few materials, like LiF:Mg,Ti, need a complex annealing procedure.

The thermal treatments normally adopted for the TLDs can be divided into three classes:

- **initialisation treatment:** this treatment is used for new (fresh or virgin) TL samples or for dosimeters which have not been used for a long time. The aim of this thermal treatment is to stabilise the trap levels, so that during subsequent uses the intrinsic background and the sensitivity are both reproducible. The time and temperature of the initialisation annealing are, in general, the same as those of the standard annealing.
- **erasing treatment** or **standard annealing** (also called **pre-irradiation annealing** or **post-readout annealing**): this treatment is used to erase any previous residual irradiation effect which is supposed to remain stored in the crystal after the readout. It is carried out before using the TLDs in new measurements. The general aim of this thermal treatment is to bring back the traps - recombination centres structure to the former one obtained after the initialisation procedure. It may consist of one or two thermal treatments (in latter case, at two different temperatures).

- **post-irradiation or pre-readout annealing:** this kind of thermal treatment is used to erase the low-temperature peaks, if they are found in the glow-curve structure. Such low-temperature peaks are normally subjected to a quick thermal decay (fading) and possibly must not be included in the readout to avoid any errors in the dose determination.

In all cases, value and reproducibility of the cooling rate after the annealing are of great importance for the performance of a TLD system. In general, the TL sensitivity is increased using a rapid cool down. It seems that the sensitivity reaches the maximum value when a cooling rate of 50-100°C/s is used. To obtain this, the TLDs must be taken out of the oven after the pre-set time of annealing is over and placed directly on a cold metal block. The procedure must be reproducible and unchanged during the whole use of the dosimeters. It must be noted that the thermal procedures listed above can be carried out in the reader itself. This is important for TL elements embedded in plastic cards as the dosimeters used for large personnel dosimetry services. In fact, the plastic cards are not able to tolerate high temperatures and the in-reader annealing is shortened to a few seconds. However, its efficiency is to very low when high dose values are involved. The in-reader annealing procedure should be used only if the dose received by the dosimeter is lower than 10 to 20 mGy. Driscoll suggests in this case a further annealing in oven during 20 hours at 80°C for cards holding LiF:Mg,Ti; at this temperature the plastic holder does not suffer any deformation. Any way, excluding cards, for bare TL solid chips or TL materials in powder form, the annealing must be performed in an oven [60]

### 3.5. Thermal Fading

If the TL signal from a TLD sample is unstable with time, specifically, if it decreases with time after irradiation the signal is said to have faded. Fading can have several causes, but the most prevalent is thermal fading. Rearrangement of equation 2.1 reveals that the time constant for the thermally induced release of trapped charge from a defect is given by:

$$\tau_f = p^{-1} = s^{-1} \exp\left\{\frac{E}{kT}\right\} \quad (3.6)$$

where all the terms have been previously defined in chapter 2. Accordingly, “half life” for thermal fading may be defined as:

$$\tau_f = \ln(2)\tau_f \tag{3.7}$$

In principle, the two parameters which dictate the thermal fading rate are thus the trap depth  $E$  and frequency factor  $s$ . As a result evaluation of these for particular dosimetric peaks has been an important part of the TLD material characterisation. Nevertheless, the thermally induced loss of the TL signal with time can also be caused by process other than the simple charge release mechanisms alluded to above. The high temperature pre-irradiation annealing conditions employed with main TLD materials to ensure re-usability place the samples in thermodynamically metastable states. It is advisable, therefore, to use (i.e. to irradiate and read out) the material as soon as possible after the pre-irradiation annealing treatment.

Unwanted fading of the light of the TL signal can also occur by optical excitation of the charge from the traps. Absorption of photons of energy  $\geq$  optical trap depth will result in a release of trapped charge and a corresponding reduction in the TL signal. Other mechanisms have also been suggested to explain the reduction of a TL signal due to optical bleaching. Whatever the mechanism is for a particular TLD material, optical fading is certainly detrimental to the material performance and needs to be tested for and characterised. Often one finds that optical effects are “thermally assisted” in that the optical transitions raise the electron into a metastable excited state from where thermal activation into the delocalised bands may occur. As expected, all the optical effects show a strong wavelength dependency. In addition to the environmental properties of heat and light upon a TLD material the effects of moisture and humidity are also important environmental factors.

## CHAPTER 4

### EXPERIMENTAL PROCEDURE

The materials, equipments and experimental procedures utilized in this work are described below.

#### 4.1 Materials

Either natural fluoride which contains, depending on its origin, a wide variety of different impurities acting as activators, or synthetic  $\text{CaF}_2$  as a host lattice with artificial dopants such as Tm, Dy, and Mn have been used. The samples used in this study were  $\text{CaF}_2$ :Dy (TLD-200),  $\text{CaF}_2$ :Tm (TLD-300),  $\text{CaF}_2$ :Mn (TLD-400), crystal chips (3.2mm x3.2mmx 0.89mm) obtained from Harshaw Chemical Company, Ohio, USA and Al-doped Lithium Triborate ( $\text{LiB}_3\text{O}_5$ ) obtained from Middle East Technical University (METU).

#### 4.2 Experimental Procedure and Equipments

Before the subsequent irradiation, the samples were first annealed to erase any residual information and then quickly cooled in air at 75 °C/min to room temperature. For this reason the  $\text{CaF}_2$ :Dy (TLD-200) samples were annealed at  $500 \pm 1$  °C for 1 hour,  $\text{CaF}_2$ :Tm (TLD-300) samples were annealed at  $400 \pm 1$  °C for 1 hour and  $\text{CaF}_2$ :Mn (TLD-400) samples were annealed at  $400 \pm 1$  °C for 30 min through the experiments. All annealing treatments were carried out with a specially designed microprocessor- controlled electrical oven which is able to control the temperature within  $\pm 1.0$  °C. The samples were irradiated at room temperature with beta rays from a calibrated  $^{90}\text{Sr}$ - $^{90}\text{Y}$  source. The activity of  $\beta$ -source is about 100 mCi. It is calibrated by manufacturer on March, 10, 1994. The recommended working life-time is about 15 years. Stronium-90 emits high energy beta particles from their daughter products ( $^{90}\text{Sr}$   $\beta$ -0.546 MeV together with  $^{90}\text{Y}$   $\beta$ -2.27 MeV). Beta radiation is absorbed by air, so its intensity declines with distance much more rapidly than inverse square law calculations would indicate.

The maximum range of Y-90 beta particles in air is approximately 9 meter. The typical strength of a 100 mCi Sr-90  $\beta$ -source installed in a 9010 Optical Dating System is 2.64 Gy/minute=0.0438 Gy/Sec for fine grains on aluminium, or 3,3 Gy/min=0.055 Gy/sec for 100 m quartz on stainless still. The irradiation equipment is an additional part of the 9010 Optical Dating System which is purchased from Little More Scientific Engineering, UK [61]. The irradiated samples were read out with a Harshaw QS 3500 manual type reader that is interfaced to a PC where the TL signals were studied and analyzed. It economically provides high reliability. The basic block diagram of reader is shown in figure 4.1. A standard clear glass filter was always installed in the reader between the planchet and photomultiplier tube to eliminate the emitted infrared lights from the reader plus samples. All functions are divided between the reader and the specialized TLDSHELL software that runs on the PC. All data storage, instrument control, and operator inputs are performed on the PC. Signal acquisition and conditioning are performed in the reader. In this way, each glow curve can be analyzed using a best-fit computer program based on a Marquardt algorithm minimisation procedure, associated to first-order and general-order kinetic expressions. The program resolves the individual peaks present in the curve, giving the best values for the different peak parameters. The instrument includes a sample change drawer for inserting and removing the TLD elements. The reader uses contact heating with a closed loop feedback system that produces adjustable linearly ramped temperatures from 1 °C to 50 °C per second accurate to within  $\pm 1$  °C to 600 °C in the standard reader.

The Time Temperature Profile (TTP) is user defined in three segments: Preheat, Acquire, and Anneal, each with independent times (Pre-read anneal: adjustable 0 to 1000 sec, Linear ramp: adjustable from 1 °C to 50 °C per second, Post-read anneal: 0 to 1000 sec) and temperature (Pre-read anneal: room temperature to 200 °C, Post-read anneal: up to 400 °C). The typical time temperature profile is shown in figure 4.2. To improve the accuracy of low-exposure readings and to extend planchet life, the 3500 provides for nitrogen to flow around the planchet. By eliminating oxygen in the planchet area, the nitrogen flow eliminates the unwanted oxygen-induced TL signal. Nitrogen is also routed through the photo-multiplier tube (PMT) chamber to eliminate moisture caused by condensation. Glow curves were measured using a platinum planchet at linear heating rates of 1 °C/s and 10 °C/s. The time duration between irradiation and necessary TL operation was always kept

constant at about 1 min, except for the storage time experiment. The storage time experiments were performed for different time periods. We also investigated the optical fading at room temperature under the tungsten filament lamp of 55 lux which is located at a distance of 20 cm from the sample. The experimental equipments are shown in figure 4.3.

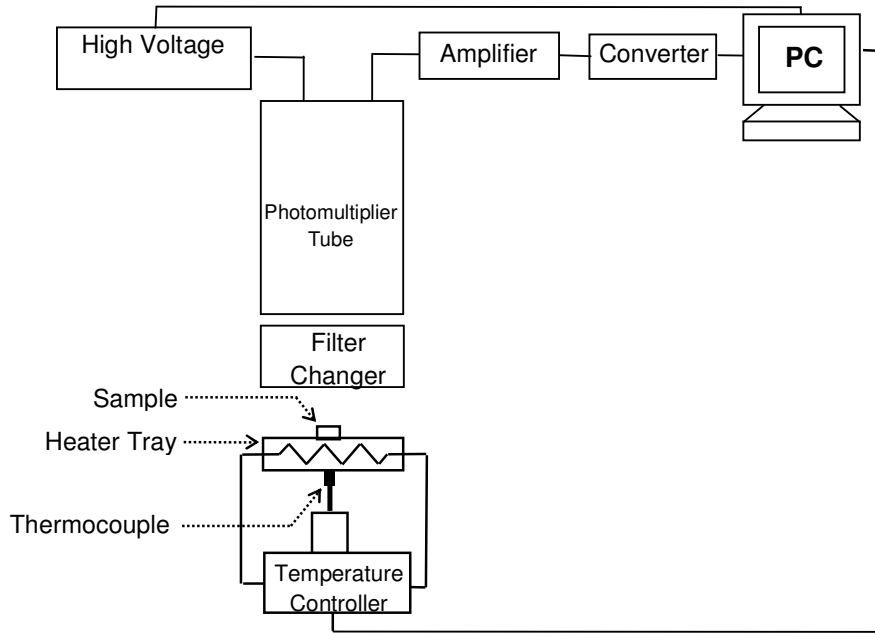


Figure 4.1 Basic block diagram of TL reader. [61]

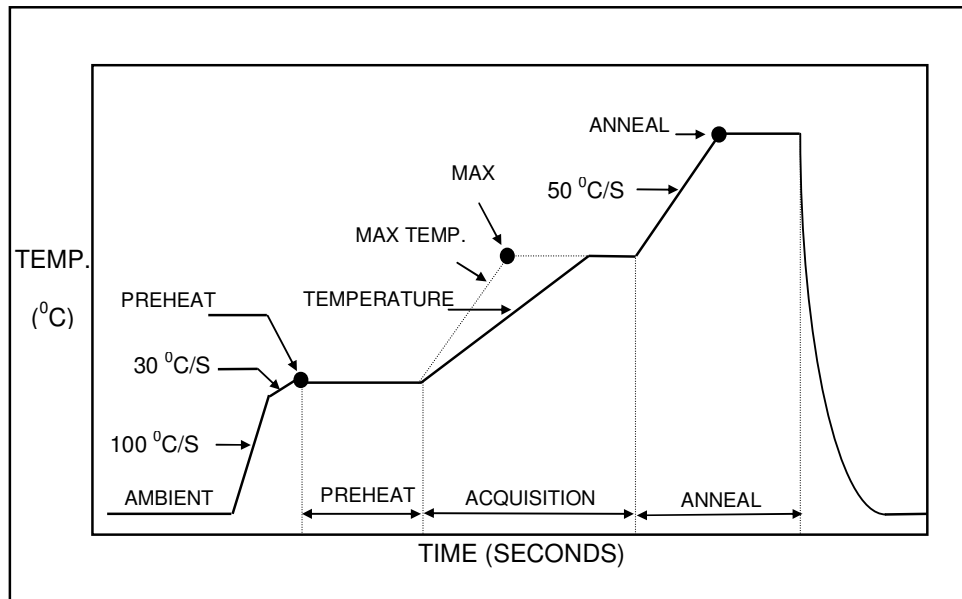
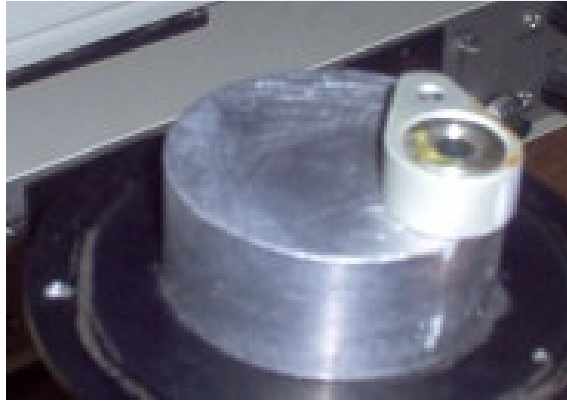


Figure 4.2 Typical time temperature profile (TTP). [61]



(a)



(b)



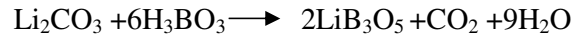
(c)

Figure 4.3 Experimental equipments (a)  $^{90}\text{Sr}$ - $^{90}\text{Y}$   $\beta$ -source (b) 9010 Optical Dating System (c) Harshaw TLD System 3500



### 4.3 Synthesis of Lithium Triborate (LBO)

Lithium triborate (LBO) samples were synthesized in an inert atmosphere using  $\text{Li}_2\text{CO}_3$  and  $\text{H}_3\text{BO}_3$ . Stoichiometric quantities of the starting materials,  $\text{Li}_2\text{CO}_3$  and  $\text{H}_3\text{BO}_3$ , were weighed separately ( $\text{Li}_2\text{O}:3\text{B}_2\text{O}_3$ ) and dissolved into 15 ml distilled water. The mixture was stirred and heated in order to evaporate extra water until a viscous gel resulted. The hot gel was transferred into a platinum crucible and then was put into electrical furnace and heated at  $750\text{ }^\circ\text{C}$  for 1 hour in air atmosphere. The estimated reaction is given below.



Lithium triborate sample was then doped with Al-elements in the form of oxides.  $\text{LiB}_3\text{O}_5$  and  $\text{Al}_2\text{O}_3$  samples were weighed separately and ground together in an agate mortar to obtain homogenization and then transferred into a porcelain crucible. The mixture was heated at  $750\text{ }^\circ\text{C}$  for 7 h and ground in an agate mortar. The doping procedure was based on the study performed by Özdemiir et al [62-63]. The concentration of Al-ions doped into  $\text{LiB}_3\text{O}_5$  is 5 % by wt. 20 mg sample was used in each measurement. The samples were firstly annealed at  $350\pm 1\text{ }^\circ\text{C}$  for 15 min prior to irradiation with a specially designed microprocessor controlled electrical oven and then they are irradiated at room temperature with a newly calibrated  $^{90}\text{Sr}$ - $^{90}\text{Y}$  beta source. The glow curves were obtained by using a Harshaw QS 3500 Manual type TL reader interfaced to a PC where the TL signals were analyzed. Glow curve readout was carried out on a platinum planchet at a linear heating rate of  $1\text{ }^\circ\text{C/s}$  up to  $400\text{ }^\circ\text{C}$ .

## CHAPTER 5

### EXPERIMENTAL RESULTS

In this study we have investigated the effect of heating rate on the linearity and dose response characteristics of  $\text{CaF}_2:\text{Dy}$  (TLD-200),  $\text{CaF}_2:\text{Tm}$  (TLD-300) and  $\text{CaF}_2:\text{Mn}$  (TLD-400) crystals by using the supralinearity index  $f(D)$  and superlinearity index  $g(D)$  at two linear heating rates of 1 °C/s and 10 °C/s and the effect of various heating rates on the glow curve and total peak area of these crystals between 1 °C/s and 30 °C/s and also the stability of the glow peaks at room temperature both in the dark and under light. We have also determined the trapping parameters of dosimetric thermoluminescent glow peak of Lithium TriBorate ( $\text{LiB}_3\text{O}_5$ ) activated by Aluminum using different experimental methods such as, additive dose (AD), variable heating rate (VHR), peak shape methods (PS), three points method (TPM), computer glow curve deconvolution (CGCD) method.

#### 5.1 The effect of heating rate on the dose response of $\text{CaF}_2:\text{Dy}$ (TLD-200)

Calcium fluoride doped with Dy is available as single crystals, as polycrystalline chips, or as powders. Single crystal  $\text{CaF}_2:\text{Dy}$  suitable for dosimetry can be grown using the Bridgman-Stockbarger technique with a Dy doping level of 3 mol % in the melt. Generally, doping levels in the final dosimetric material are less than this and, typically, for 3 mol % Dy in the melt, one can expect approximately 1.5 mol % in the dosimeter [3]. The mechanism of TL production in rare earth doped  $\text{CaF}_2$  is not perfectly understood, but some general outlines can be sketched. The standard model suggested to account for TL emission above room temperature follows from an in-depth study of the TL emission below room temperature by Merz and Pershan [64]. These authors noted the TL in this latter temperature region in oxygen-free samples (such as TLD-200) is initiated by the release of holes from different varieties of perturbed  $V_k$  centres recombining with electrons at divalent rare earth ions in cubic symmetry. Thus, in the case of Dy, irradiation reduces cubic  $\text{Dy}^{+3}$  to  $\text{Dy}^{+2}$  with the holes trapped elsewhere at  $V_k$ . Fong [65] examined the TL above

room temperature in CaF<sub>2</sub>:Dy and also observed the formation of divalent Dy<sup>+2</sup> after irradiation. CaF<sub>2</sub>:Dy (TLD-200, Harshaw Chem. Co.) is one of the high-sensitivity thermoluminescence dosimetry (TLD) phosphors. Binder and Cameron [66] have studied its glow curve behaviour as well as the spectral character of the thermoluminescence (TL) emission. They observed six glow peaks at temperatures of about 120, 140, 200, 240, 340 and 400 °C. The TL emission spectrum reported by these authors consists of sharp bands at 460, 484 and 577 nm for all the glow peaks. Sunta [67] extended the study of the spectrum further up to 800 nm and observed two more groups of bands at 660-670 and 750-760 nm. The thermoluminescence (TL) behaviour of a phosphor depends on the dose received [68]. In general, each TL glow peak exhibits different phases as the dose varies, such as: linear, supralinear, saturation and decreasing [69]. Peaks appear (practically above a certain threshold dose) grow and perhaps disappear completely. The above behaviour is a result of the relative number of the appropriate TL traps of the crystal, the relative cross section of filling the traps with electrons (or holes) and the creation and destruction of the traps by radiation. Radiation induces new traps as well as destroying old ones, via several channels. The above behaviour, as is clear, is of interest both as regards the physics of the TL process itself and also the application of TL, for instance in dosimetry [70]. Recently, Yazici *et al* [71, 72] have analyzed these parameters for all glow peaks between room temperature and 600 °C, and they observed that the glow curve of this material has five peaks (P1-P5) between room temperature and 250 °C called low temperature peaks (LTPs) and three peaks (P6-P8) between 260 and 600 °C called high temperature peaks (HTPs), at a linear heating rate of 1 °C/s. In this study the dose response behavior of CaF<sub>2</sub>: Dy (TLD-200) has been investigated at two linear heating rates of 1 °C and 10 °C by using the dose response functions  $f(D)$  and  $g(D)$ . TLD-200 crystal chips were firstly annealed at 500 °C for 1 hour before the subsequent irradiation and then cooled in air to room temperature. Then the sample was irradiated immediately after the standard annealing at room temperature with  $\beta$  rays from a <sup>90</sup>Sr- <sup>90</sup>Y source ( $\approx 0.04$  Gy/s) between 0.04 Gy and 34.5 kGy dose level. The stability of the glow curves were also investigated at room temperature for different environmental condition i.e. in dark and under light. The crystal chip was annealed with same annealing procedure and exposed to 12 Gy then left fading for different storage time periods. Typical glow curves of TLD-200 sample, using a linear heating rate of 1 °C/s is shown in Figure 5.1a and 5.1b.

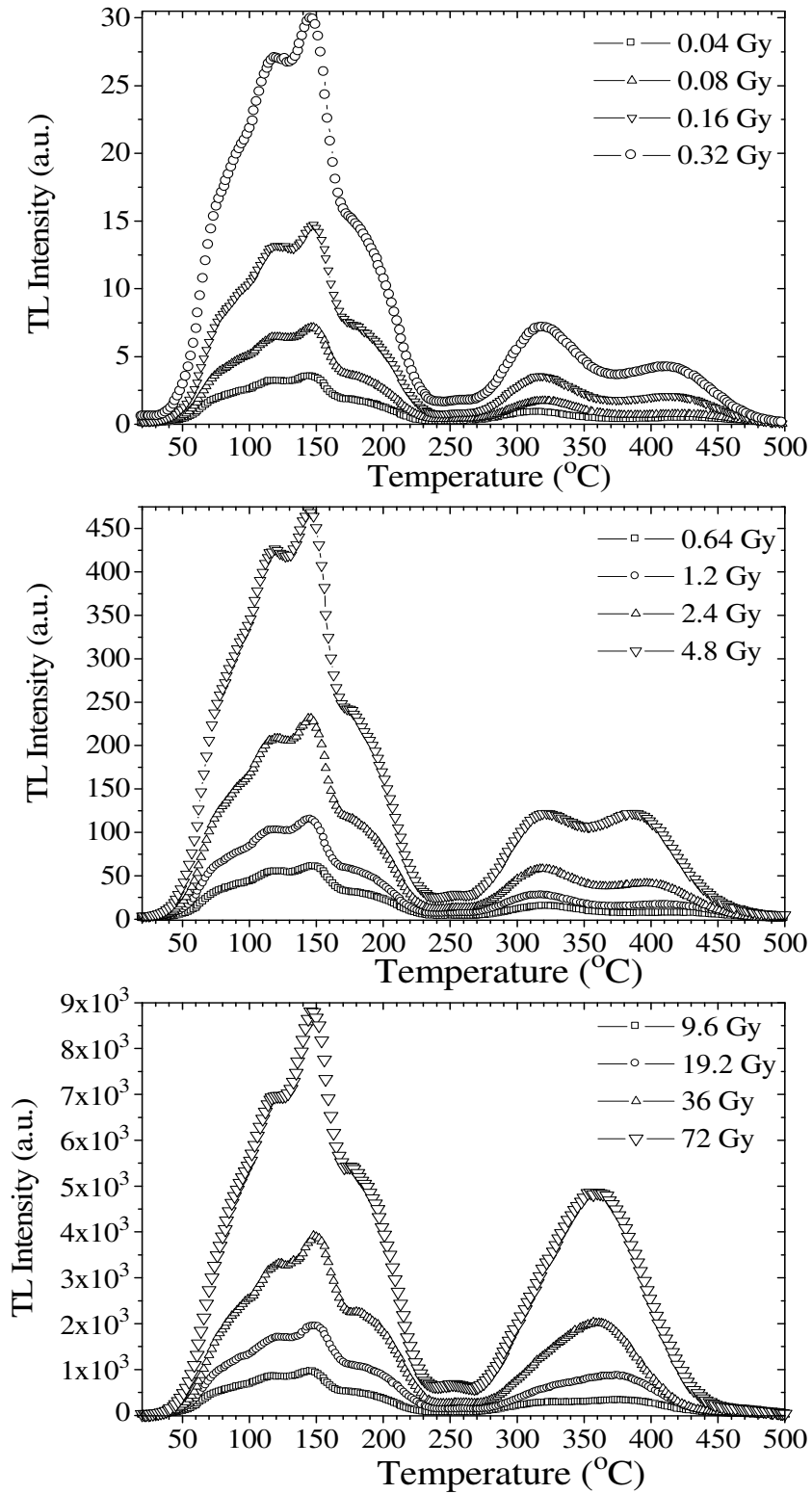


Figure 5.1a A typical glow curve of TLD-200 measured after an annealing procedure of  $500 \pm 1^\circ\text{C}$  for 1 hour by irradiation at room temperature from exposed to beta rays from 0.04 Gy up to 72 Gy and readout at a linear heating rate of  $\beta = 1^\circ\text{C/s}$

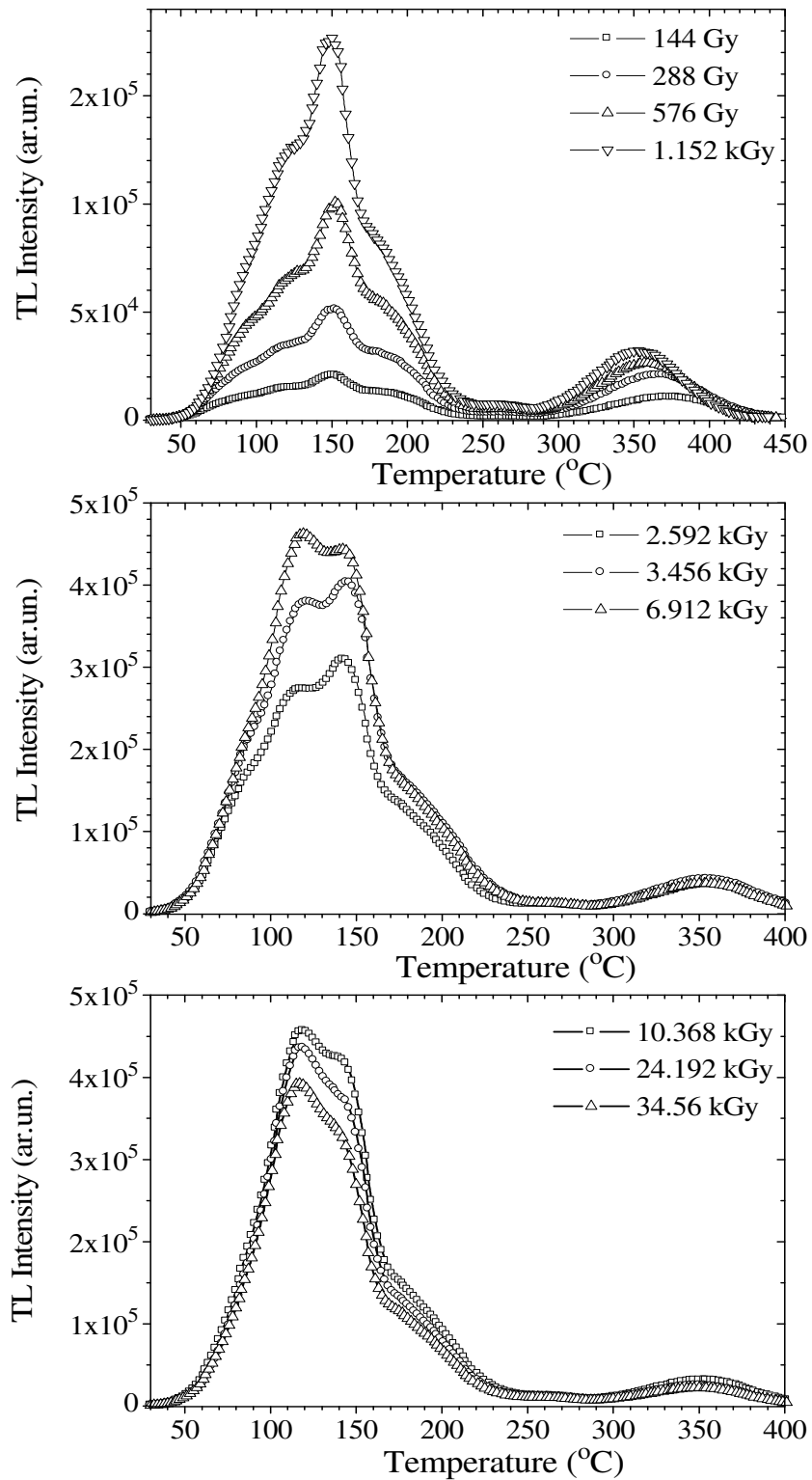


Figure 5.1b A typical glow curve of TLD-200 measured after an annealing procedure of  $500 \pm 1 \text{ }^\circ\text{C}$  for 1 hour by irradiation at room temperature from exposed to beta rays from 144 Gy up to 34.5 kGy and readout at a linear heating rate of  $\beta = 1 \text{ }^\circ\text{C/s}$

Figure 5.2 shows the growth of the height of the peaks as a function of dose. As seen from this figure, P1 and P2 shows linear behaviour up to 10 Gy, after a region of supralinear region these peaks go into the sublinear region after  $10^3$  Gy. The linearity of the P3 continues nearly up to  $10^3$  Gy then this peak goes to the sublinear region. P4 also shows linear behaviour up to  $10^2$  Gy then this peak shows supralinear behaviour, after  $10^3$  Gy the peak saturates and goes into sublinear region. P5 also shows linear behaviour up to 10 Gy then this peak shows supralinear behaviour nearly up to  $10^3$  Gy after that P5 saturates and shows sublinear behaviour. Consequently, if one investigated the peaks between the room temperature and 250 °C, P1-P5, and high temperature peaks P6-P8, it is clear that P1-P5 show linear behaviour nearly up to  $10^2$  Gy and going to the supralinear region up to  $10^3$  Gy then these peaks saturate at high doses showing sublinear behaviour. The linearity of the P6-P8 continues up to 10 Gy then these peaks show supralinear behaviour up to  $10^3$  Gy then going into the sublinear region.

Even figure 5.2 explains the growth of the height of the peaks as a function of dose, to best understand the dose rate behaviour of the peaks the dose response function,  $f(D)$ , is evaluated by using equation 3.3. As seen from the figure 5.3 the curves exhibit the main features characteristic of the dose response. For peak 1 and 2  $f(D)$  of this material, namely a linear ( $f(D)=1$ ) region up to 1 Gy, followed by a region of supralinear growth ( $f(D)>1$ ), gradually going into a region of sublinear growth ( $f(D)<1$ ) near  $10^3$  Gy. Peak 3 shows linear behaviour nearly up to  $10^3$  Gy then it saturates after that dose and shows a sublinear behaviour. Peak 4 shows linear behaviour up to 10 Gy, followed by a region of supralinear growth up to  $10^3$  Gy, gradually going into a region of sublinear growth near  $10^4$  Gy. Similar to peak 3, peak 5 also shows linear characteristic only at low doses than reaching its maximum nearly  $10^2$  Gy having  $f(D) \sim 2.5$  then it saturates nearly  $10^4$  Gy showing sublinear behaviour. The total area of high temperature peaks (P6+P7+P8) shows linear characteristic ( $f(D)=1$ ) nearly up to 1 Gy followed by a region of supralinear growth ( $f(D)>1$ ). Then, the peaks gradually go into a region of sublinear growth ( $f(D)<1$ ) after a dose level of  $10^3$  Gy.

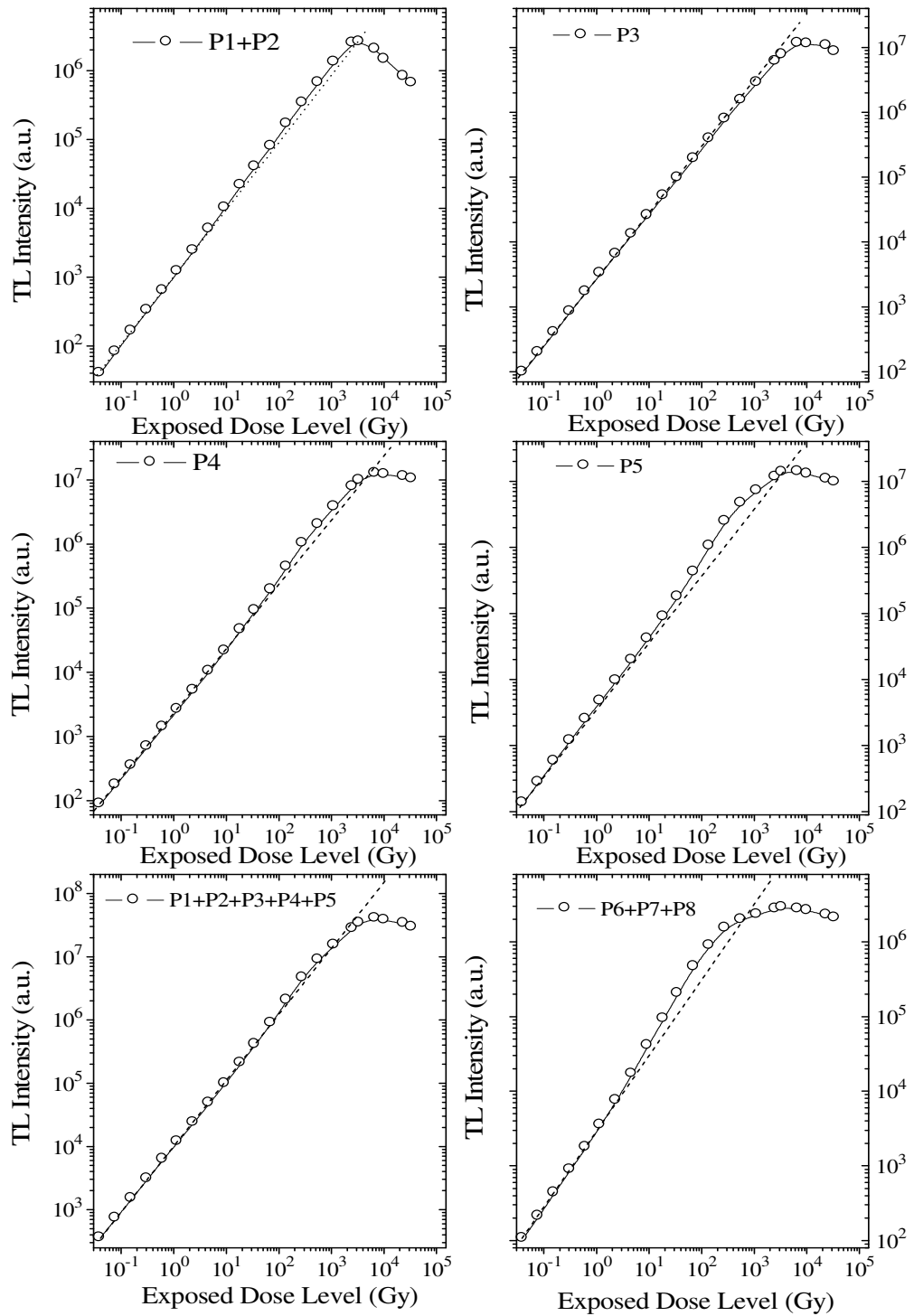


Figure 5.2 The growth of the height of the peaks from TLD-200 as a function of dose at a linear heating rate of  $\beta = 1 \text{ }^\circ\text{C/s}$

It is also seen from figure 5.3 that the total area of glow peaks (P1+P2+P3+P4+P5) between RT and  $250 \text{ }^\circ\text{C}$  shows linear behavior ( $f(D)=I$ ) at low doses nearly up to 1 Gy then gradually going into a region of supralinear growth ( $f(D)>I$ ).

The peaks saturates after a dose level of  $10^4$  Gy showing sublinear behaviour ( $f(D) < 1$ ) at a linear heating rate of  $1\text{ }^\circ\text{C/s}$ . The dose response function of the low temperature and high temperature of the peaks is also depicted in figure 5.4.

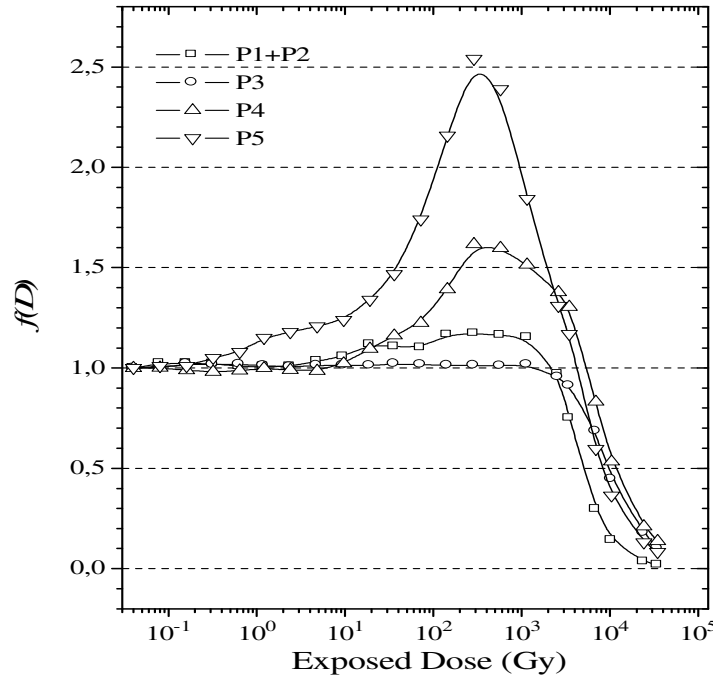


Figure 5.3 The dose response function  $f(D)$  vs  $D$  of TLD-200 ( $\beta=1\text{ }^\circ\text{C/s}$ )

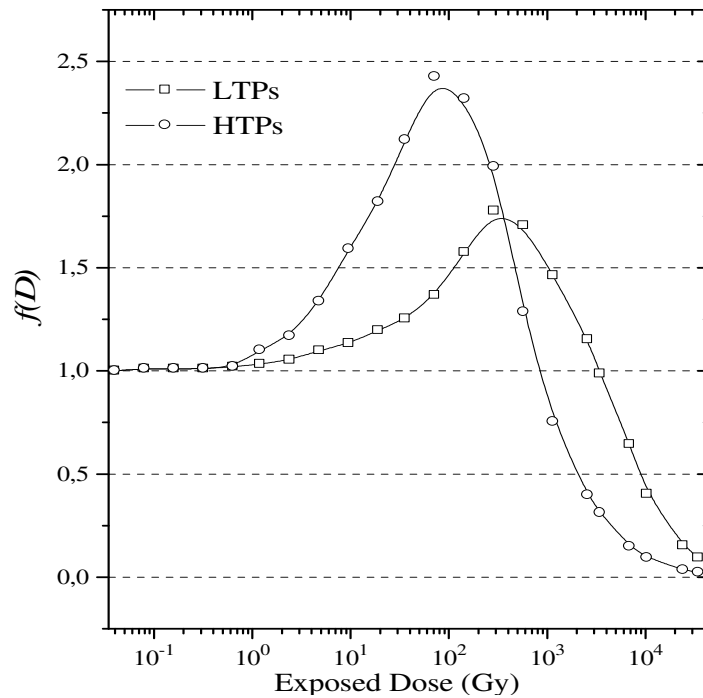


Figure 5.4 The dose response function  $f(D)$  vs  $D$  of the LTPs and HTPs of TLD-200 ( $\beta=1\text{ }^\circ\text{C/s}$ )



In this study we have also defined the *superlinearity index*,  $g(D)$ , for total peak area of the low temperature and high temperature peaks of this crystal to better understand the dose rate behaviour of the peaks. To evaluate the superlinearity index  $g(D)$  we used the function 5.1 by using the glowfit program.

$$S(x) = \frac{a + cx}{1 + bx + dx^2} \quad (5.1)$$

Where  $S$  is the measured TL signal- i.e. the maximum intensity, or the total area of a glow peak-  $x$  is the absorbed dose.  $a$ ,  $b$ ,  $c$  and  $d$  are the constants which are shown in table 5.1. The superlinearity function was evaluated by using equation 3.1.

$$g(D) = \left[ \frac{4 + 2bx}{1 + x(b + dx)} + \frac{2(c - a(b + dx))}{a(b + 2dx) + c(-1 + dx^2)} - 1 \right] \quad (5.2)$$

Table 5.1 The constants used in the superlinearity function

Low Temperature Peaks	High Temperature Peaks
a= -135493.77	a= 2956.2629
b= 0.000689	b= 0.003455
c= 42411.819	c= 109.11
d= $4.123 \times 10^{-8}$	d= $1.032 \times 10^{-7}$

The superlinearity index  $g(D)$  is shown in figure 5.5. As shown from this figure that the curves exhibit the main features characteristic of the superlinearity function,  $g(D)$ , namely, the LTPs shows a linear region ( $g(D)=1$ ) up to about 10 Gy followed by a region of superlinear growth ( $g(D)>1$ ), gradually going into a region of sublinear growth ( $g(D)<1$ ) after a dose level of  $10^4$  Gy dose. The HTPs also shows linear characteristics ( $g(D)=1$ ) up to 10 Gy, after this dose level the curves gradually go into a superlinear growth ( $g(D)>1$ ). This also saturates and shows sublinear behaviour after  $10^3$  Gy.

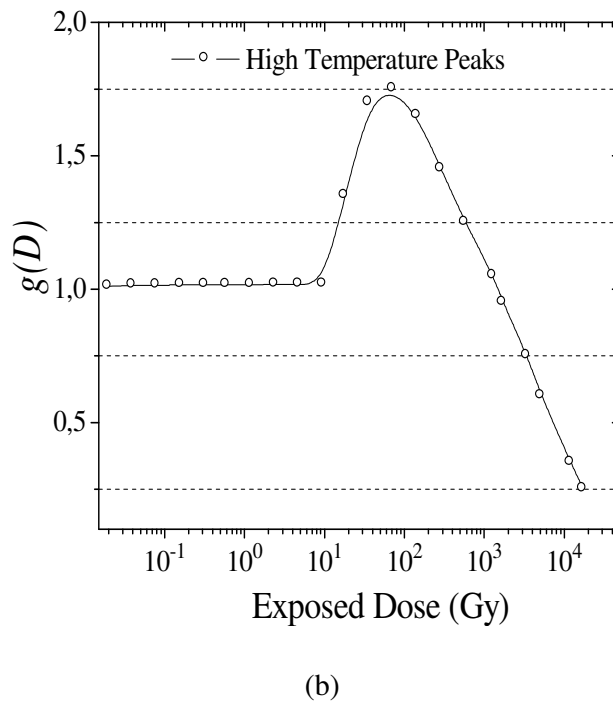
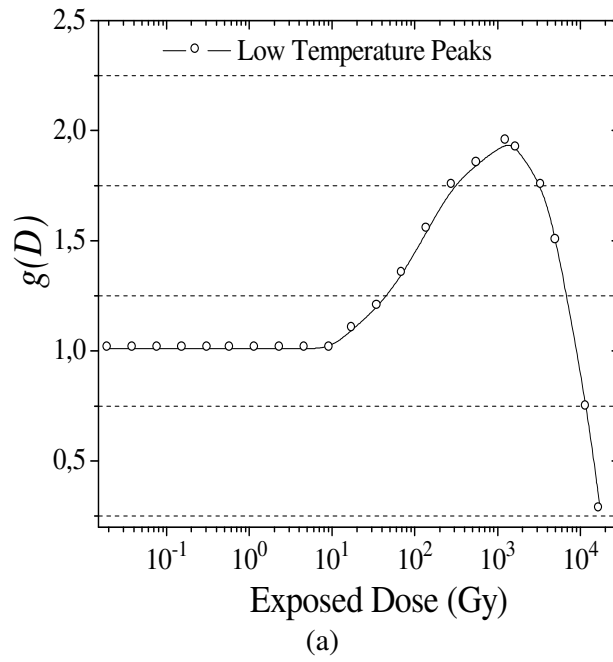


Figure 5.5 The superlinearity function  $g(D)$  vs  $D$  of TLD-200 (a) LTPs, (b) HTPs ( $\beta=1\text{ }^{\circ}\text{C/s}$ )

The dose response characteristics of the glow peaks of TLD-200 were also obtained by recording the glow curves at a linear heating rate of  $10\text{ }^{\circ}\text{C/s}$ . Figure 5.6a and 5.6b show some of the selected glow curves of TLD-200 after different dose levels using a linear heating rate of  $10\text{ }^{\circ}\text{C/s}$ .

Figure 5.7 shows the growth of the height of the peaks as a function of dose. As seen from this figure, P1 and P2 shows linear behaviour up to 50 Gy, after a region of supralinear growth these peaks go into the sublinear region after  $10^3$  Gy. The linearity of the P3 continues nearly up to 10 Gy after a region of supralinear growth this peak goes to the sublinear region after  $10^3$  Gy dose level. P4 also shows linear behaviour nearly up to  $10^2$  Gy then this peak shows supralinear behaviour, after  $10^3$  Gy the peak saturates and goes into sublinear region. P5 also shows linear behaviour up to 50 Gy then this peak shows supralinear behaviour nearly up to  $10^4$  Gy after that P5 saturates and shows sublinear behaviour. Consequently, if one investigated the peaks between the room temperature and 250 °C, LTPs, and high temperature peaks, HTPs, it is clear that LTPs show linear behaviour nearly up to 50 Gy and going to the supralinear region up to  $10^3$  Gy then these peaks saturate at high doses showing sublinear behaviour. The linearity of the HTPs continues up to 10 Gy then these peaks show supralinear behaviour up to  $10^3$  Gy then going into the sublinear region after this dose level.

The dose response function,  $f(D)$ , is also evaluated by using equation 3.3 at a linear heating rate of 10 °C/s. As seen from the figure 5.8 and 5.9 the curves exhibit the main features characteristic of the dose response. The total area of peaks 1 and 2 show linear characteristics ( $f(D)=1$ ) up to 50 Gy, followed by a region of supralinear growth ( $f(D)>1$ ), these peaks gradually go into a region of sublinear growth ( $f(D)<1$ ) after  $10^3$  Gy. Peak 3 shows linear behaviour, ( $f(D)=1$ ), nearly up to 10 Gy, after a region of supralinear growth, ( $f(D)>1$ ), this peak saturates after  $10^3$  Gy dose level and shows a sublinear, ( $f(D)<1$ ), behaviour. Peak 4 shows linear behaviour, ( $f(D)=1$ ), up to 10 Gy, followed by a region of supralinear growth, ( $f(D)>1$ ), this peak gradually goes into a region of sublinear growth, ( $f(D)<1$ ), near  $10^4$  Gy. Similar to peak 3, peak 5 also shows linear characteristic, ( $f(D)=1$ ), up to 10 Gy. Then the supralinearity index reaches its maximum value nearly at 600 Gy, having  $f(D) \sim 2.4$ , then it saturates after  $10^4$  Gy showing sublinear behaviour, ( $f(D)<1$ ). The total area of high temperature peaks (HTPs) shows linear characteristic ( $f(D)=1$ ) nearly up to 50 Gy followed by a region of supralinear growth ( $f(D)>1$ ). The peaks gradually go into a region of sublinear growth ( $f(D)<1$ ) after a dose level of  $10^4$  Gy.

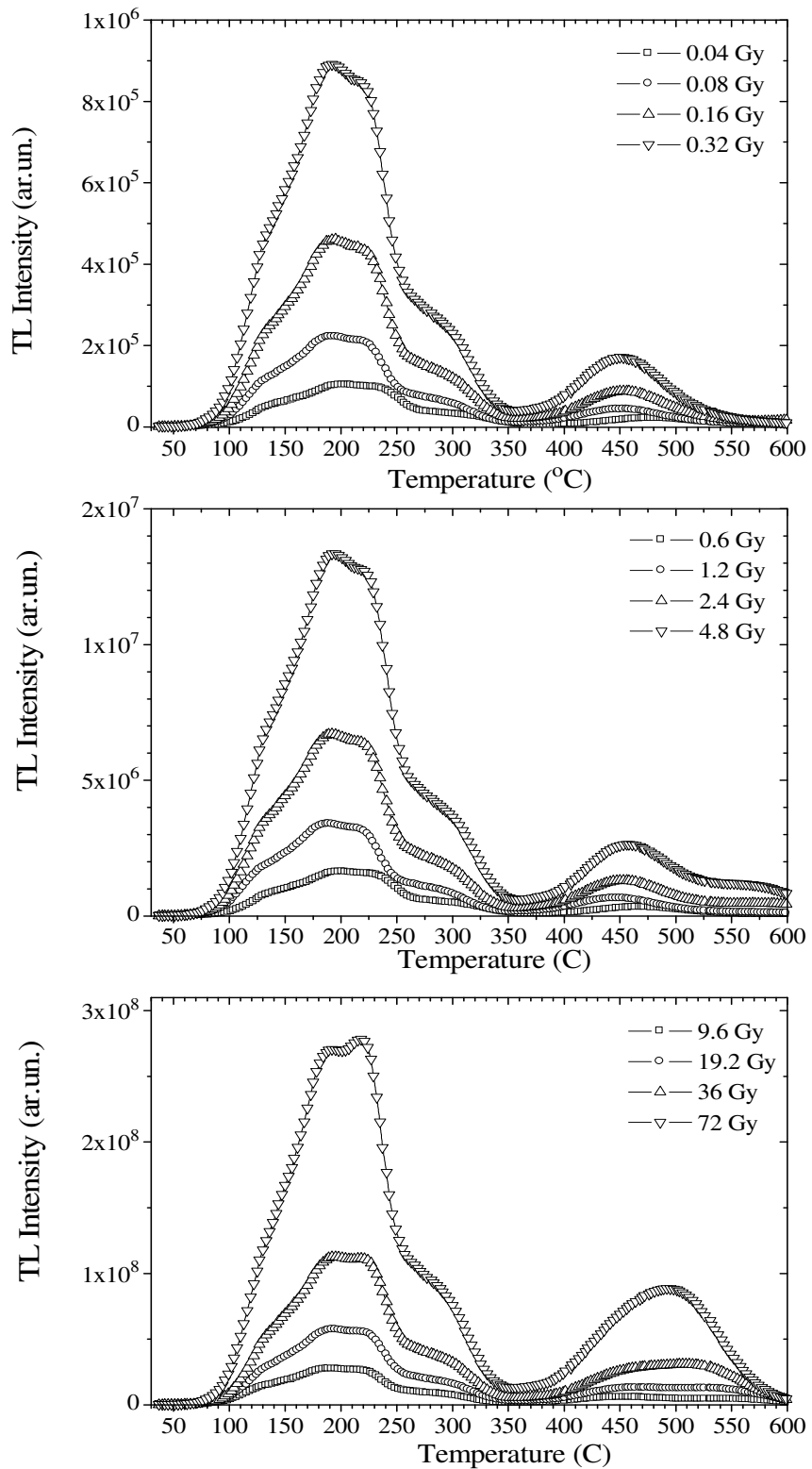


Figure 5.6a A typical glow curve of TLD-200 measured after an annealing procedure of  $500 \pm 1$  °C for 1 hour by irradiation at room temperature from exposed to beta rays from 0.04 Gy up to 72 Gy and readout at a linear heating rate of  $\beta = 10$  °C/s

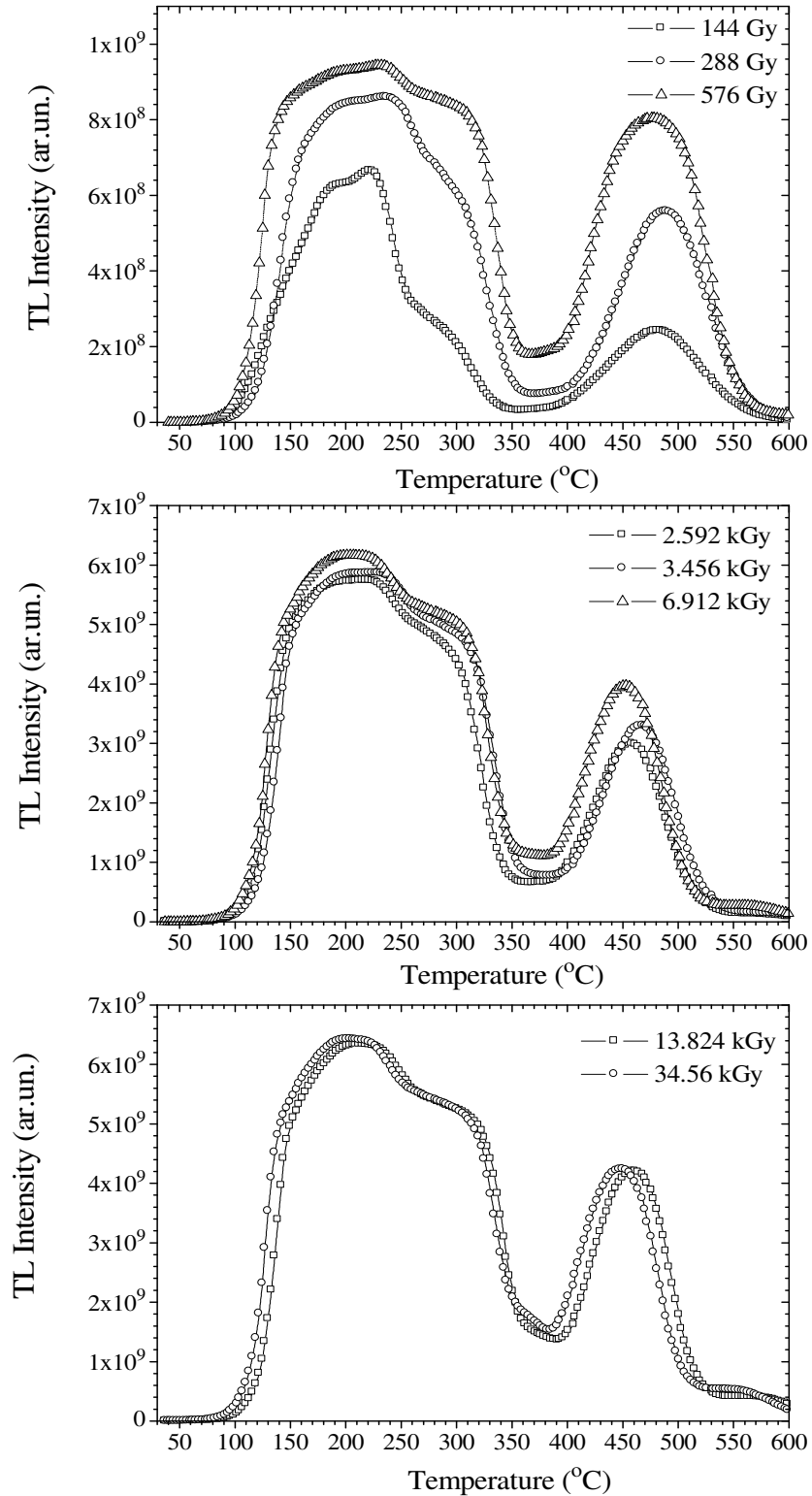


Figure 5.6b. A typical glow curve of TLD-200 measured after an annealing procedure of  $500 \pm 1$  °C for 1 hour by irradiation at room temperature from exposed to betarays from 144 Gy up to 34.5 kGy and readout at a linear heating rate of  $\beta = 10$  °C/s

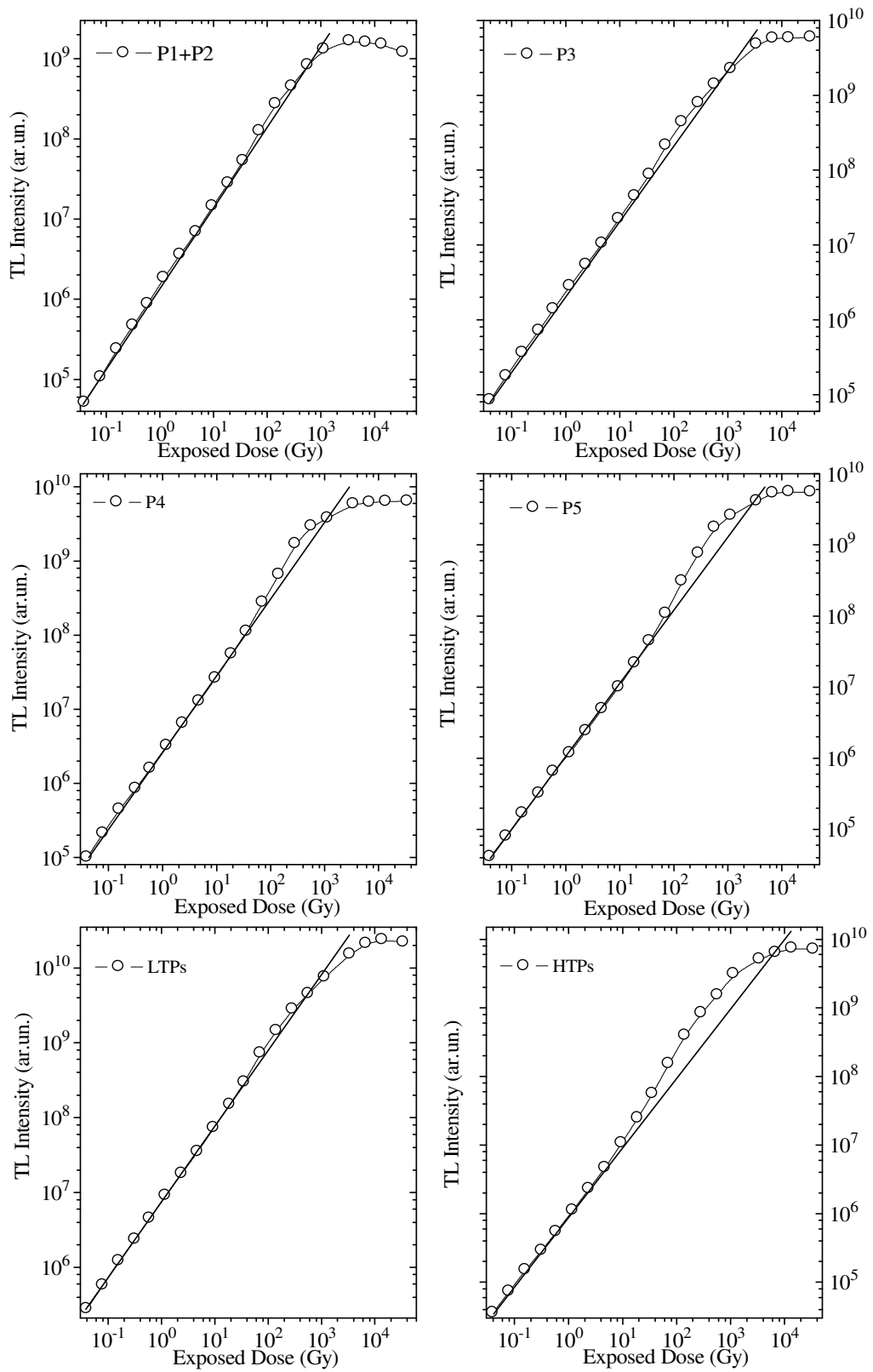


Figure 5.7 The growth of the height of the peaks from TLD-200 as a function of dose at a linear heating rate of  $\beta = 10$  °C/s

It is also seen from figure 5.9 that the total area of low temperature glow peaks (LTPs) show linear behavior ( $f(D)=1$ ) nearly up to 50 Gy then gradually go into a region of supralinear growth ( $f(D)>1$ ). The peaks saturate after a dose level of  $10^3$  Gy showing sublinear behavior ( $f(D)<1$ ) at a linear heating rate of  $10^\circ\text{C/s}$ .

The *superlinearity index*,  $g(D)$ , for total peak area of the low temperature and high temperature peaks of this crystal is also evaluated at a linear heating rate of  $10^\circ\text{C/s}$  using the function 5.3. Where  $S$  is the measured TL signal- i.e. the maximum intensity or the total area of a peak-  $x$  is the absorbed dose.  $a$ ,  $b$ ,  $c$  and  $d$  are the constants which are shown in table 5.2. The superlinearity function was evaluated by using equation 3.1.

$$S(x) = (a + bx + cx^2 + dx^3 + ex^4 + fx^5 + gx^6) \quad (5.3)$$

$$g(D) = \left[ \frac{2(c + x(3d + x(6e + 10fx + 15gx^2)))}{b + 6gx^5 + x((2c + 3dx + 4ex^2 + 5fx^3))} \right] + 1 \quad (5.4)$$

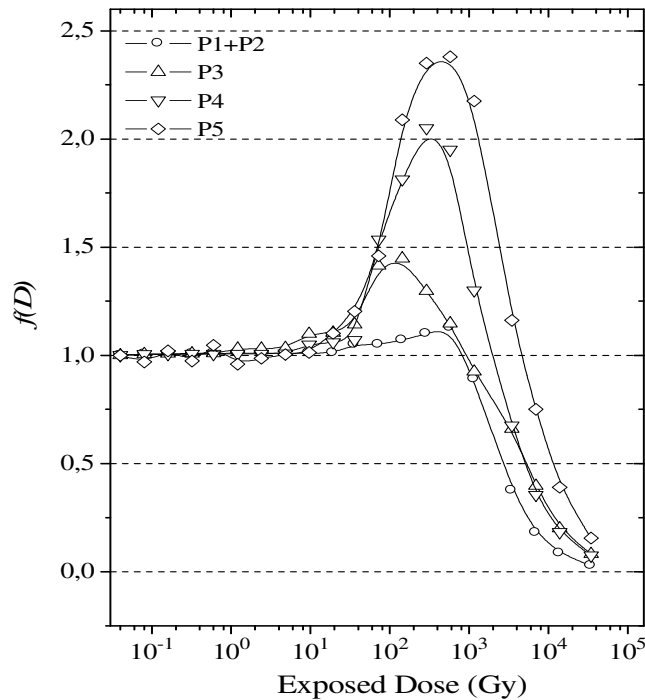


Figure 5.8 The dose response function  $f(D)$  vs  $D$  of TLD-200 ( $\beta=10^\circ\text{C/s}$ )

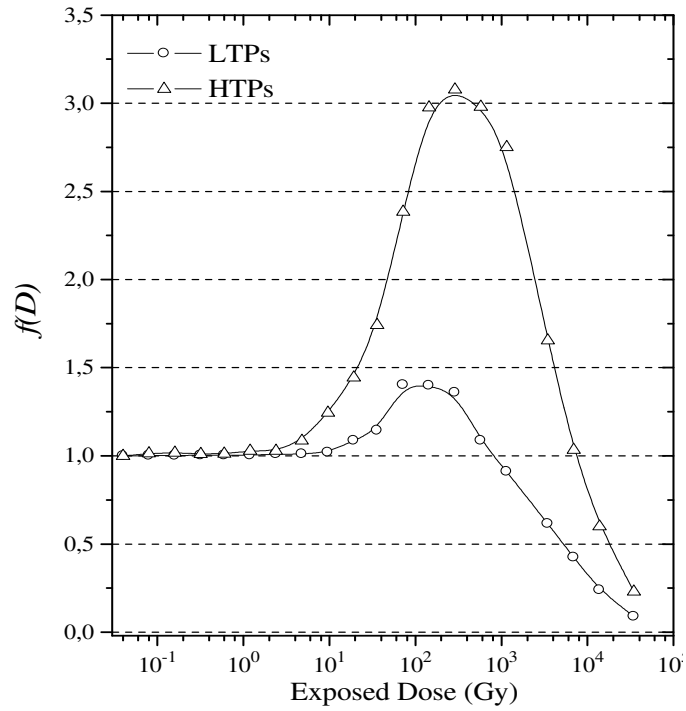


Figure 5.9 The dose response function  $f(D)$  vs  $D$  of the LTPs and HTPs of TLD-200 ( $\beta=10$  °C/s)

Table 5.2 The constants used in the superlinearity function

Low Temperature Peaks	High Temperature Peaks
a= -2055.8511	a= -167.3167
b= 632.09159	b= 192.701
c= 0.103226	c= 0.05484
d= $3.0062 \times 10^{-8}$	d= $7.229 \times 10^{-7}$
e= $1.61305 \times 10^{-9}$	e= $3.865 \times 10^{-10}$
f= $1.3302 \times 10^{-13}$	f= $6.332 \times 10^{-15}$
g= $2.504 \times 10^{-18}$	



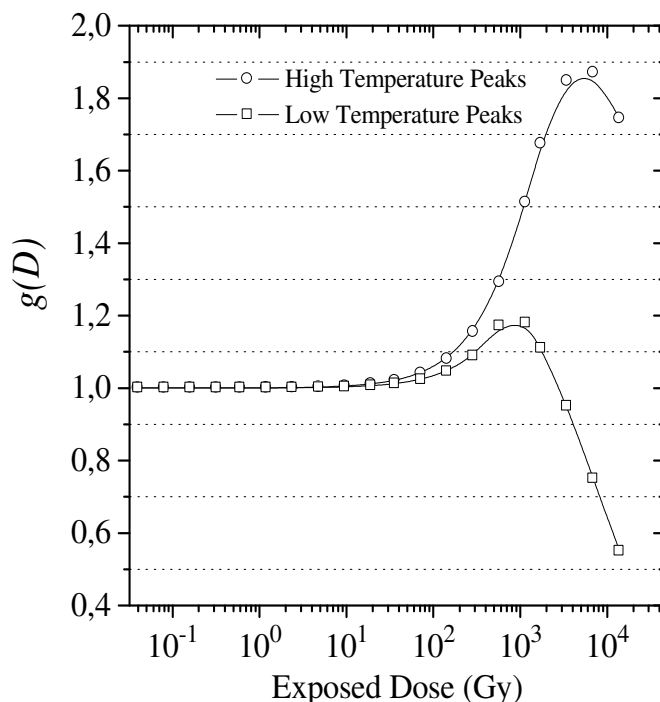


Figure 5.10 The superlinearity function  $g(D)$  vs  $D$  of TLD-200 ( $\beta=10$  °C/s)

As seen from the superlinearity index,  $g(D)$ , in figure 5.10, the LTPs show linear characteristics up to nearly 50 Gy, ( $g(D)=1$ ), followed by a region of superlinear growth ( $g(D)>1$ ), the peaks gradually go into a region of sublinear growth ( $g(D)<1$ ) after a dose level of  $10^3$  Gy dose. The HTPs also shows linear characteristics ( $g(D)=1$ ) up to 50 Gy, after this dose level the curves gradually go into a superlinear growth ( $g(D)>1$ ). These peaks also saturate and show sublinear behaviour after  $10^4$  Gy dose level.

The behaviour of the glow curves and the effect of thermal quenching due to the heating rate on the total peak area of glow curves were also investigated at different linear heating rates between 1 °C/s and 30 °C/s. Figure 5.11 shows some of the selected glow curves of CaF<sub>2</sub>: Dy (TLD-200) at linear heating rates between 1 °C and 30 °C. As seen from this figure the peak temperatures of all peaks are shifted higher temperatures when the heating rate increases as expected in theory. It is seen from figure 5.12, the total peak area of the glow curves decreases as the heating rate increases. The total area of the glow curves were normalized at the lower heating rate (1 °C s<sup>-1</sup>) and it can be seen that the decrease in the integrated area of the peaks by about 30 %.

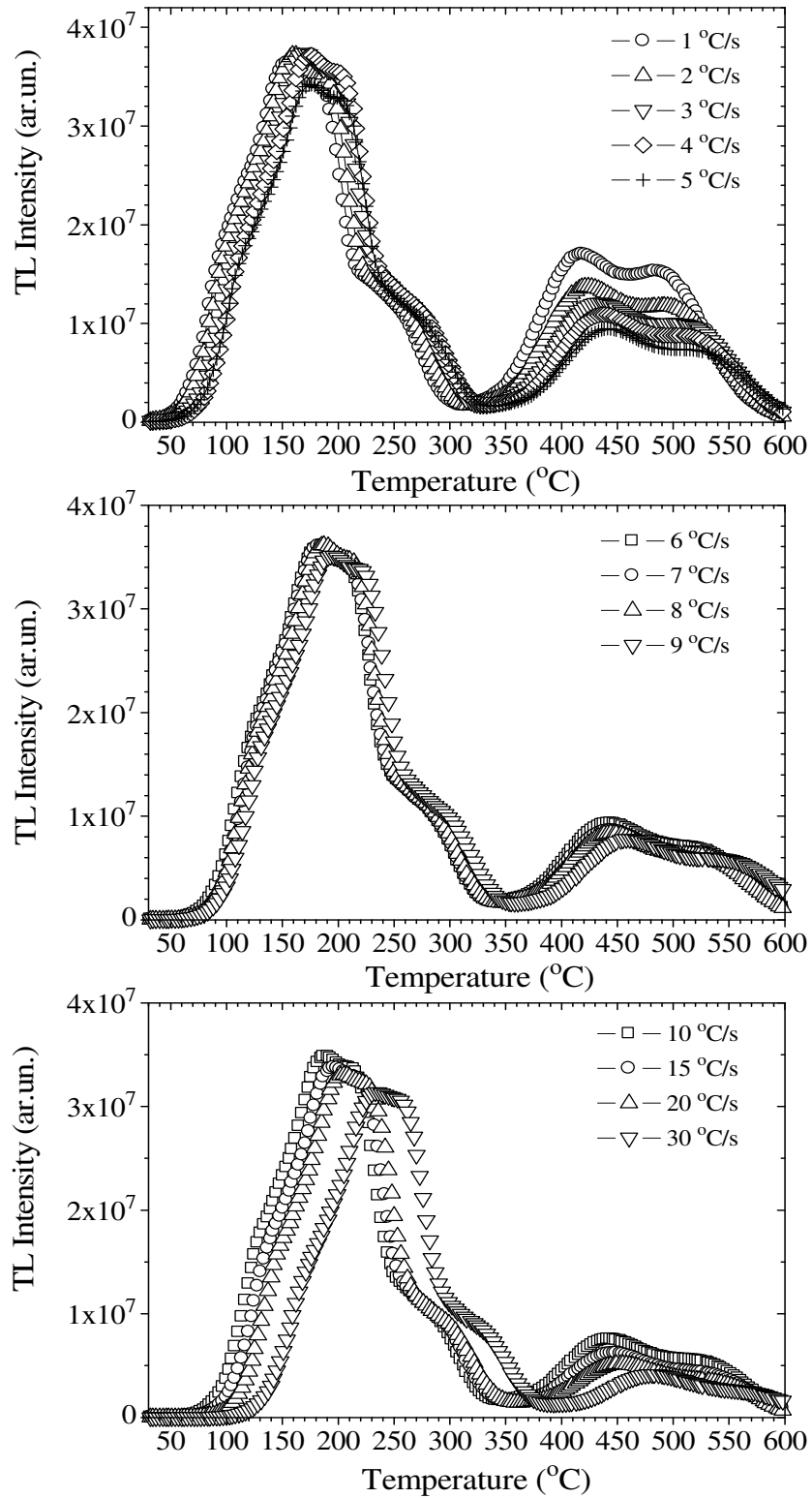


Figure 5.11 The glow curves of TLD-200 crystals irradiated with  $^{90}\text{Sr}$ - $^{90}\text{Y}$  beta source at linear heating rates between 1 °C/s and 30 °C/s ( $D=12$  Gy)

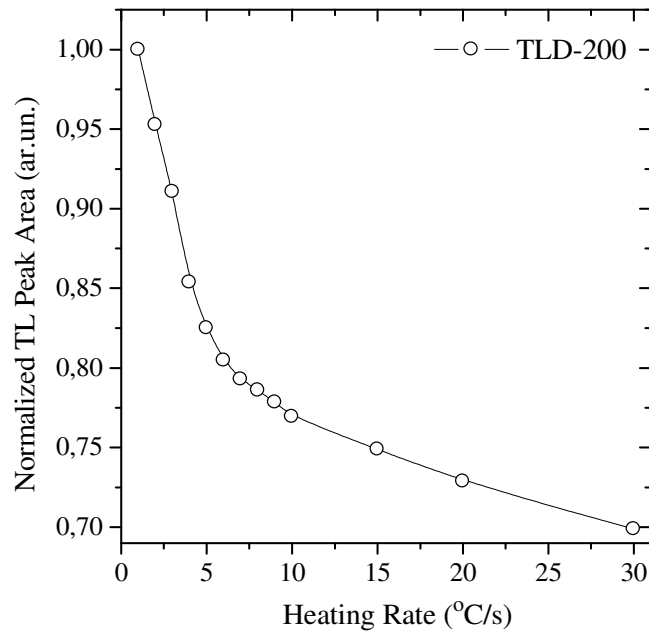
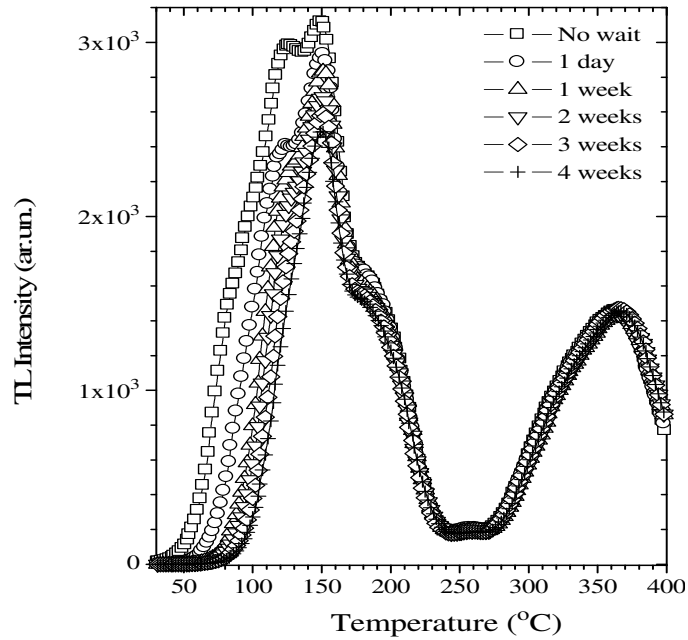


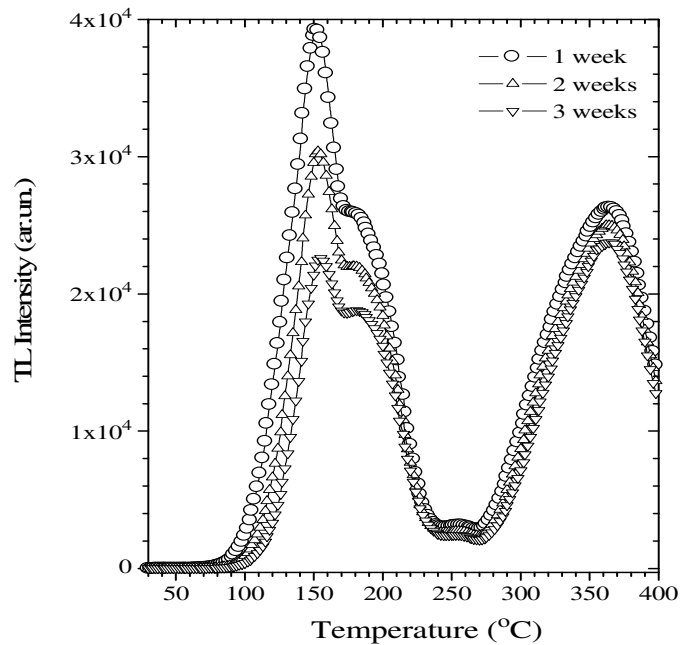
Figure 5.12 The normalized total TL peak area of TLD-200 crystals irradiated with  $^{90}\text{Sr}$ - $^{90}\text{Y}$  beta source at linear heating rates between 1 °C/s and 30 °C/s (D=12 Gy)

The most important problem in thermoluminescence (TL) technique applied to different fields of dosimetry, i.e., personnel, environmental and clinical dosimetry, is related to the loss of the stored TL signal after irradiation, commonly called thermal fading (trapped charge effects) and to its estimation. The release of electrons from their traps and their consequent recombination in luminescence centres is a statistical phenomenon, the probability of which is a function of temperature. The TL emission, glow curve, is related to traps which lie at different depths in the band gap, between the conduction and valance bands of a solid. Trap levels which are near the conduction band (shallow traps) are heavily affected by fading at room temperature [73]. For the storage time experiment the sample was annealed at  $500 \pm 1$  °C for 1 hour than, 12 Gy dose exposed each time and left fading. The storage time experiments were performed for different time periods from 1 day to 4 weeks for dark fading, and from 1 week to 3 weeks for light fading. The measured glow curves of  $\text{CaF}_2: \text{Dy}$  at the end of the planned storage periods are shown in figure 5.13. As seen from this figure, peak 1 was neglected after 1 week storage time due to its fast fading. The low temperature peaks 1-5 are quickly decreased while high temperature peaks 6-8 are not sufficiently influenced from storage periods at room temperature in the dark. As seen from figure 5.14, P1-P5 reduced to typically 40 % of their original value after 4 weeks. The storage time experiment performed in the light, the situation

is different; both low and high temperature peaks were highly affected from the storage times such as P1-P5 reduced to nearly 75% and P6-P8 reduced to 25% of their original value.



(a)



(b)

Figure 5.13 A set of TL glow curves for TLD-200 crystal measured after different storage times at room temperature (a) in the dark, (b) under light. All glow curves were read out at  $1^{\circ}\text{C} / \text{s}$  after the samples were exposed to an irradiation of 12 Gy

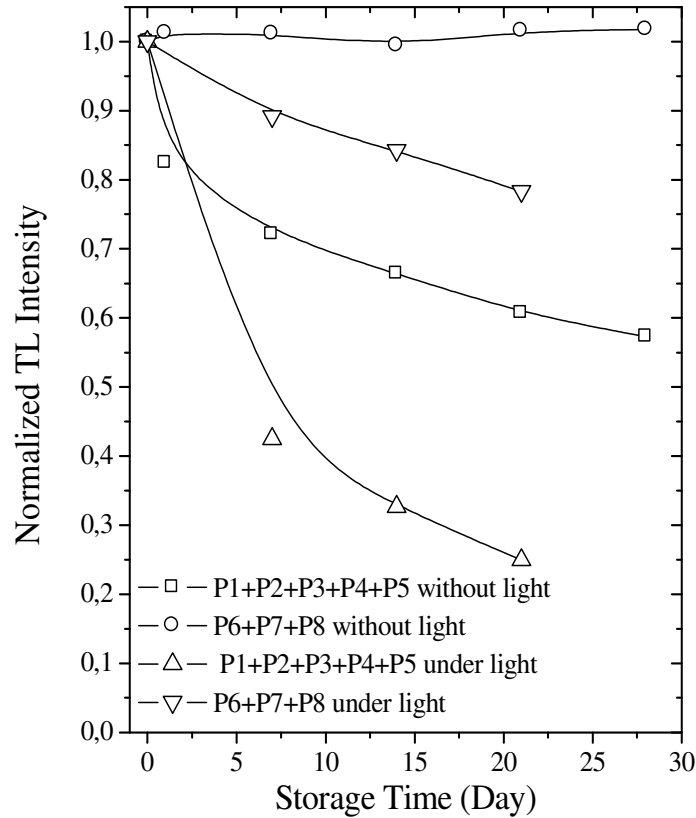


Figure 5.14 The normalized TL intensity of the glow curves after planned storage time periods both in the dark and under light

## 5.2 The effect of heating rate on the dose response of $\text{CaF}_2: \text{Tm}$ (TLD-300)

Thulium-doped calcium fluoride,  $\text{CaF}_2: \text{Tm}$ , dosimeters may be obtained as single crystals, extruded rods and hot chips. Available sizes are the same as those of the other popular  $\text{CaF}_2$  materials (viz.  $0.32 \times 0.32 \times 0.9 \text{ mm}^3$ ) and the methods of growth are also the same.  $\text{CaF}_2: \text{Tm}$  TL dosimeters were first introduced in 1977 [74] and are sold commercially by Bicron-NE (Harshaw) as TLD-300. Dosimetric quality material contains about 0.35 mol% Tm. TLD-300 are known to be particularly useful for the dosimetry of densely ionising radiation. The glow curve of these detectors consists of two well-separated peaks (called peaks 3 and 5), each exhibiting a different dependence on the ionisation density of the radiation (Linear Energy Transfer, LET). The ease with which peaks 3 and 5 can be separated in the glow curve and their good stability, make this TL detector particularly useful in certain applications, such as estimation of radiation quality or dose measurements in mixed

radiation fields in spite of its high  $Z_{\text{eff}} = 16.3$ .  $\text{CaF}_2: \text{Tm}$ , first mentioned by Lukas and Kapsar (1977), has been receiving considerable attention ever since [75].

Bos and Dielhof [76] reported that the main peaks (peak 3 and 5) have activation energies of 1.15 eV and 1.54 eV respectively, with corresponding frequency values,  $s$ , of  $4 \times 10^{12} \text{s}^{-1}$  and  $1 \times 10^{14} \text{s}^{-1}$ . They have also demonstrated that the kinetics for all the peaks is first order. Unlike LiF, the trapping parameters found for the TL peaks in  $\text{CaF}_2: \text{Tm}$  are found to be invariant with heating rate. This suggests that the complex defect interactions during heating found in LiF:Mg dosimeters are not active in this material. This is consistent with what is known about the thermal stability of the rare earth defects (aggregates) in alkaline earth fluorides [77]. The main emission peaks are at 360 nm, 450 nm, 465 nm and 650 nm in the visible region corresponding to internal Tm transitions. In addition to these visible emission bands, strong luminescence in the infrared, at 795 nm, is also observed [78].

The mechanism for TL production in Tm-doped  $\text{CaF}_2$  are suggested to be similar to those for Dy-doped material with the emission stemming from  $\text{Tm}^{+3}$  ions in centres of lower symmetry than cubic [3]. Phototransfer studies by Lakshman and Tiwari [79] indicate that peak 5 complex near 270 °C is caused by the release of electrons (from unknown sites), with the emission of  $\text{Tm}^{+3}$  being stimulated by energy transfer. Hole release rather than  $\text{F}^{\circ}$  interstitial movement is preferred by these authors as the source of the TL emission at lower temperatures, i.e. up to and including peak 3. Clearly the actual mechanisms are far from certain and, as with most dosimetric forms of  $\text{CaF}_2$ , not enough detailed studies have been performed to enable a clear picture to emerge.

As seen from figure 5.15 the glow curve structure of  $\text{CaF}_2: \text{Tm}$  consist of six first order peaks located at temperatures  $\approx 90$  (P1),  $\approx 110$  (P2),  $\approx 150$  (P3),  $\approx 180$  (P4),  $\approx 245$  (P5), and  $\approx 270$  (P6) °C. The glow curves of TLD-300 are shown in Fig. 5.16a and 5.16b measured after an annealing procedure of  $400 \pm 1$  °C for 1 hour by irradiation at room temperature from exposed to beta rays between 0.04 Gy and 14 kGy and readout at a linear heating rate of  $\beta = 1$  °C/s.

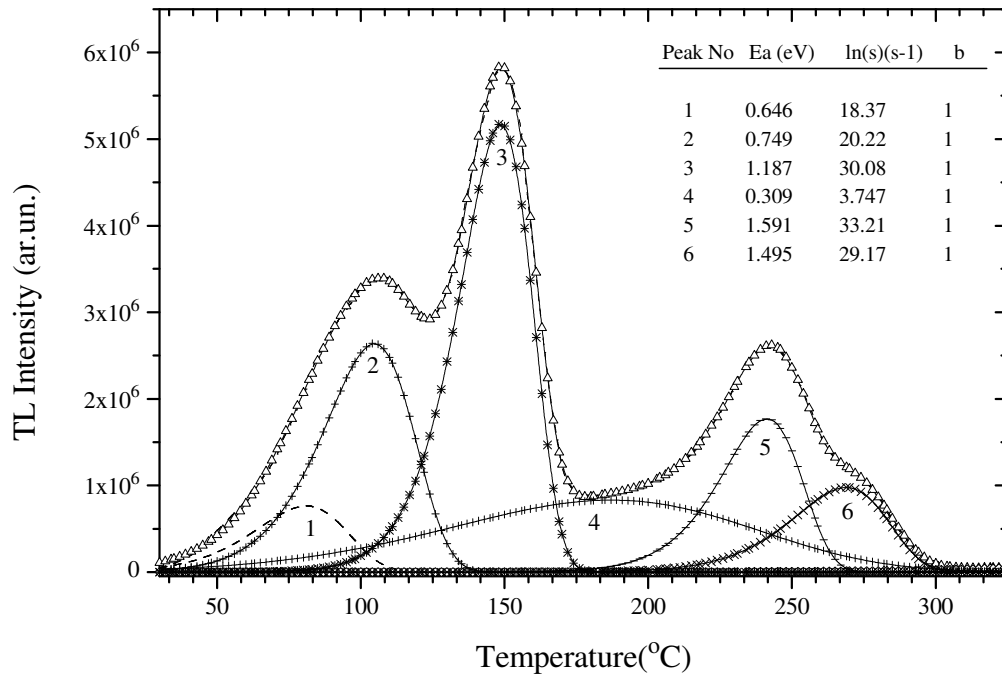


Figure 5.15 The CGCD analyzed glow curves of Tm-doped CaF<sub>2</sub> measured after 12 Gy irradiation by beta ray at room temperature after an annealing procedure of 1 hour at 400 °C

Figure 5.17 shows the growth of the height of the peaks as a function of dose. As seen from this figure, P1 and P2 shows linear behaviour up to 10 Gy, after a region of supralinear region these peaks go into the sublinear region after 10<sup>3</sup> Gy. The linearity of the P3 continuous nearly up to 10 Gy then this peak goes to the sublinear region. P4 also shows linear behaviour up to 10 Gy then this peak shows supralinear behaviour, after 10<sup>3</sup> Gy the peak saturates and goes into sublinear region. P5 also shows linear behaviour up to 10 Gy then this peak shows supralinear behaviour nearly up to 10<sup>4</sup> Gy after that P5 saturates and shows sublinear behaviour. P6 shows linear behaviour nearly up to 5 Gy and going to the supralinear region up to 10<sup>3</sup> Gy then these peaks saturate after this dose level showing sublinear behaviour at a linear heating rate of 1 °C/s.

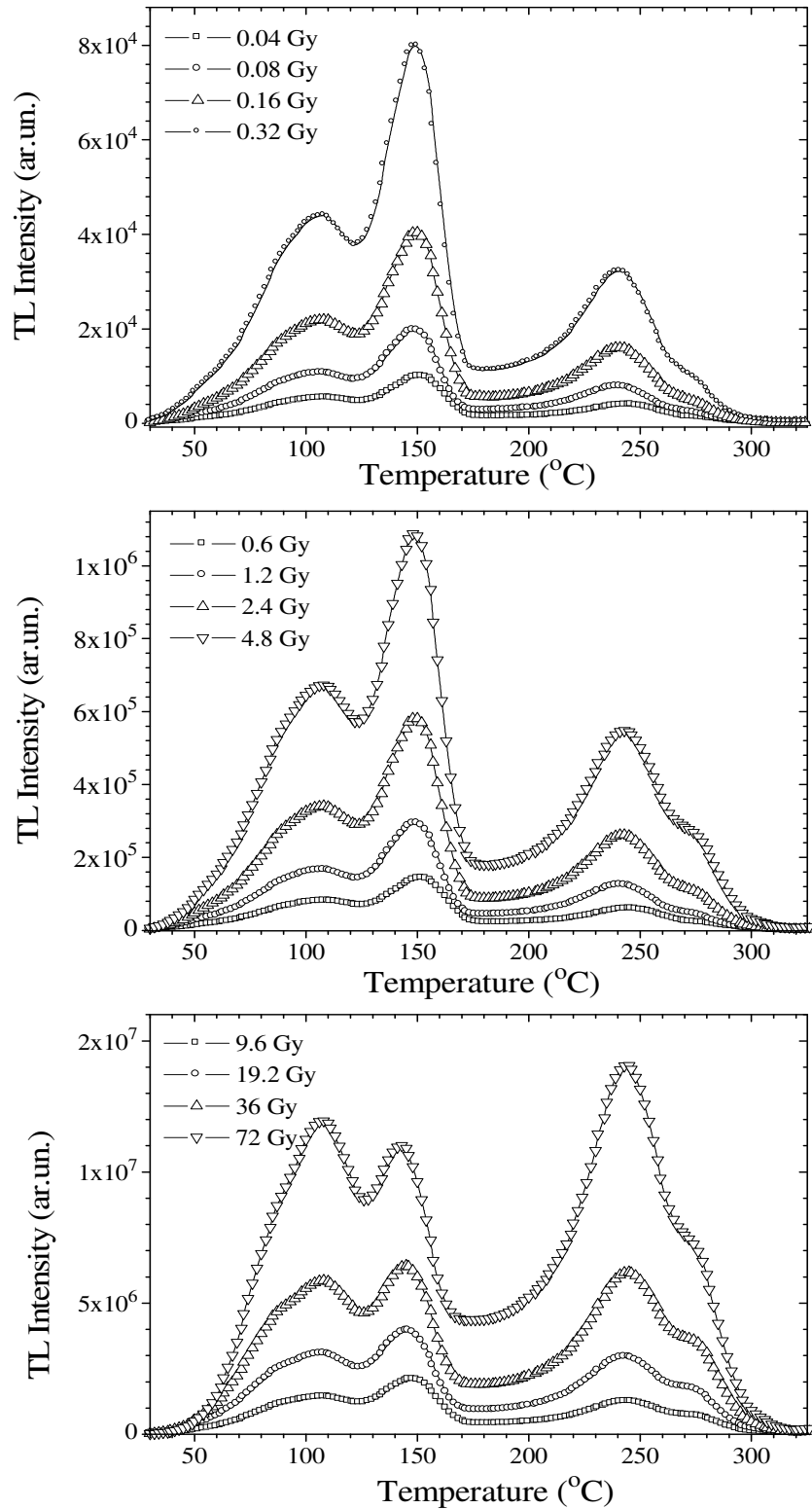


Figure 5.16a A typical glow curve of TLD-300 measured after an annealing procedure of  $400 \pm 1$  °C for 1 hour by irradiation at room temperature from exposed to beta rays from 0.04 Gy up to 72 Gy and readout at a linear heating rate of  $\beta = 1$  °C/s



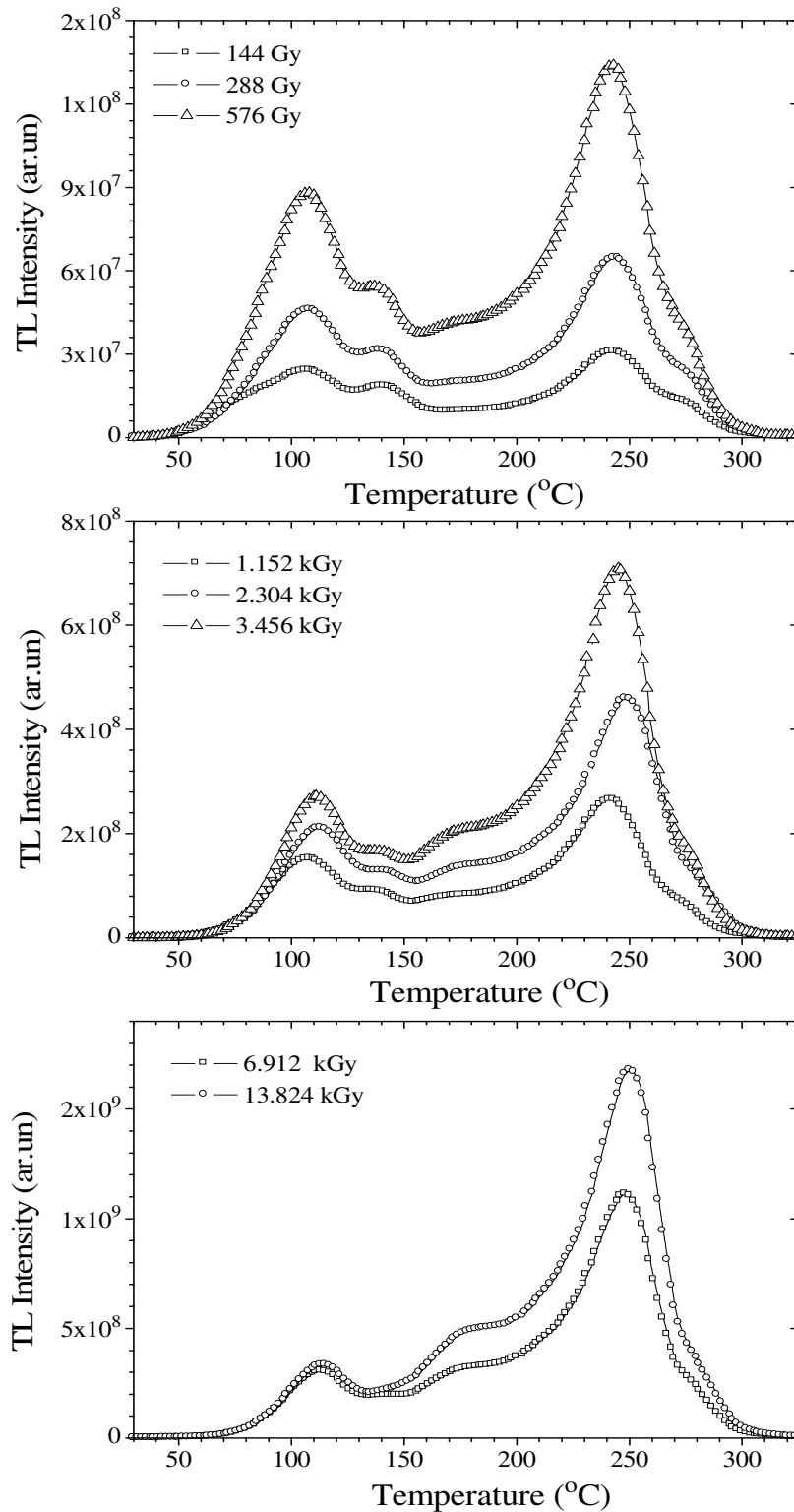


Figure 5.16b A typical glow curve of TLD-300 measured after an annealing procedure of  $400 \pm 1$  °C for 1 hour by irradiation at room temperature from exposed to beta rays from 144 Gy up to 14 kGy and readout at a linear heating rate of  $\beta = 1$  °C/s

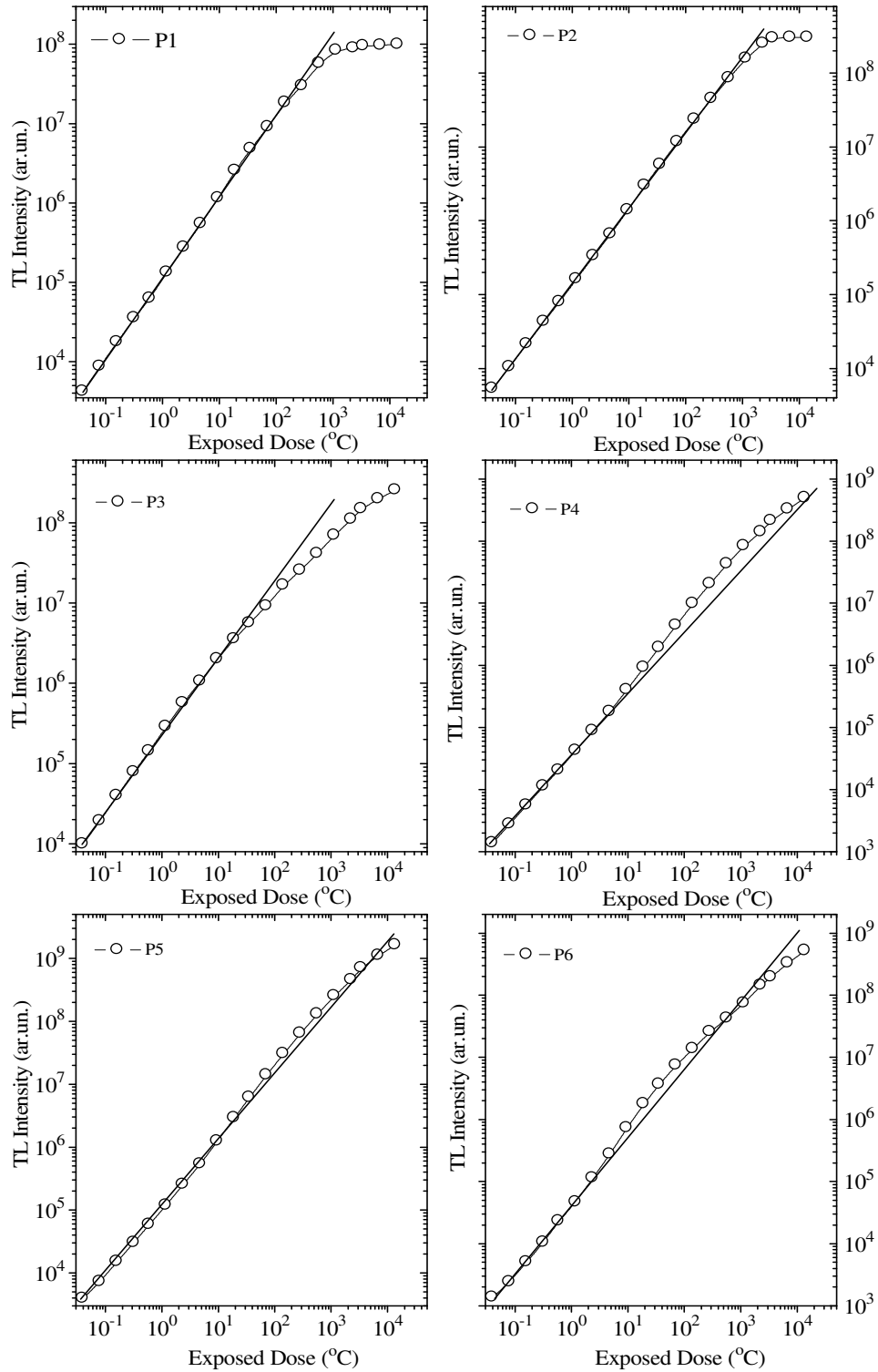


Figure 5.17 The growth of the height of the peaks from TLD-300 as a function of dose at a linear heating rate of  $\beta = 1$  °C/s

It is also seen from the figure 5.18 that, P1 shows linear characteristics ( $f(D)=1$ ) up to 1 Gy, followed by a region of supralinear growth ( $f(D)>1$ ), this peak gradually go into a region of sublinear growth ( $f(D)<1$ ) after  $10^3$  Gy. Peak 2 shows linear behaviour, ( $f(D)=1$ ), nearly up to 1 Gy, after a region of supralinear growth, ( $f(D)>1$ ), this peak saturates at a dose of  $10^4$  Gy and shows a sublinear, ( $f(D)<1$ ), behaviour. Peak 3 shows linear behaviour, ( $f(D)=1$ ), up to 5 Gy, followed by a region of supralinear growth, ( $f(D)>1$ ), this peak gradually goes into a region of sublinear growth, ( $f(D)<1$ ), after this dose level. Peak 4 also shows linear characteristic, ( $f(D)=1$ ), up to 1 Gy, after a region of supralinear growth, ( $f(D)>1$ ), this peak also saturates after at high dose level, and shows sublinear characteristics, ( $f(D)<1$ ). P5 and P6 show similar characteristics, i.e: both peaks are linear up to 1 Gy, ( $f(D)=1$ ), after the supralinear region, ( $f(D)>1$ ), these peaks saturates and go into the sublinear region, ( $f(D)<1$ ).

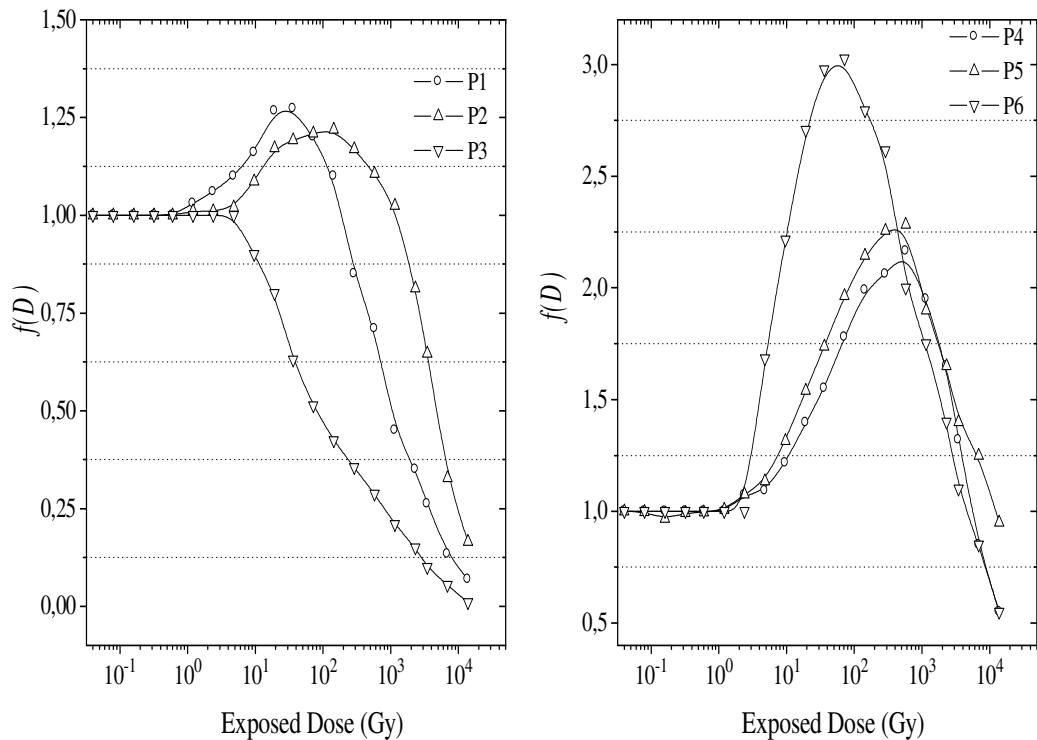


Figure 5.18 The dose response function  $f(D)$  vs  $D$  of TLD-300 ( $\beta=1$  °C/s)

The dose rate behavior of the total peak area of the glow peaks of TLD- 300 crystal was also investigated by using the supralinearity index,  $f(D)$ , and superlinearity index,  $g(D)$ . To evaluate the superlinearity index, equation 5.5 was used. Where the constants are:  $a= 4.456$ ,  $b= 2.201$ ,  $c= -0.000701$ ,  $d= 1.3144$  and  $e= -9.3711$ .

$$S(x) = (a + bx + cx^2 + dx^3 + ex^4) \quad (5.5)$$

$$g(D) = \left[ \frac{2x(c + 3x(d + 2ex))}{b + x((2c + x(3d + 4ex))} \right] + 1 \quad (5.6)$$

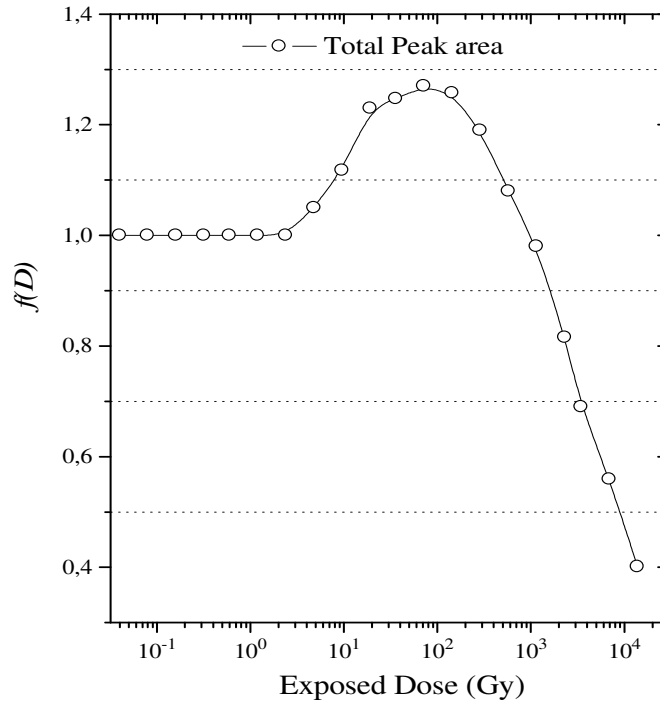


Figure 5.19 The dose response function  $f(D)$  vs  $D$  of TLD-300 ( $\beta=1$  °C/s)

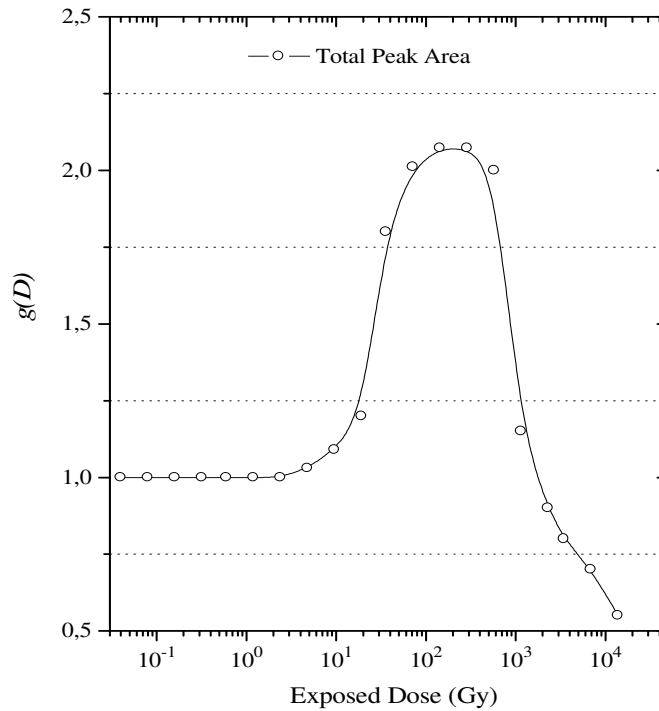


Figure 5.20 The superlinearity function  $g(D)$  vs  $D$  of TLD-300 ( $\beta=1$  °C/s)

As shown from figures 5.19 and 5.20 the total peak area of the glow peaks shows linear characteristics nearly up to 5 Gy ( $f(D)=1$  and  $g(D)=1$ ), after a region of nonlinear growth ( $f(D)>1$  and  $g(D)>1$ ), it goes into a sublinear region after  $10^3$  Gy dose level having  $f(D)<1$  and  $g(D)<1$ .

The dose response characteristics of the glow peaks of TLD-300 were also obtained by recording the glow curves at a linear heating rate of 10 °C/s. Figure 5.21a and 5.21b show some of the selected glow curves of TLD-300 after different dose levels using a linear heating rate of 10 °C/s. Figure 5.22 shows the growth of the height of the peaks as a function of dose. As seen from this figure, P1 shows linear behaviour up to 5 Gy, after a region of supralinear growth up to  $10^3$  Gy, this peak goes into the sublinear region after  $10^3$  Gy. The linearity of the P2 continuous nearly up to  $10^3$  Gy, after this dose level this peak goes to the sublinear region. P3 shows linear behaviour nearly up to 10 Gy then this peak also saturates and goes into sublinear region after this dose level. The linearity of the P4 continuous up to 50 Gy, then this peak shows supralinear behaviour nearly up to  $10^4$  Gy after this dose; P4 saturates and shows sublinear behaviour. P5 shows linear characteristics nearly up to 50 Gy, after a region of supralinear growth, it saturates and goes into the sublinear region after  $10^3$  Gy dose level. P6 shows linear behaviour up to high doses, but it

saturates after  $10^3$  Gy dose before showing supralinear growth at a linear heating rate of  $10$  °C/s.

The dose response function,  $f(D)$ , is also evaluated by using equation 3.3 at a linear heating rate of  $10$  °C/s. As seen from the figure 5.23 the curves exhibit the main features characteristic of the dose response that, P1 shows linear characteristics ( $f(D)=1$ ) up to 1 Gy, followed by a region of supralinear growth ( $f(D)>1$ ), this peak gradually goes into a region of sublinear growth ( $f(D)<1$ ) after  $10^3$  Gy. Peak 2 shows linear behaviour, ( $f(D)=1$ ), nearly up to 1 Gy, after a region of supralinear growth, ( $f(D)>1$ ), this peak saturates near to a dose level of  $10^4$  Gy and shows a sublinear, ( $f(D)<1$ ), behaviour. Peak 3 shows linear behaviour, ( $f(D)=1$ ), up to 5 Gy, followed by a region of supralinear growth, ( $f(D)>1$ ), this peak gradually goes into a region of sublinear growth, ( $f(D)<1$ ), after this dose level. Peak 4 also shows linear characteristic, ( $f(D)=1$ ), up to 1 Gy, after a region of supralinear growth, ( $f(D)>1$ ), this peak also saturates after at high dose level, and shows sublinear characteristics, ( $f(D)<1$ ). P5 and P6 show similar characteristics, i.e: both peaks are linear up to 1 Gy, ( $f(D)=1$ ), after the supralinear region, ( $f(D)>1$ ), these peaks saturates and go into the sublinear region, ( $f(D)<1$ ), after  $10^3$  Gy dose level.

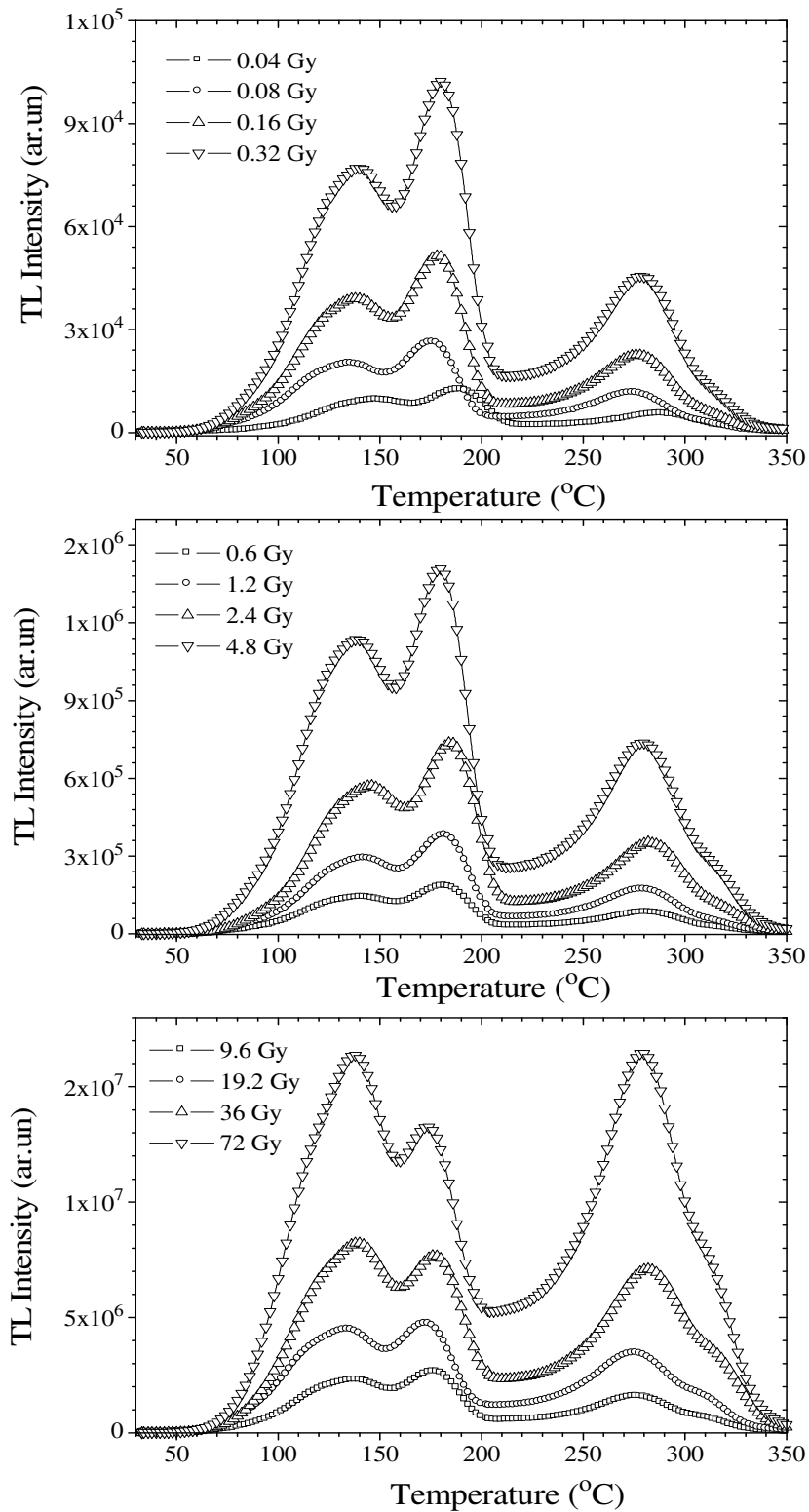


Figure 5.21a A typical glow curve of TL D-300 measured after an annealing procedure of  $400 \pm 1$  °C for 1 hour by irradiation at room temperature from exposed to beta rays from 0.04 Gy up to 14 kGy and readout at a linear heating rate of  $\beta = 10$  °C/s

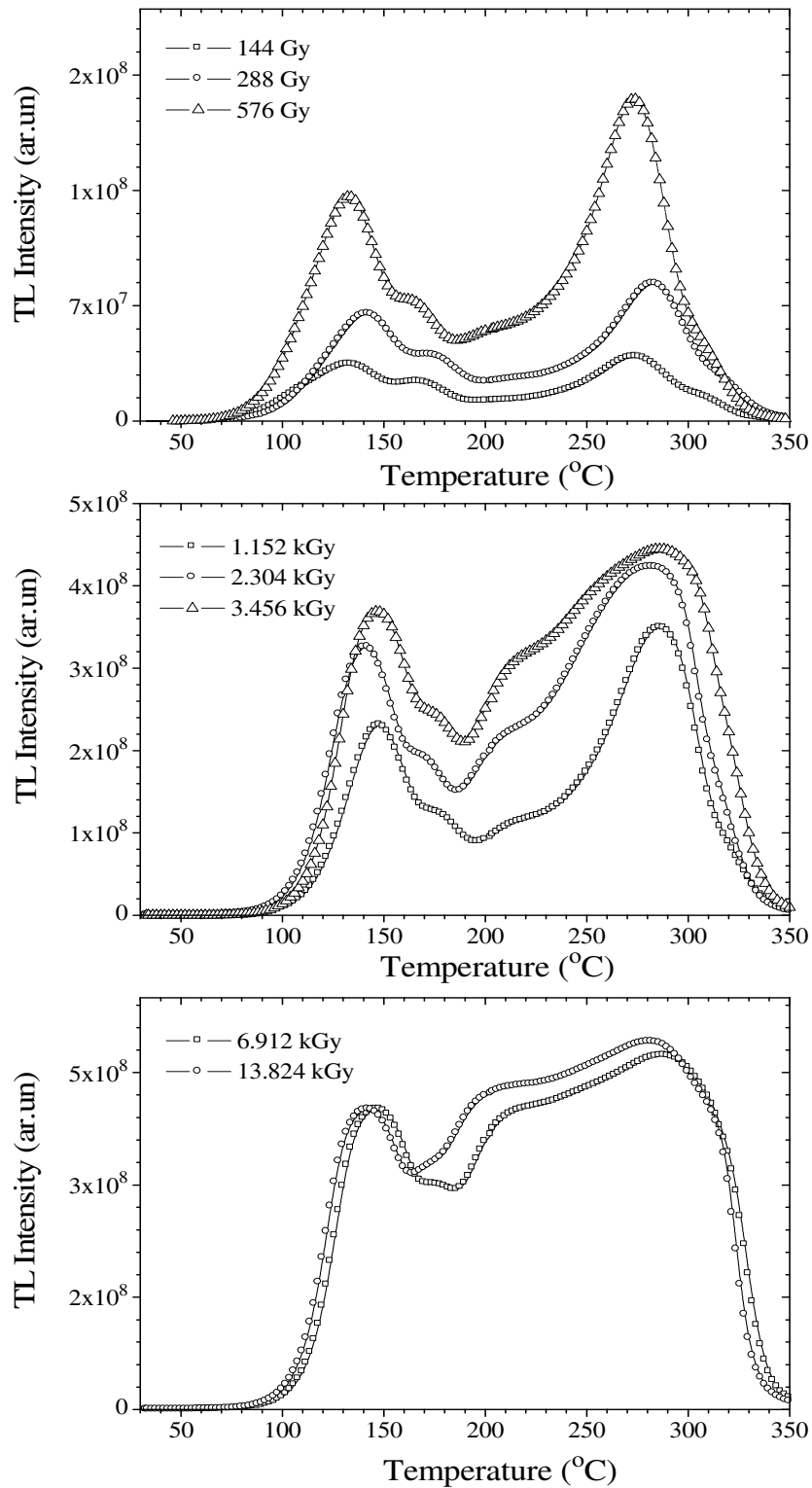


Figure 5.21b A typical glow curve of TLD-300 measured after an annealing procedure of  $400 \pm 1$  °C for 1 hour by irradiation at room temperature from exposed to beta rays from 0.04 Gy up to 14 kGy and readout at a linear heating rate of  $\beta = 10$  °C/s



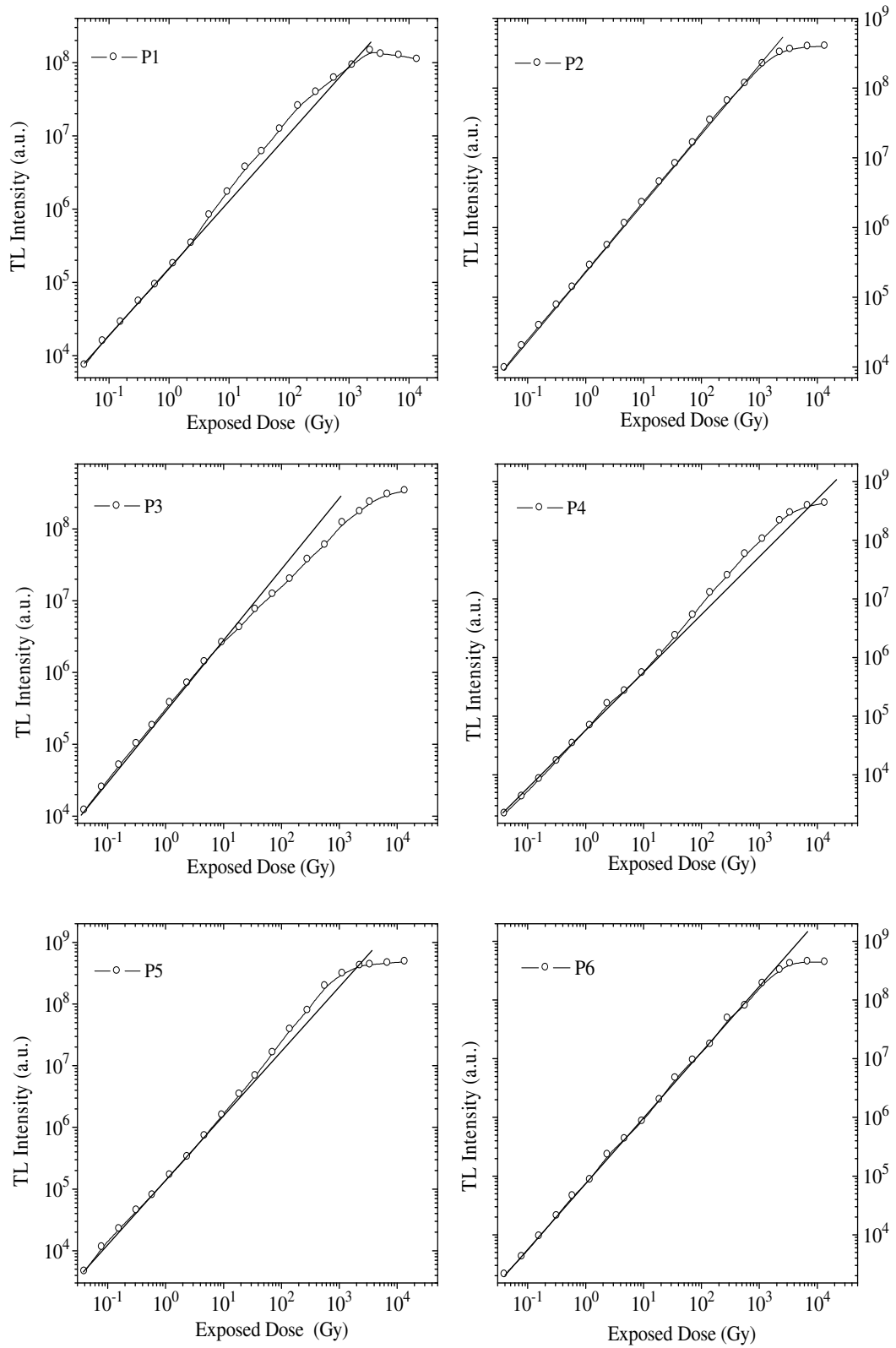
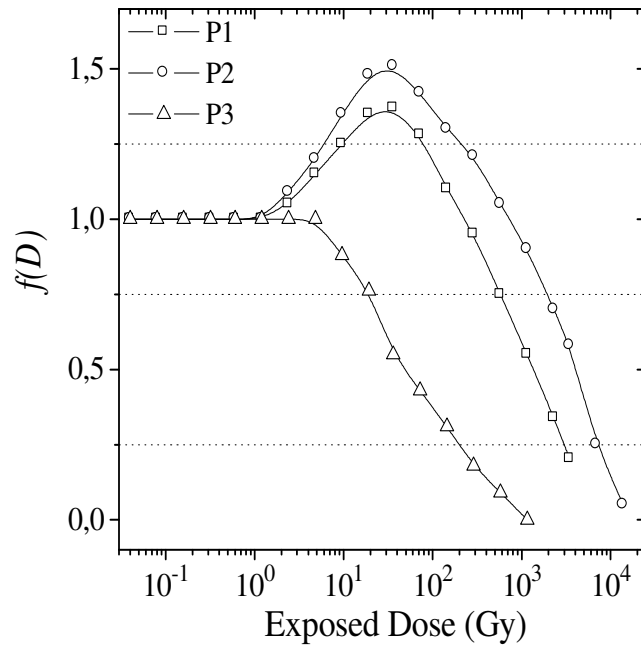
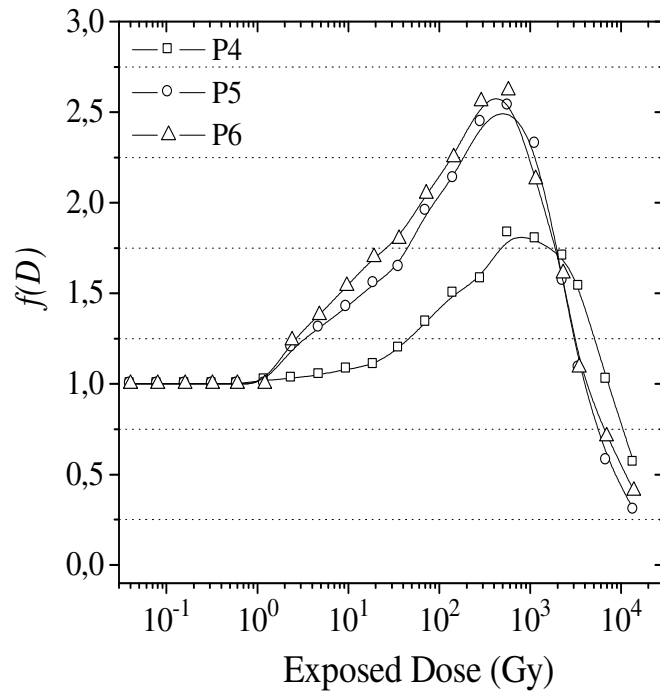


Figure 5.22 The growth of the height of the peaks from TLD-300 as a function of dose at a linear heating rate of  $\beta = 10 \text{ }^\circ\text{C/s}$



(a)



(b)

Figure 5.23 The dose response function  $f(D)$  vs  $D$  of TLD-300 (a) P1, P2, P3 (b) P4, P5, P6 ( $\beta=10$  °C/s)

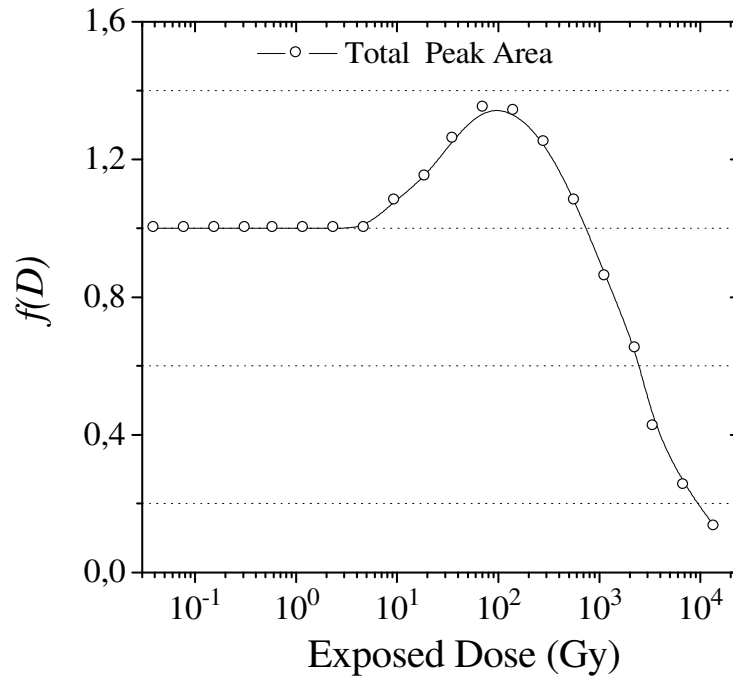
The dose response functions  $f(D)$  and  $g(D)$  were also evaluated for the total peak area of the glow peaks of TLD-300 crystal at a linear heating rate of  $10\text{ }^\circ\text{C/s}$ . To calculate the superlinearity index, equation 5.7 was used. Where the constant are:  $a= -13.517$ ,  $b= 0.001$ ,  $c= 3.970$  and  $d= 4.754 \times 10^{-8}$

$$S(x) = \frac{a + cx}{1 + bx + dx^2} \quad (5.7)$$

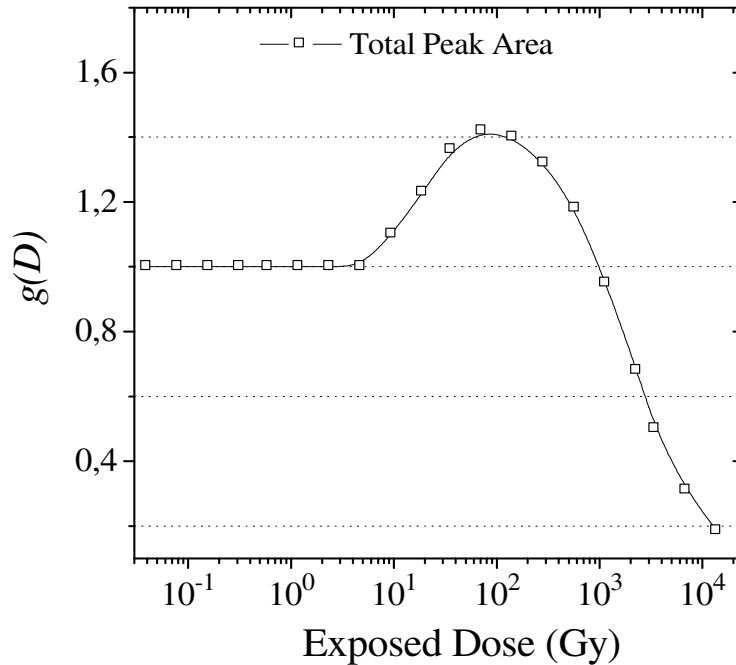
By applying the definition of superlinearity index as stated in equation 3.1, it can be found that;

$$g(D) = \frac{4 + 2bx}{1 + x(b + dx)} + \frac{2(c - a(b + dx))}{a(b + 2dx) + c(-1 + dx^2)} - 1 \quad (5.8)$$

As seen from figure 5.24, the total peak area of the glow peaks of TLD-300 crystal shows linear behaviour nearly up to 5 Gy (both  $f(D)$  and  $g(D)=1$ ), after a region of nonlinear growth, (both  $f(D)>1$  and  $g(D)>1$ ), saturation effect set in after  $10^3$  Gy dose level, (both  $f(D)<1$  and  $g(D)<1$ ).



(a)



(b)

Figure 5.24 The dose response functions (a)  $f(D)$  and (b)  $g(D)$  vs  $D$  of TLD-300 ( $\beta=10\text{ }^\circ\text{C/s}$ )

The behaviour of the glow curves and the effect of thermal quenching due to the heating rate on the total peak area of glow curves were also investigated for  $\text{CaF}_2:\text{Tm}$  (TLD-300) at different linear heating rates between  $1\text{ }^\circ\text{C/s}$  and  $30\text{ }^\circ\text{C/s}$ . Figure 5.25 shows some of the selected glow curves of TLD-300 at linear heating rates between  $1\text{ }^\circ\text{C}$  and  $30\text{ }^\circ\text{C}$ . As seen from this figure the peak temperatures of all peaks are shifted higher temperatures when the heating rate increases as expected in theory. It is seen from figure 5.26, the total peak area of the glow curves decreases as the heating rate increases. The total area of the glow curves were normalized at the lower heating rate ( $1\text{ }^\circ\text{C s}^{-1}$ ) and it can be seen that the decrease in the integrated area of the peaks by about 50 %.

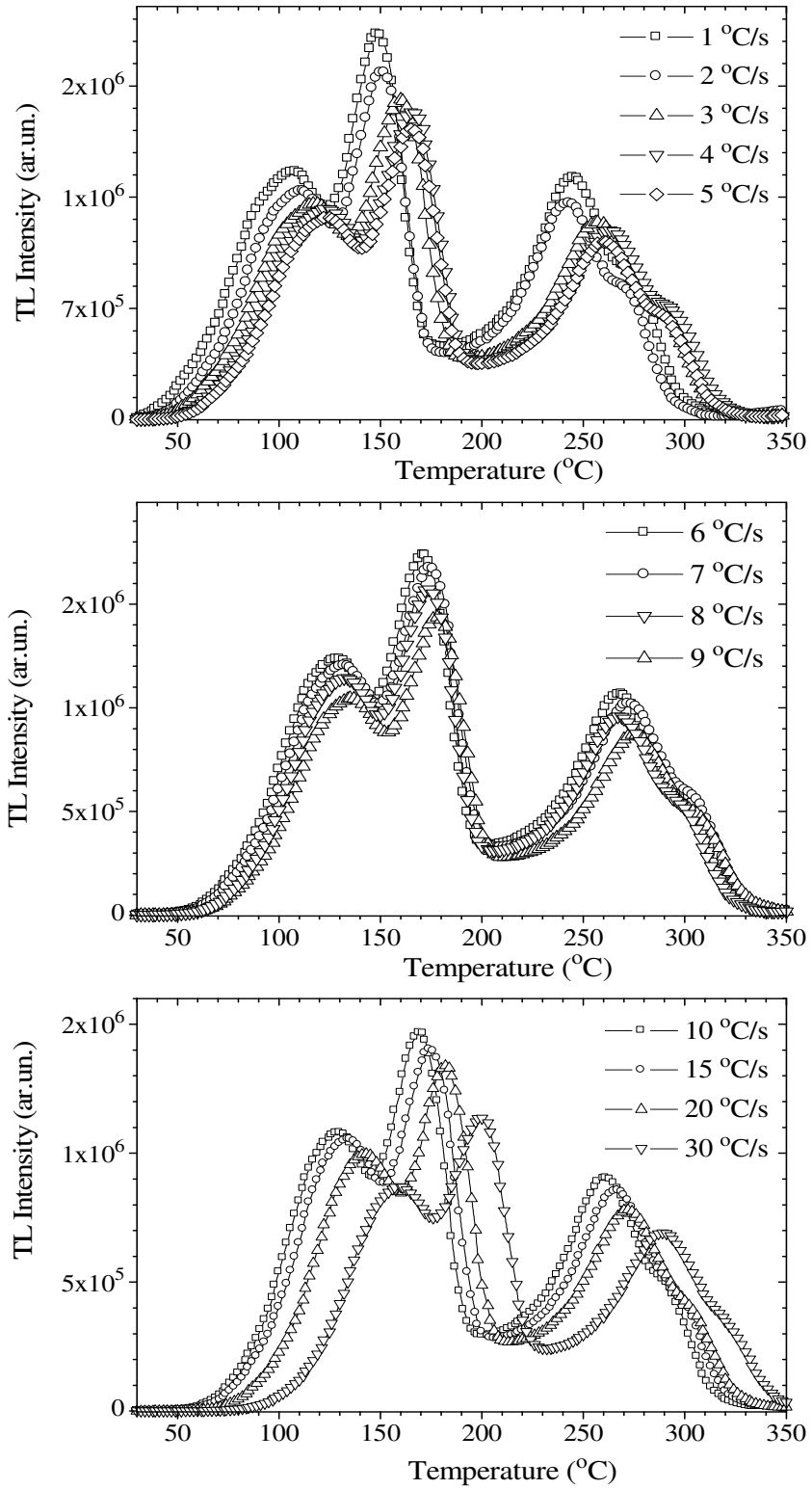


Figure 5.25 The glow curves of TLD-300 crystals irradiated with  $^{90}\text{Sr}$ - $^{90}\text{Y}$  beta source at linear heating rates between 1 °C/s and 30 °C/s ( $D=12$  Gy)

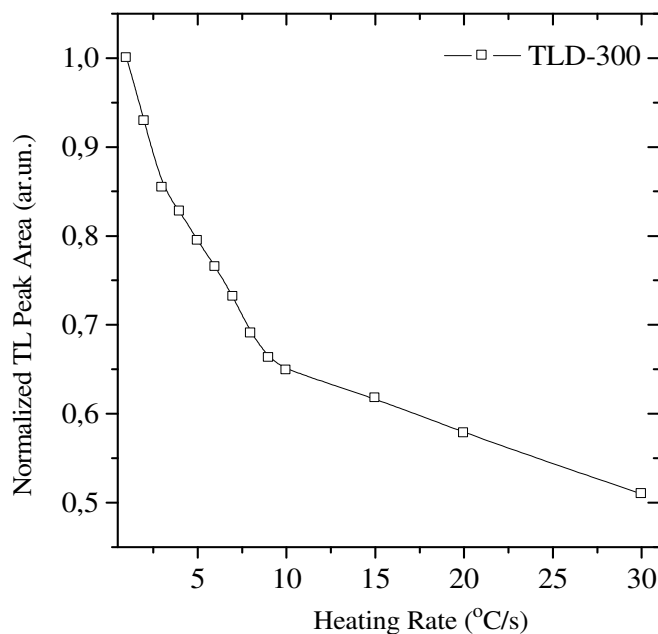
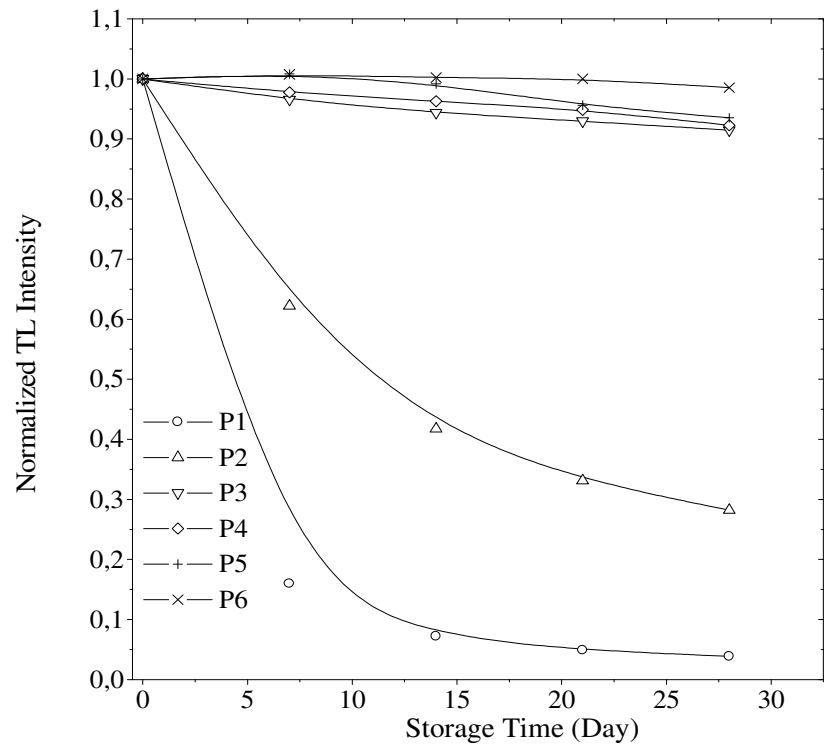
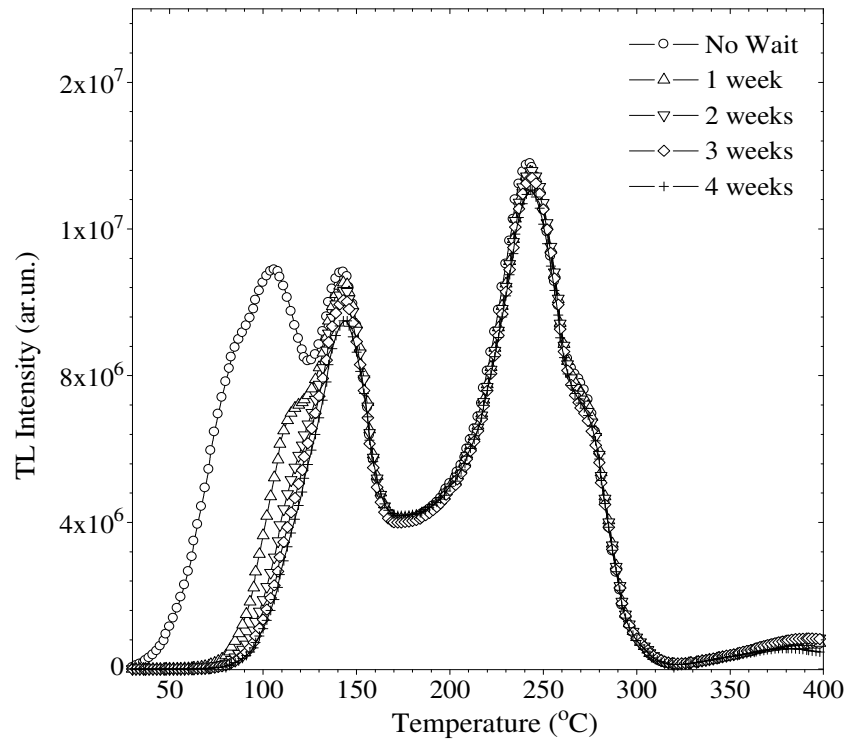


Figure 5.26 The normalized total TL peak area of TLD-300 crystals irradiated with  $^{90}\text{Sr}$ - $^{90}\text{Y}$  beta source at linear heating rates between 1 °C/s and 30 °C/s (D=12 Gy)

For the storage time experiment the sample was annealed at  $400 \pm 1$  °C for 1 hour than, 72 Gy dose exposed each time and left fading. The storage time experiments were performed for different time periods from 1 day to 4 weeks for dark fading, and from 1 week to 3 weeks for light fading. The measured glow curves of  $\text{CaF}_2$ : Tm at the end of the planned storage periods are shown in figure 5.27. As seen from this figure, P1 reduced to 95 %, P2 70 % of their original values. P3, P4 and P5 are reduced to nearly 5 % of their original values but P6 is not affected from the planned storage time period of 4 weeks, performed in the dark. In the optical fading experiment, P1 reduced to 98 % and P2 reduced to 85 % of their original values. P3 reduced to 10 % and P4 reduced to 3 % of their original value. P5 and P6 are almost not affected from the storage time period of 3 weeks.



(a)

Figure 5.27a A set of TL glow curves for TLD-300 crystal measured after different storage times at room temperature and normalized TL intensity for dark fading. All glow curves were read out at  $1^{\circ}\text{C} / \text{s}$  after exposing to an irradiation of 72 Gy

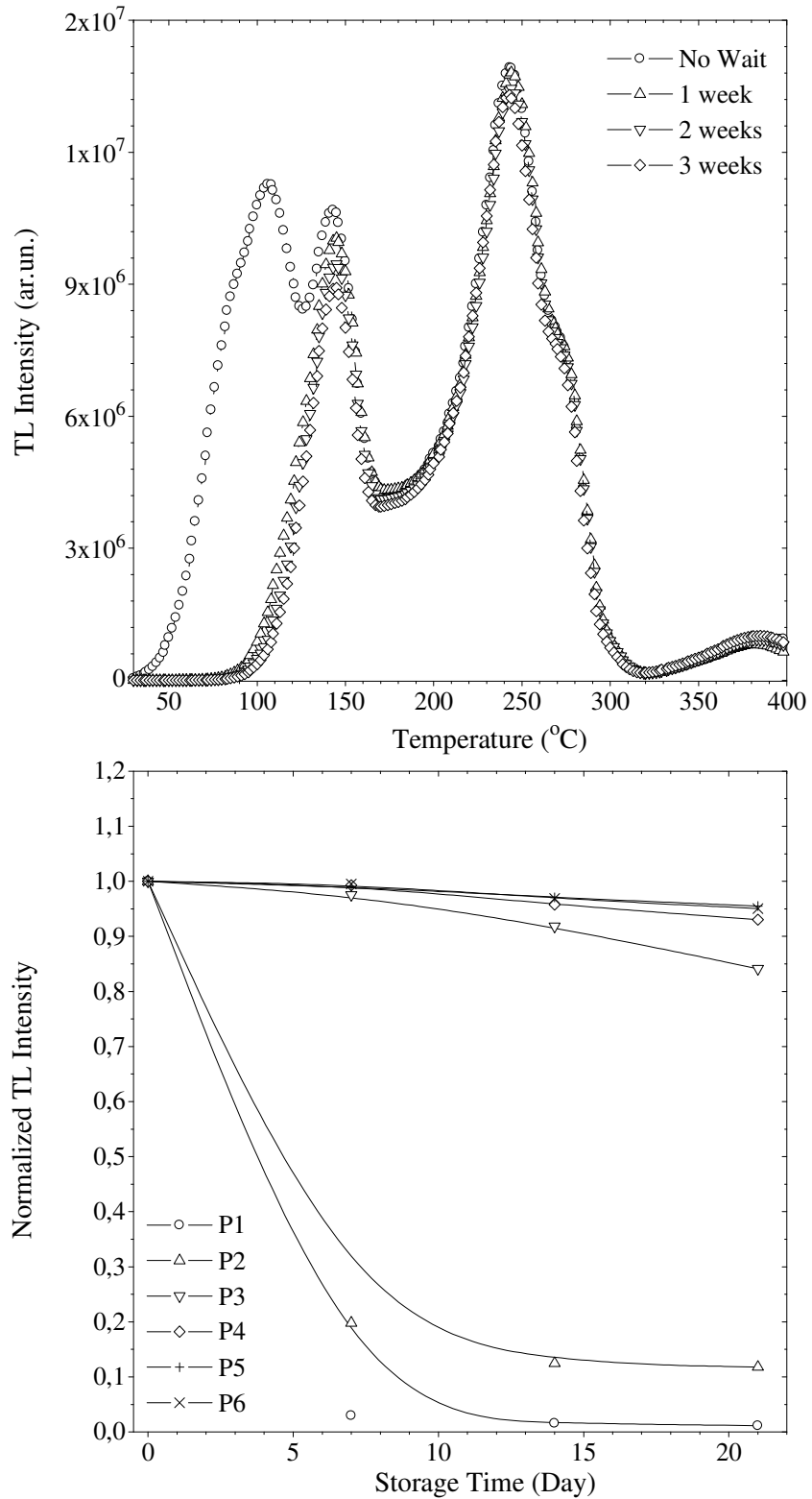


Figure 5.27b A set of TL glow curves for TLD-300 crystal measured after different storage times at room temperature and normalized TL intensity for optical fading. All glow curves were read out at  $1^{\circ}\text{C} / \text{s}$  after exposing to an irradiation of 72 Gy



### 5.3 The effect of heating rate on the dose response of CaF<sub>2</sub>: Mn (TLD-400)

CaF<sub>2</sub>: Mn (TLD-400) dosimeters may be obtained as single crystals, extruded rods and hot pressed chips. Single crystal CaF<sub>2</sub>: Mn suitable for dosimetry can be grown using the Bridgman-Stockbarger technique with a Mn doping level of 3 mol% in the melt. Generally, doping levels in the final dosimetric material are less than this and, typically, for 3 mol% Dy in the melt, one can expect approximately 1.5 mol% in the dosimeter [3]. The lattice of CaF<sub>2</sub> could be represented as two cubic lattices inserted one into another: a cubic lattice composed of F<sup>-</sup> ions and a face-centred cubic lattice composed of Ca<sup>2+</sup> ions. Manganese substitutes for calcium at regular sites of CaF<sub>2</sub> lattice, and only divalent Mn<sup>2+</sup> is suitable to substitute Ca<sup>2+</sup> and to give luminescence. The smaller ionic radius of Mn<sup>2+</sup> compared to Ca<sup>2+</sup> (ionic radii of 8-coordinate Mn<sup>2+</sup> and Ca<sup>2+</sup> are 0.110 and 0.126 nm, respectively, causes lattice strains in doped with Mn CaF<sub>2</sub>. This makes the solid solution sensitive to the Mn concentration and complicates doping technologies. So, one needs to introduce Mn into CaF<sub>2</sub> lattice as uniformly as possible and to avoid oxidation of Mn<sup>2+</sup> to higher oxidation states at annealing. Once oxidised, manganese becomes unstable in the lattice and falls out of the solid solution. This causes TL dosimeters to degrade during cycled annealing while they are practically used, due to further oxidation and losses of Mn<sup>2+</sup>. Mechanical mixing of the dopant with CaF<sub>2</sub> followed by annealing produces non-uniform and unstable solid solutions due to the low diffusion rate of Mn<sup>2+</sup> at the temperature of final annealing. The dopant is distributed more uniformly only when the starting material is obtained by co-precipitation of MnF<sub>2</sub> together with CaF<sub>2</sub> from the initial solution [80].

Mn<sup>2+</sup> doped CaF<sub>2</sub> has been used over the past four decades as an important thermoluminescent (TL) dosimetry due to its high sensitivity (compared to TLD-100) to doses as low as 50 µGy and a simpler glow curve structure. Therefore, it has found widespread use in the field of environmental and personnel radiation dosimetry, despite some problems associated with batch-to-batch irreproducibility, anomalous fading, degradation during re-use, perennial zero dose problem and its poor energy response resulting from its high effective atomic number compared with tissue. The lack of tissue equivalence precludes its regular use as a personal dosimeter, but its higher sensitivity make it an excellent environmental dosimetric material since exposure time in the field can be reduced accordingly [81,82]. In the

zero dose problems, TLDs without exposure to radiation read a dose of 0.1 mGy or more above the natural background level when stored in the dark (dependent on the prior exposure history of the sample). Over the past years much effort has been spent to identify the cause of this chronic problem and it was observed that the peak near 390 °C has a vital role on the dosimetric performance of this material [83]. Unless this peak is thoroughly cleaned either by heating the TLDs beyond 400 °C, the dosimetric peak near 290 °C is regenerated without further exposure to radiation and therefore the TLDs will produce a zero dose problem depending upon the previous dose and elapsed time after readout. On the other hand, when the high-temperature traps near and above 400 °C are completely depleted, optically or thermally, this problem is removed. Moreover, laser cleaning of this trap is preferred, because, this process, being performed at room temperature, will not reduce the sensitivity of the TLDs which might happen with heating above 400 °C. Another way to minimize the zero dose problems is lowering the concentration of  $Mn^{2+}$  in the material. This would reduce the formation of  $Mn^{2+}$  pairs which are thought to be the origin of the center responsible for zero dose problems.

As seen from 5.28 the glow curve structure of  $CaF_2: Mn$  consist of three first order peaks located at temperatures  $\approx 255$  (P1),  $\approx 295$  (P2),  $\approx 330$  (P3), °C at a heating rate of 1 °C/s. Before the investigation of TL properties of Mn-doped  $CaF_2$ , an annealing procedure was usually utilized to improve the performance of TL material before the irradiation, because; it is known that the heat-treatment before the irradiation is generally re-established the defect equilibrium that exists in the material and the heating can also empty the deep traps to avoid its influence on the TL sensitivity of a given peak since they can act as competitors. Some of the selected glow curves after different dose levels are shown in Fig. 5.29a and 5.29b. The experimental observations have clearly shown that there were no significant changes in the peak temperature of glow peak of  $CaF_2: Mn$  with increasing dose level. The positions of peak temperature of this peak are within the experimental error  $\pm 4$  °C for all the doses. This result indicates that the main glow peak or at least all of the individual glow peaks in the dosimetric glow peak of  $CaF_2: Mn$  should have first-order kinetics. On the other hand, the slight variations in the shape of the glow peak with increasing dose levels indicate that this peak no longer retains the original single

pattern. This observation reveals the fact that the main glow peak consists of more than one glow peak.

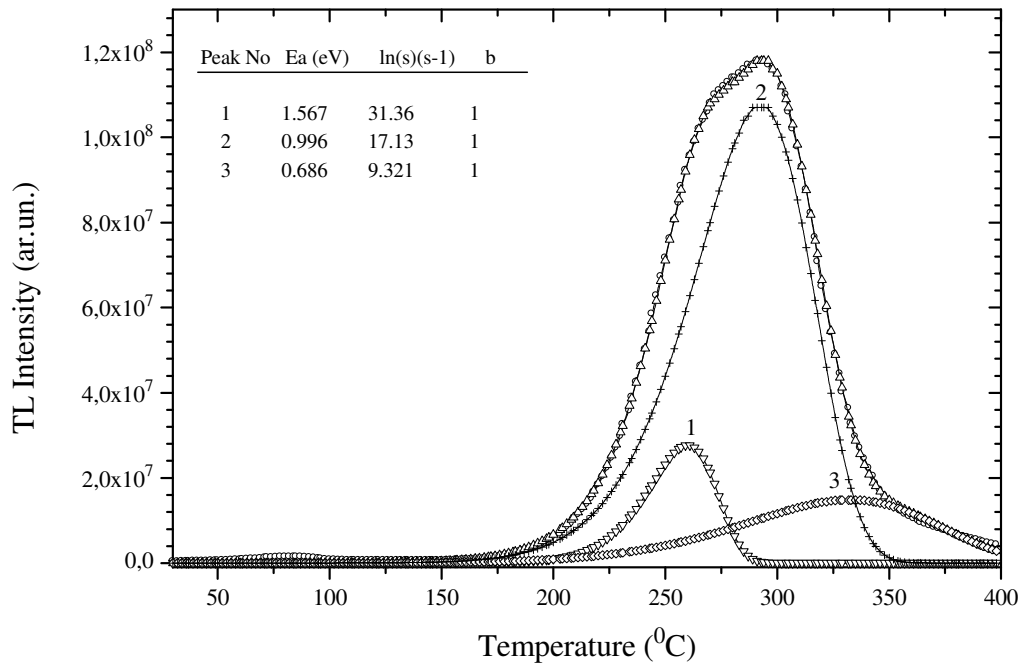


Figure 5.28 The CGCD analyzed glow curves of Mn-doped CaF<sub>2</sub> measured after 12 Gy irradiation by beta ray at room temperature after an annealing procedure of 30 min. at 400 °C

Figure 5.30 shows the variations of the peak areas of glow peaks of TLD-400 as a function of applied dose  $\beta=1$  °C/s. It is seen that the peak area of peak 1 shows linear behaviour up to  $\approx 10^2$  Gy. Then it goes into a supralinear region and saturates above  $\approx 10^4$  Gy. The dose response characteristics of peak 2 and 3 are similar to each other. As seen, they have linear behaviour nearly up to  $10^3$  Gy. Then, they saturate after this dose level. In figure 5.31, the  $f(D)$  functions of glow peaks of TLD-400 are depicted. As seen from this figure, the peaks 2 and 3 show linear characteristic ( $f(D)=1$ ) nearly up to 10 Gy, then they go into a region of supralinear growth ( $f(D)>1$ ) after this dose level. The linearity of peak 1 continues up to  $\approx 100$  Gy. After a region of supralinear growth ( $f(D)>1$ ), it saturates showing sublinear behavior ( $f(D)<1$ ) after  $10^4$  Gy dose level. Figure 5.32 shows growth of the height of the total area of the glow curve of TLD-400 and dose response function  $f(D)$  vs dose respectively. As it is seen from this figure that the total area of the glow curve shows linear characteristics up to 50 Gy ( $f(D)=1$ ), after a region of supralinear growth ( $f(D)>1$ ), a sublinear behavior sets in after a dose level of  $10^3$  Gy ( $f(D)<1$ ).

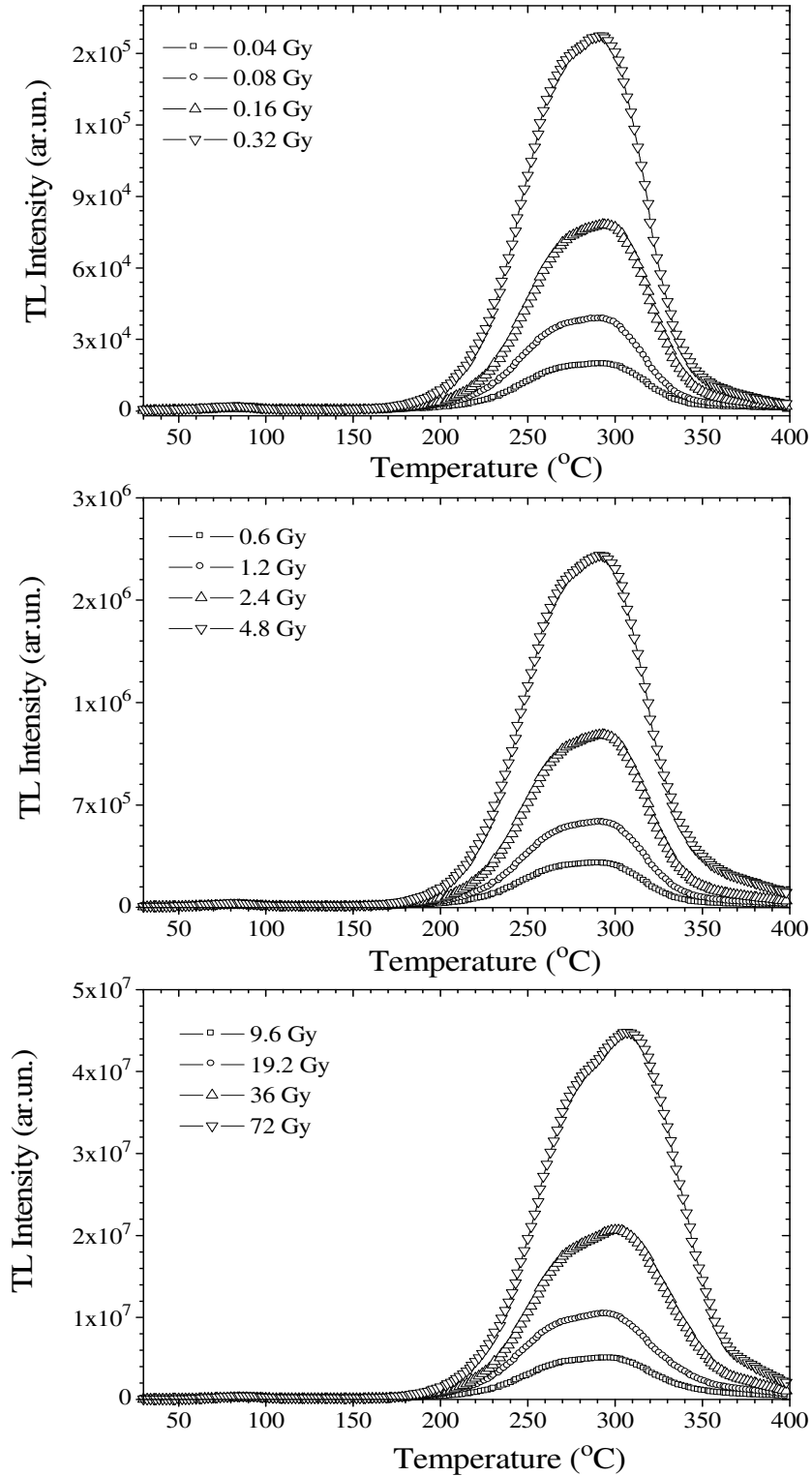


Figure 5.29a A typical glow curve of TLD-400 measured after an annealing procedure of  $400 \pm 1$  °C for 30 min by irradiation at room temperature from exposed to beta rays from 0.04 Gy up to 14 kGy and readout at a linear heating rate of  $\beta = 1$  °C/s

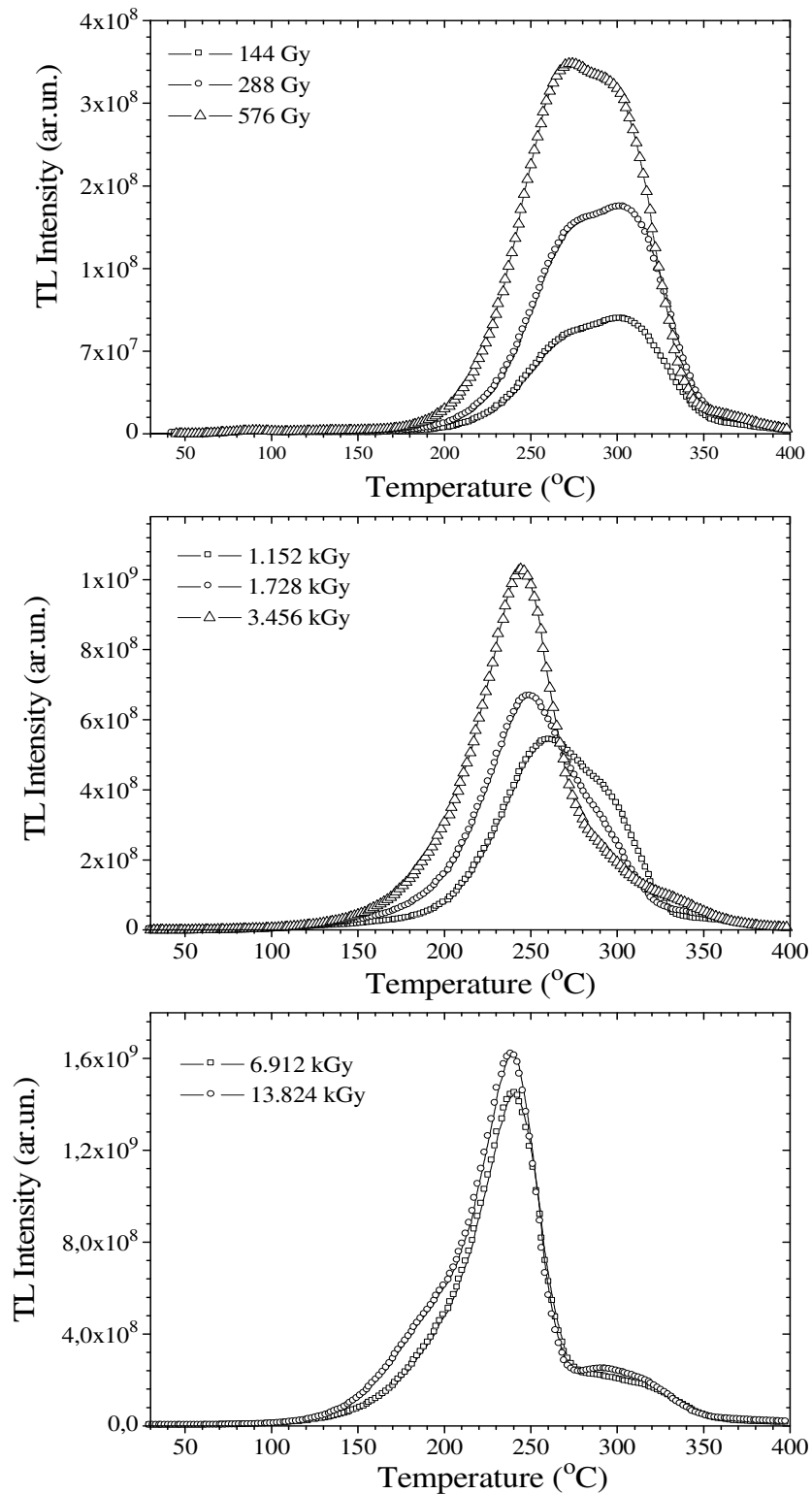


Figure 5.29b A typical glow curve of TLD-400 measured after an annealing procedure of  $400 \pm 1$  °C for 30 min by irradiation at room temperature from exposed to beta rays from 0.04 Gy up to 14 kGy and readout at a linear heating rate of  $\beta = 1$  °C/s

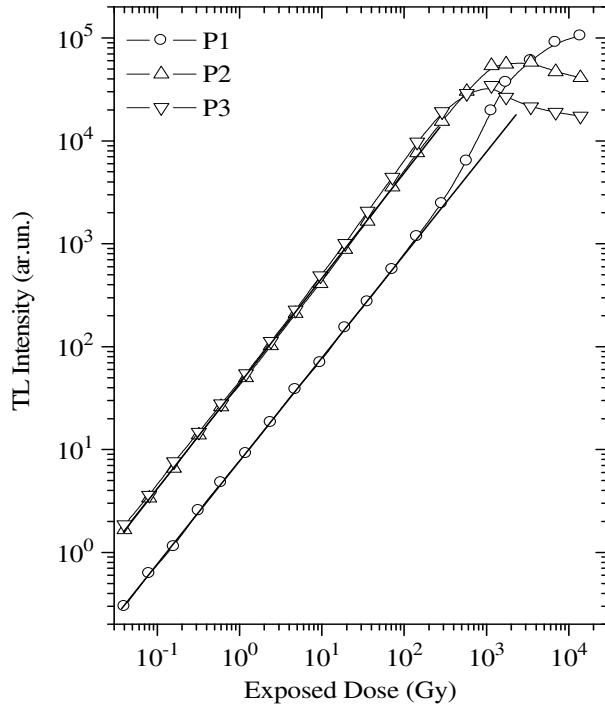


Figure 5.30 The growth of the peak areas of glow peaks of TLD-400 as a function of applied dose ( $\beta=1$  °C/s)

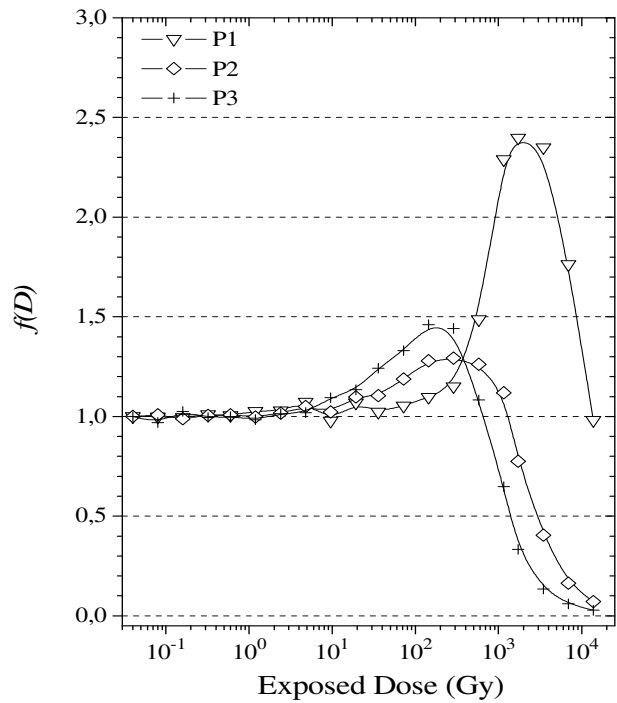


Figure 5.31 The dose response function  $f(D)$  vs  $D$  of TLD-400 ( $\beta=1$  °C/s)

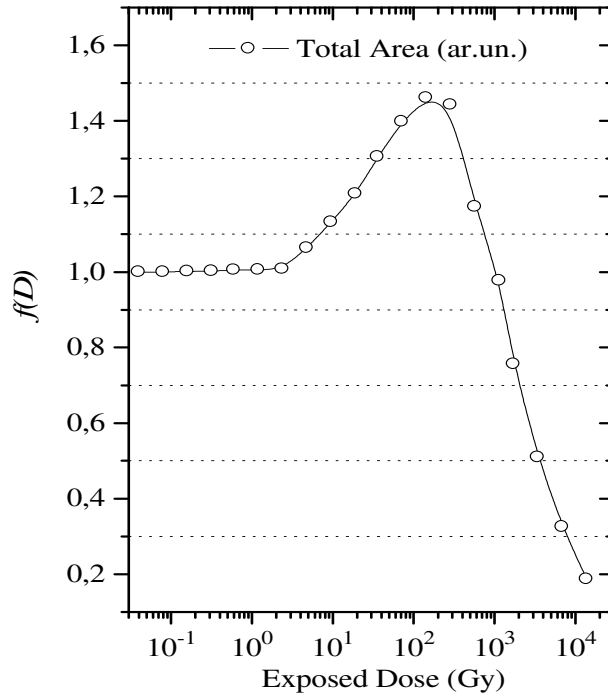


Figure 5.32 The dose response function  $f(D)$  vs  $D$  of TLD-400. ( $\beta=1$  °C/s)

The superlinearity function  $g(D)$  has also been evaluated for the total peak area of the glow curve of  $\text{CaF}_2:\text{Mn}$  (TLD-400) at a linear heating rate of 1 °C/s using equations 5.9 and 5.10. Where the constants are:  $a= 25.871$ ,  $b= 0.00115$ ,  $c= 4.8581$ .

$$S(x)= \frac{a + cx}{1 + bx} \quad (5.9)$$

$$g(D) = \left[ \frac{-2bx}{1 + bx} + 1 \right] \quad (5.10)$$

It can be seen from the figure 5.33 that, the total area of the glow curve of TLD-400 crystal at a linear heating rate of 1 °C/s shows linear behaviour up to nearly 5 Gy ( $g(D)=1$ ), after the superlinear region, ( $g(D)>1$ ), the saturation effect sets in after  $10^3$  Gy ( $g(D)<1$ ).

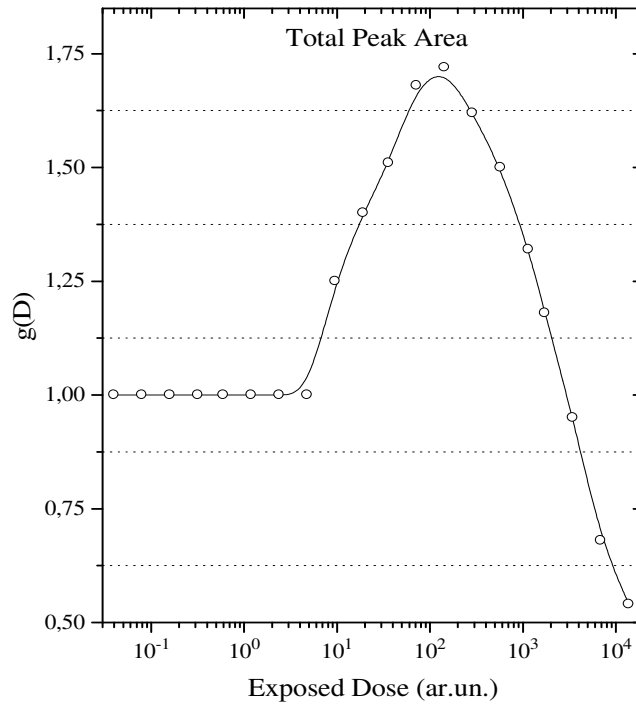


Figure 5.33 The superlinearity function  $g(D)$  vs  $D$  of the total peak area of the TL peaks from TLD- 400 at linear heating rates of  $1\text{ }^{\circ}\text{C}\cdot\text{s}^{-1}$

The dose response characteristics of the glow peaks of TLD-400 were also obtained by recording the glow curves at a linear heating rate of  $10\text{ }^{\circ}\text{C}/\text{s}$ . Figure 5.34a and 5.34b show some of the selected glow curves of TLD-400 after different dose levels using a linear heating rate of  $10\text{ }^{\circ}\text{C}/\text{s}$ . Figure 5.35 shows the growth of the height of the peaks as a function of dose. As seen from this figure, that all peaks show linear behavior nearly up to  $10^2\text{ Gy}$  then they go into a supralinear region and saturate after dose level of  $10^3\text{ Gy}$ . In figure 5.36, the dose response functions ( $f(D)$ ) of all glow peaks are depicted. As seen, all peaks show linear characteristic ( $f(D)=1$ ) nearly up to  $10^2\text{ Gy}$ , then they go into a region of supralinear growth ( $f(D)>1$ ) after this dose level. Then, peaks 2 and 3 start to saturate and show sublinear behavior ( $f(D)<1$ ) above  $10^3\text{ Gy}$ . On the other hand, peak 1 show a sublinear behavior ( $f(D)<1$ ) above  $10^4\text{ Gy}$ .



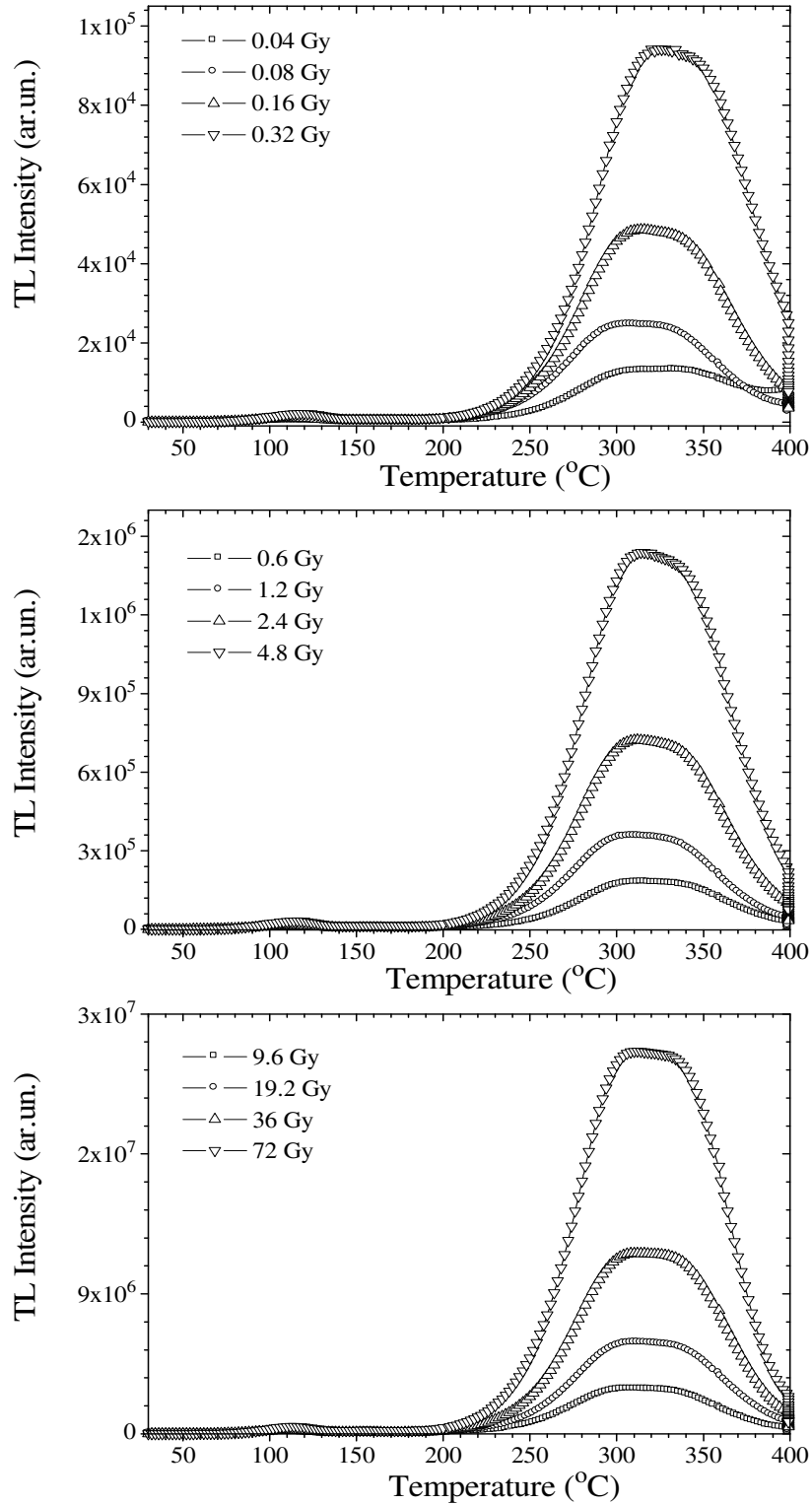


Figure 5.34a A typical glow curve of TLD-400 measured after an annealing procedure of  $400 \pm 1$  °C for 30 min by irradiation at room temperature from exposed to beta rays from 0.04 Gy up to 14 kGy and readout at a linear heating rate of  $\beta = 10$  °C/s

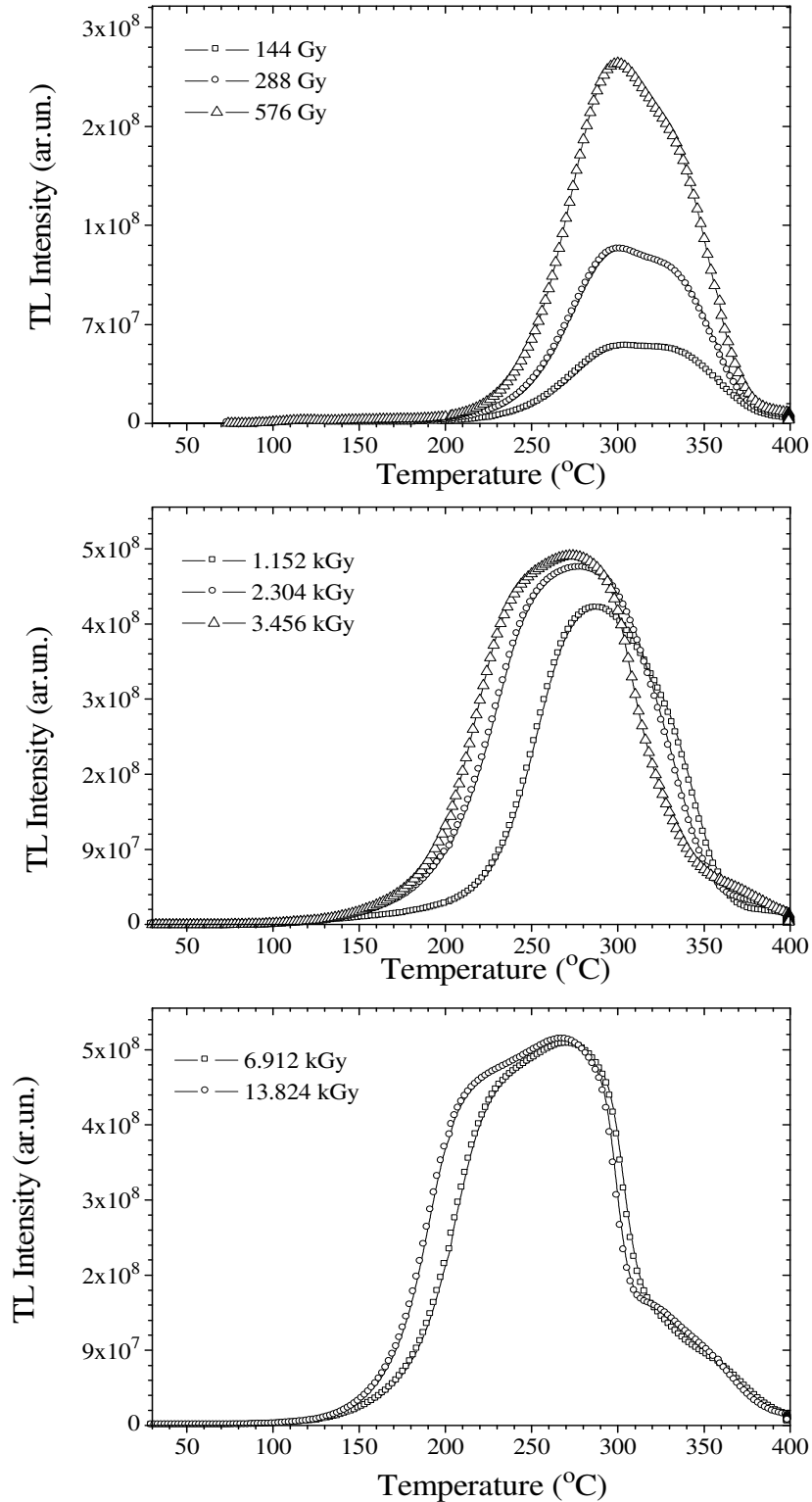


Figure 5.34b A typical glow curve of TLD-400 measured after an annealing procedure of  $400 \pm 1$  °C for 30 min by irradiation at room temperature from exposed to beta rays from 0.04 Gy up to 14 kGy and readout at a linear heating rate of  $\beta = 10$  °C/s

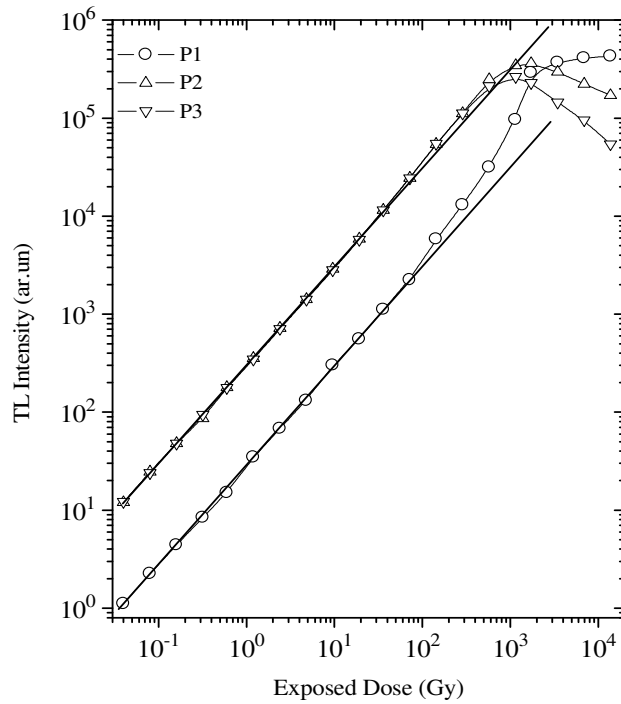


Figure 5.35 The growth of the peak areas of glow peaks of TLD-400 as a function of applied dose ( $\beta=10\text{ }^{\circ}\text{C/s}$ )

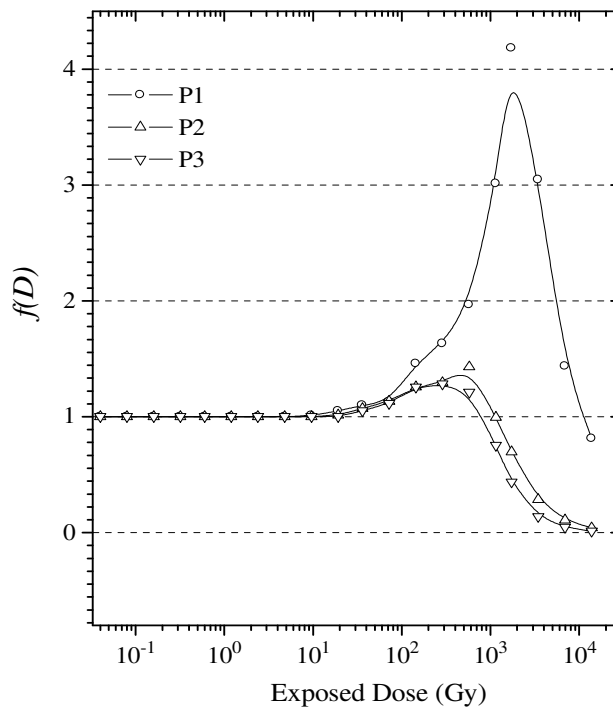


Figure 5.36 The dose response function  $f(D)$  vs  $D$  of TLD-400 ( $\beta=10\text{ }^{\circ}\text{C/s}$ )

The dose response functions,  $f(D)$  and  $g(D)$ , have also been evaluated for the total area of the glow curve for heating rate of  $10\text{ }^\circ\text{C/s}$ . The superlinearity function was found according to the peak area of the TL glow curve by using equations 5.11 and 5.12, from the definition of the superlinearity index in equation 3.1. Where the constants are:  $a= -474.049$ ,  $b= 1887.4$ ,  $c= 4.1817$ ,  $d= -0.0110547$ . It can be concluded from the figures 5.37 and 5.38 that the total area of the glow curve at a heating rate of  $10\text{ }^\circ\text{C/s}$  shows linear behaviour up to 50 Gy (both  $f(D)$  and  $g(D)=1$ ), after a region of nonlinear growth, ( $f(D)$  and  $g(D)>1$ ), saturation effect sets in and the glow peak area goes to the sublinear region, ( $f(D)$  and  $g(D)>1$ ), after  $10^3$  Gy dose level.

$$S(x)= a + bx + cx^2 + dx^3 \quad (5.11)$$

$$g(D)= \left[ \frac{x(2c + 6dx)}{b + 2cx + 3dx^2} + 1 \right] \quad (5.12)$$

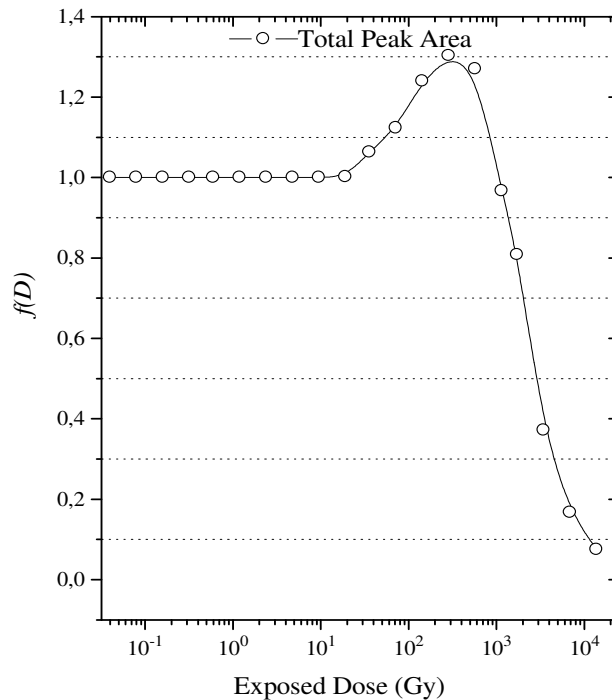


Figure 5.37 The dose response function  $f(D)$  vs  $D$  of TLD-400 ( $\beta=10\text{ }^\circ\text{C/s}$ )

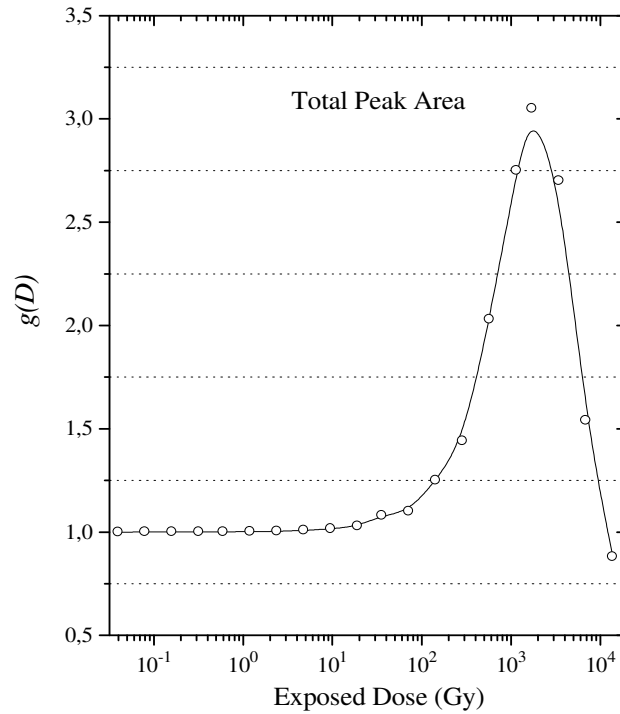


Figure 5.38 The dose response function  $g(D)$  vs  $D$  of TLD-400 ( $\beta=10\text{ }^{\circ}\text{C/s}$ )

The behaviour of the glow curves and the effect of thermal quenching due to the heating rate on the total peak area of glow curves were also investigated for  $\text{CaF}_2:\text{Mn}$  (TLD-400) at different linear heating rates between  $1\text{ }^{\circ}\text{C/s}$  and  $30\text{ }^{\circ}\text{C/s}$ . Figure 5.39 shows some of the selected glow curves of TLD-400 at linear heating rates between  $1\text{ }^{\circ}\text{C}$  and  $30\text{ }^{\circ}\text{C}$ . As seen from this figure the peak temperatures of all peaks are shifted to higher temperatures when the heating rate increases as expected in theory. It is seen from figure 5.40, the total peak area of the glow curves decreases as the heating rate increases. The total area of the glow curves were normalized at the lower heating rate ( $1\text{ }^{\circ}\text{C s}^{-1}$ ) and it can be seen that the decrease in the integrated area of the peaks by about 60 %.

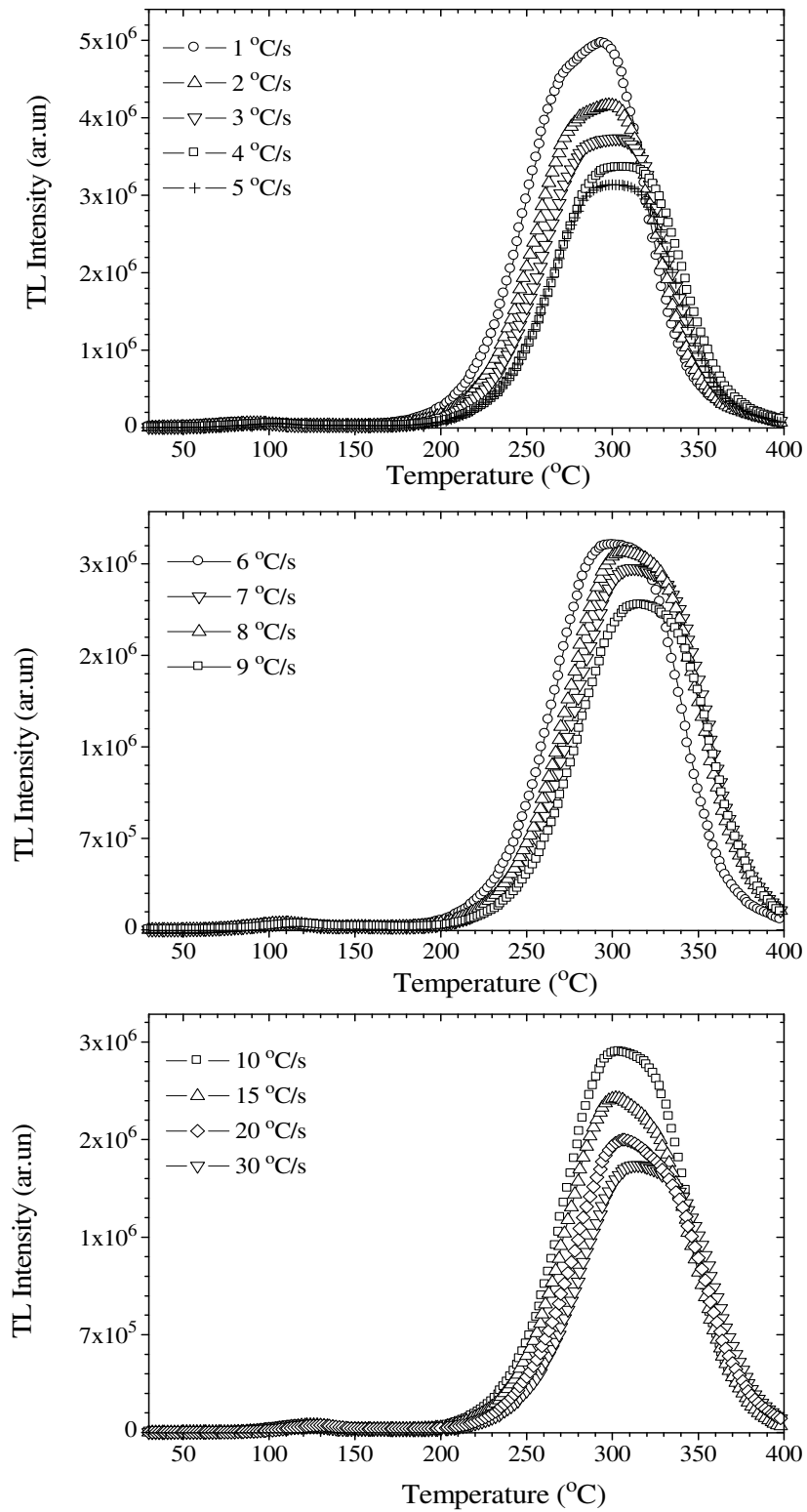


Figure 5.39 The glow curves of TLD-400 crystals irradiated with <sup>90</sup>Sr-<sup>90</sup>Y beta source at linear heating rates between 1 °C/s and 30 °C/s ( $D=12$  Gy)

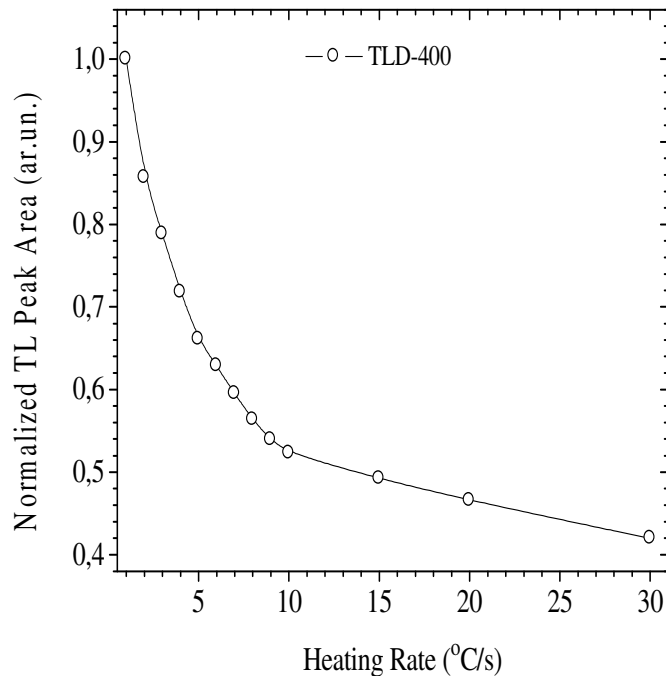
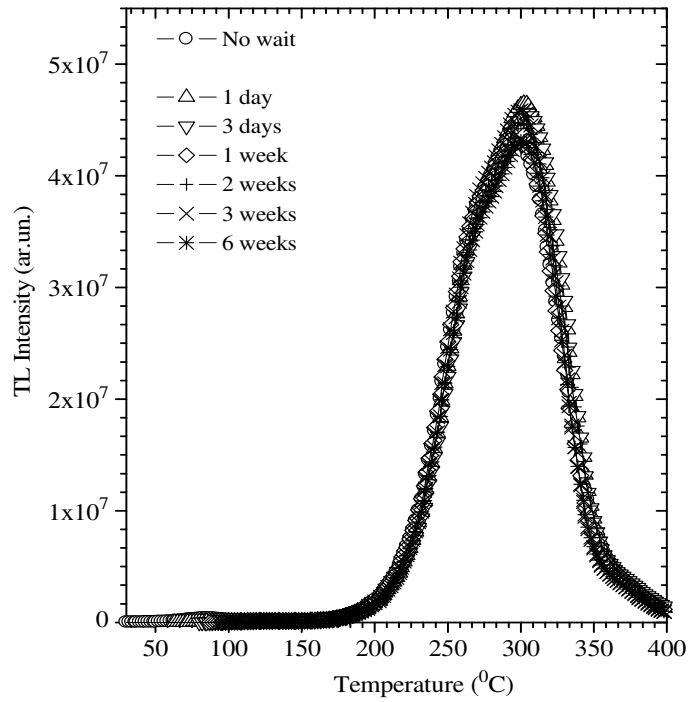


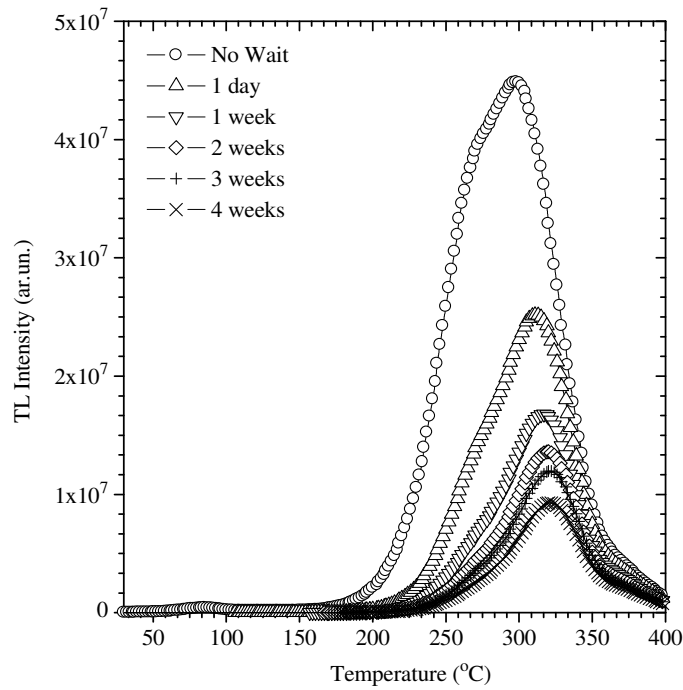
Figure 5.40 The normalized TL peak area of TLD-300 crystals irradiated with  $^{90}\text{Sr}$ - $^{90}\text{Y}$  beta source at linear heating rates between 1 °C/s and 30 °C/s (D=12 Gy)

For the storage time experiments TLD- 400 crystal were annealed at  $400 \pm 1$  °C for 30 min and irradiated up to 36 Gy. The storage time experiments were performed for different time periods. Also the optical fading at room temperature was investigated under the tungsten filament lamp of 55 lux which is located at a distance of 20 cm from the sample.

The measured glow curves of  $\text{CaF}_2: \text{Mn}$  at the end of the planned storage periods are shown in figure 5.41. As seen from this figure, the peaks are not highly affected from the storage time periods performed in the dark. According to figure 5.42, P1 reduced to typically 15 %, P2 and P3 reduced to 5% of their original value after 6 weeks. In the optical fading experiment, the situation is different; P1 reduced to 95%, P2 reduced to 90% and P3 reduced to nearly 85 % of their original values after 3 weeks. This illustrates that the peaks are highly affected from the optical condition.



(a)



(b)

Figure 5.41 A set of TL glow curves for TLD-400 crystal measured after different storage times at room temperature (a) in the dark, (b) optical fading. All glow curves were read out at  $1\text{ }^{\circ}\text{C/s}$  after exposing to an irradiation of 36 Gy



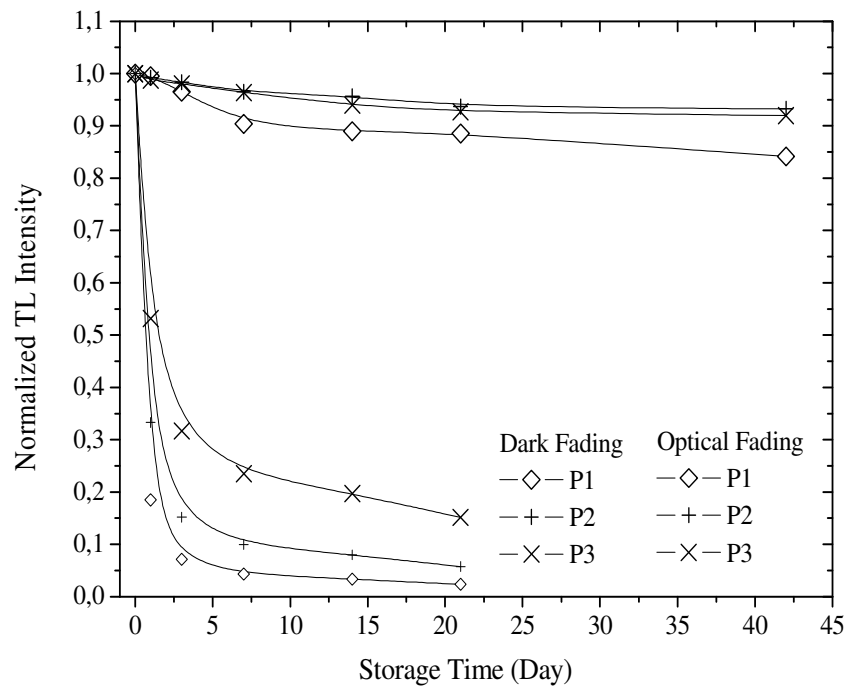


Figure 5.42 Normalized TL intensity for dark and optical fading for TLD-400

#### 5.4 The thermoluminescence properties of Lithium triborate ( $\text{LiB}_3\text{O}_5$ : Al) after $\beta$ - irradiation

Thermoluminescence dosimetry with borates has been of interest for some 15 years and has been stimulated by a number of factors. The most obvious is that materials such as  $\text{Li}_2\text{B}_4\text{O}_7$  or  $\text{MgB}_4\text{O}_7$  have a close tissue equivalence and rare thus worth considering for their TL properties. Indeed the lithium borate dosimeters are superior to LiF in terms of tissue-equivalence. The borates are relatively stable chemical compounds and respond without serious problems to attempts to dope them with TL sensitizers such as the rare earths, copper or manganese ions. The resultant materials now show some desirable features for TL in terms of high sensitivity, linearity and storage and many of the earlier problems of fading, light sensitivity and poor humidity behavior have been avoided.

Lithium triborate,  $\text{LiB}_3\text{O}_5$ , is one of the most known lithium borates. It is a newly developed nonlinear optical crystal. It offers the following advantages: extremely high damage threshold, large phase matching acceptance angle, very wide

transparency range and chemical stability. So it is particularly useful for making doubler or tripler for such as Nd: YAG lasers where high power density, high stability, and long time operation are required. It is an ideal nonlinear optical crystal used in laser weapon, welder, radar, tracker, surgery, communication and etc. [77].

Lithium triborate ( $\text{LiB}_3\text{O}_5$  or LBO) is an attractive material for frequency conversion applications due to its high UV transmission, large acceptance angle, small walk-off angle, good chemical stability and non-hygroscopicity. However, the relatively moderate effective non-linear coefficient of LBO has so far limited the application of this material to harmonic generation of high power laser beams. Waveguide structures have the advantage over bulk geometries of maintaining high intensities over long interaction lengths, which may make it possible to extend harmonic generation use of LBO to low power lasers, such as diode lasers. Several techniques have been developed to produce waveguide structures in materials, such as metal diffusion, ion exchange, thin film deposition and ion implantation. Because of its ability to modify the surface of materials, ion implantation has become a universal method for fabricating waveguide structures in most optical materials because it has superior controllability and reproducibility. Implantation of light ions, such as H and He, has proven to be a successful way to fabricate optical waveguides in LBO crystals. Recently, the implantation of heavy ions has attracted much attention for waveguide fabrication because it usually requires much lower doses and hence offers better confinement of light in the waveguide [84].

An interest in the study of nonlinear optical effects, in particular, to the problem of generation of the second harmonic (SHG) of laser radiation, has grown considerably nowadays, especially as solid-state laser sources started replacing gas and ion laser sources for various applications and they need frequency conversion devices. Lithium triborate exhibits excellent nonlinear optical properties luminescent properties spontaneous polarization and moderate piezoelectric coefficients parallel with high laser damage threshold required for many applications. Crystals of  $\text{LiB}_3\text{O}_5$  are widely used as nonlinear optical units and materials for integrated optical waveguides in laser weapon, welder, radar, surgery, communication, etc. So, there are lot various studies of  $\text{LiB}_3\text{O}_5$ , for example, the study of synthesis and crystal growth of  $\text{LiB}_3\text{O}_5$  infrared spectra dielectric properties specific heat at low temperatures structure and chemistry of  $\text{LiB}_3\text{O}_5$  optical surfaces etc. [85].

The tissue equivalent absorption coefficient is one of the most important properties for the TLD materials in the field of medical physics. The thermoluminescence (TL) studies of lithium borate compounds are of interest because of their near tissue equivalent absorption coefficient ( $Z_{\text{eff}}=7.3$ ), low cost and easy handling process and therefore it is particularly suited for applications in radiation dosimetry, especially radiation therapy and clinical applications. Therefore, the TL studies of lithium borate compounds were started in 1967 by the work of Schulman [86] et al and then, detailed TL studies on various alkali and alkaline earth tetra borates, especially on the lithium and magnesium borate compounds, were continued up to present times [87-89]. Recently, Prokic reported that the sintered  $\text{Li}_2\text{B}_4\text{O}_7$  doped with several impurities such as Cu, In; Cu, In, Ag; and Mg, Cu, P gives better dosimeter characteristics than the others [90]. These materials have better tissue equivalence as TL dosimeters and they show similar sensitivity like TLD-100 (LiF:Mg,Ti). In addition, doped lithium borate crystals may be potential materials for neutron detection, due to the presence of Li and B. Because of the presence of the Li and B in the structure, efficient neutron capture is expected with high-energy deposits. Since lithium borate has a low effective atomic number and low material density, it will have low efficiency for gamma ray background detection.

The dosimetric characteristics of any TL material mainly depend on the sensitivity, energy response and the kinetic parameters quantitatively describing the trapping-emitting centers responsible for the TL emission. Thus, a reliable dosimetric study of a thermoluminescent material should be based on a good knowledge of its kinetic parameters. For example, the simultaneous estimation of the dose rate and the time elapsed since exposure are closely related to the position of the trapping levels within the band gap, and therefore it is necessary to have a good knowledge of these parameters. There are various methods for evaluating the trapping parameters from TL glow curves. When one of the glow peaks is highly isolated from the others, the experimental methods such as initial rise, various heating rates and peak shape methods are suitable methods to determine them. Therefore, in the given study, the additive dose (AD),  $T_m(E_a)-T_{\text{stop}}$ , repeated initial rise (RIR), variable heating rate (VHR), peak shape (PS), isothermal decay (ID), three points methods (TPM) along with the deconvolution method have been used to

determine trapping parameters of the main dosimetric peak, namely P3, of Al-doped LiB<sub>3</sub>O<sub>5</sub>.

Previously published studies have shown that the determination of  $E_a$  and  $s$  mainly depends on the prior knowledge of kinetic order ( $b$ ) and the exact number of glow peaks in the glow curve [90-91, and 92]. In TL theory [4], the peak temperatures of glow peaks are expected to change only with heating rate for  $b=1$ . Hence, for a constant heating rate, the peak temperature should not be affected by other experimental parameters and should be fairly constant within the limit of experimental uncertainties. However, for  $b \neq 1$  and below the trap saturation points  $\{n_o \text{ (concentration of trapped electrons)} < N_t \text{ (concentration of traps)}\}$ , it is generally received that the peak temperatures are shifted to the lower-temperature side with increasing dose levels. Therefore, to form an opinion about the number of glow peaks and kinetic orders ( $b$ ) of all individual glow peaks in the glow curve structure of Al-doped LiB<sub>3</sub>O<sub>5</sub>, the AD method was first utilized in the current study. The samples were irradiated at different doses between  $\approx 0.04$  and  $\approx 114$  Gy to check the dose dependence effect on the peak positions. Some of the selected glow curves after different dose levels are shown in Figure 5.43.

The experimental observations have clearly shown that there were no significant changes in the peak temperature of glow peak of Al-doped LiB<sub>3</sub>O<sub>5</sub> with increasing dose level (Fig.5.43). As seen from this figure, the positions of peak temperature of P3 are within the experimental error  $\pm 2$  °C for all the doses. This result clearly shows that the main glow peak, P3, and also all of the glow peaks of Al-doped LiB<sub>3</sub>O<sub>5</sub> should have first-order kinetics.

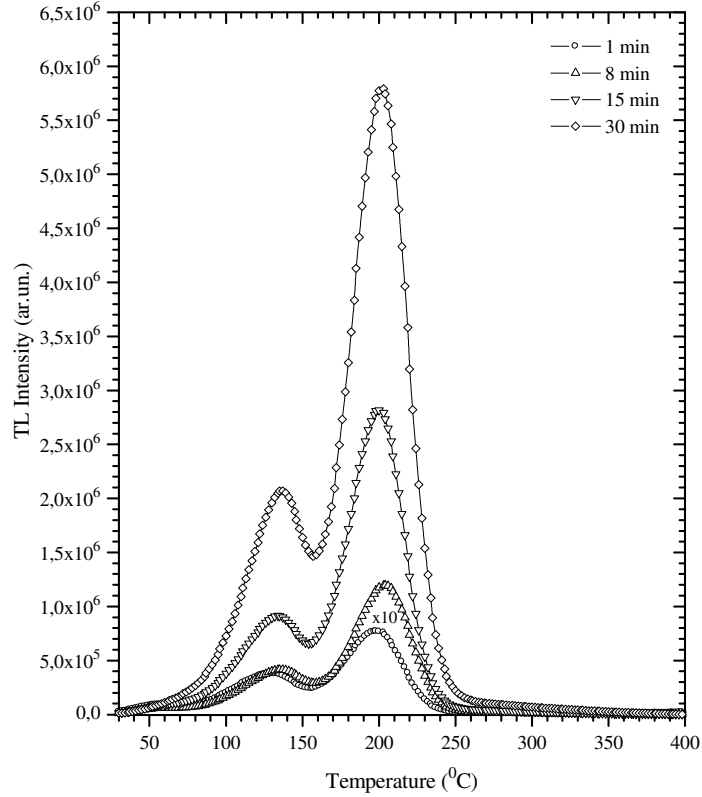


Figure 5.43 The glow curve of Al-doped  $\text{LiB}_3\text{O}_5$  measured after various radiation exposed dose levels ( $\beta=1\text{ }^\circ\text{C/s}$ )

The recorded glow curves after the AD experiments were also used to determine the kinetic parameters by the PS method. This method is based on the shape and full width at half maximum ( $\text{FWHM} = T_2 - T_1$ ) of a single glow peak and the values of  $E_a$  were determined by the modified PS method of Chen [5]. According to this method, the  $b$  of a single peak is easily obtained by means of the geometric factor  $\{\mu_g = (T_2 - T_m)/(T_2 - T_1)\}$  and  $\mu_g$  changes with the order of kinetics  $b$  from  $\approx 0.42$  to  $\approx 0.52$ , where these two limits correspond to first- and second-order kinetics, respectively. In the present case, the symmetry factor ( $\mu_g$ ) of the isolated glow peak 3 of Al-doped  $\text{LiB}_3\text{O}_5$  has been found to be 0.416 which gives a kinetic order of about 1. In addition to Chen peak shape method the kinetic parameters have also determined by using Gartia, Singh & Mazumdar [93] peak shape method which requires the prior knowledge of the kinetics order. The method uses any three points of a peak. According to this method, it is possible to calculate the activation energy as follows

$$E_a = \frac{CkT_m^2}{|T_x - T_y|} + DkT_m \quad (5.13)$$

where  $|T_x - T_y| = \tau, \delta, \omega$ . The coefficients  $C$  and  $D$  are found using the method of least squares for different order of kinetics  $b$  in the range from 0.7 to 2.5 and for  $x = 1/2, 2/3, 4/3$ . For a particular value of  $x$  the coefficients results to be dependent on  $b$  and then can be expressed as a quadratic function of  $b$  itself. So that, the previous equation can be rewritten as

$$E_a = \frac{(C_0 + C_1b + C_2b^2)kT_m^2}{|T_x - T_y|} + (D_0 + D_1b + D_2b^2)kT_m \quad (5.14)$$

Table 5.3 gives the coefficients for different values of  $x$ . The results obtained by using expression for  $x=1/2$  are more accurate than those of Chen. Furthermore, it is pointed out that  $E_\tau, E_\delta$  and  $E_\omega$  are in excellent agreement among themselves, whereas the Chen's values for  $E_\delta$  and  $E_\omega$  yield poor results [93]. The kinetic parameters calculated by this method are given in table 5.4.

Table 5.3 Numerical values of the coefficients comparing in Eq. (5.14)

Ratio	Parameter	$C_0$	$C_1$	$C_2$	$D_0$	$D_1$	$D_2$
1/2	$\tau$	1.019	0.504	-0.066	-1.059	-1.217	0.109
	$\delta$	0.105	0.926	-0.048	0.154	-0.205	-0.128
	$\omega$	1.124	1.427	-0.113	-0.902	-0.346	-0.061
2/3	$\tau$	0.684	0.426	-0.055	-0.720	-1.21	0.098
	$\delta$	0.146	0.683	-0.048	0.184	-0.432	-0.094
	$\omega$	0.830	1.108	-0.103	-0.529	-0.607	-0.029
4/5	$\tau$	0.449	0.342	-0.043	-0.0480	-1.184	0.085
	$\delta$	0.153	0.487	-0.041	0.180	-0.606	-0.062
	$\omega$	0.602	0.829	-0.084	-0.293	-0.777	-0.006

Table 5.4 The values of the activation energy  $E_a$  (eV) and frequency factor  $s$  ( $s^{-1}$ ) of main dosimetric peak of-Al doped  $LiB_3O_5$  determined by the modified PS method of Gartia et al. [93]

	1 / 2 ratio			2 / 3 ratio			4 / 5 ratio		
	$E_\tau$	$E_\delta$	$E_\omega$	$E_\tau$	$E_\delta$	$E_\omega$	$E_\tau$	$E_\delta$	$E_\omega$
<b><math>E_a</math> (eV)</b>	1.05	1.08	1.07	1.09	1.02	1.06	1.00	1.20	1.09
<b><math>ln(s)</math> (<math>s^{-1}</math>)</b>	22.81	23.48	23.24	23.81	22.18	23.06	21.6	26.56	23.75

Recently, Rasheedy [94] has developed another technique (TPM) to obtain the trap parameters of glow peaks. According to this method, the order of kinetics  $b$  and the activation energy  $E_a$  are given in equations 2.60 and 2.61 respectively. In this thesis, the trapping parameters evaluated from the TPM are the results of calculations from the maximum intensity at temperature 200 °C (P3) up to 10% of the maximum intensity. The average values of the parameters involved for peak 3 are found equal to  $b=1.1$ ,  $E_a=1.02$  eV and  $ln(s) = 22.17 s^{-1}$ . In order to obtain the trapping parameters of peak 3, the isothermal decay method has also been used in which the TL sample temperature is kept constant near the peak temperature of glow peak and the light emission can be recorded as a function of time. Generally, in the isothermal decay method, the following equation is solved for constant  $T$  for the first order kinetic

$$I(T) = -c \frac{dn}{dt} = c \frac{n_0}{\tau} \exp\left(-\frac{t}{\tau}\right) \quad (5.15)$$

where  $n_0$  is the initial value of  $n$  and  $\tau = s^{-1} \exp\left(\frac{E_a}{kT}\right)$ .

The above equation shows that at a constant temperature  $T_f$ , the light emission will decay exponentially with time  $t$  and a plot of  $ln(I)$  against  $t$  will give a straight line with a slope  $m = s \exp\left(-\frac{E_a}{kT}\right)$ . In order to find  $E_a$  and  $s$ , the experiments are carried out at two different constant temperatures  $T_1$  and  $T_2$ , resulting in two different slopes  $m_1$  and  $m_2$ . Thus the activation energy can be determined by using the following equation:

$$E = \frac{k}{\left(\frac{1}{T_2} - \frac{1}{T_1}\right)} \ln\left(\frac{m_1}{m_2}\right) \quad (5.16)$$

The isothermal decay method is not applicable to higher order kinetics. In 1979; a method has been proposed by Kathuria and Sunta [81] to calculate the order of kinetics from the isothermal decay of thermoluminescence. According to this method; if the decaying intensity from the sample is held at a constant temperature, the plot of  $I^{\left(\frac{1}{b}-1\right)}$  versus  $t$  gives a straight line, when the proper value of  $b$  is chosen. Therefore, various  $b$  values are tried and the correct one is that giving a straight line. Figure 5.44 shows the isothermal decay curve at  $190\pm 1$ ,  $195\pm 1$ ,  $200\pm 1$ ,  $205\pm 1$ ,  $210\pm 1$  °C of the sample after 5 min beta-irradiation. Decay intensity values are normalized at  $t=0$  s for all decay. An ambiguous method to ascertain that the order of kinetics followed by any given TL glow peak is first-order is to see whether the ID of the TL intensity follows an exponential law. The fact that none of these curves in figure 5.44 follows an exact exponential pattern is a sufficient proof against first-order kinetics. The exact value of the order of kinetics is determined by plotting the decay data in the form  $I^{\frac{1}{b}-1}$  versus time for various value of  $b$  (Fig. 5.45) [95]. As it is seen from the figure 5.45 all curves have a part of straight line. On the other hand, the linearity of the plots changes according to the kinetic order  $b$  and chosen decaying temperature ( $T_f$ ). Therefore, the extraction of the order of kinetic  $b$  of dosimetric glow peak from these curves is not sufficiently possible. As seen for  $b=1.01$ , a straight line plot is obtained only up to approximately 20 s in all decay curves. Moreover, the linearity of curves increases with increasing decaying temperature ( $T_f$ ). As the kinetic order increases, the plots are more linear than previous graphs up to  $b=1.5$  for  $T_f$  at 200 °C, 205 °C and 210 °C. When the kinetic order values go beyond  $b=1.5$ , the linearity of some decaying curves were again start to decrease. These results indicate that the linearity of decaying curves is not only depend upon the kinetic order  $b$  of glow peak but also the decaying temperature  $T_f$  and decaying time. It is seen from this figure that during the initial decay of the peak, the order of kinetics is close to 1, but as the decaying proceeds the order of kinetic is found to be continuously changing. This means that the kinetic order  $b$  of P3 depends on the populated number of the traps belong to this peak and the ratio of empty and



filled number of traps. Simply, as the decay progress, more and more empty traps become available to enable an increase the retrapping. As mentioned previously, the isothermal decay method is not applicable to higher order kinetics and variable kinetic order. Therefore, this method was not applied to obtain the activation energy and frequency factor of studied glow peak of Al-doped  $\text{LiB}_3\text{O}_5$ .

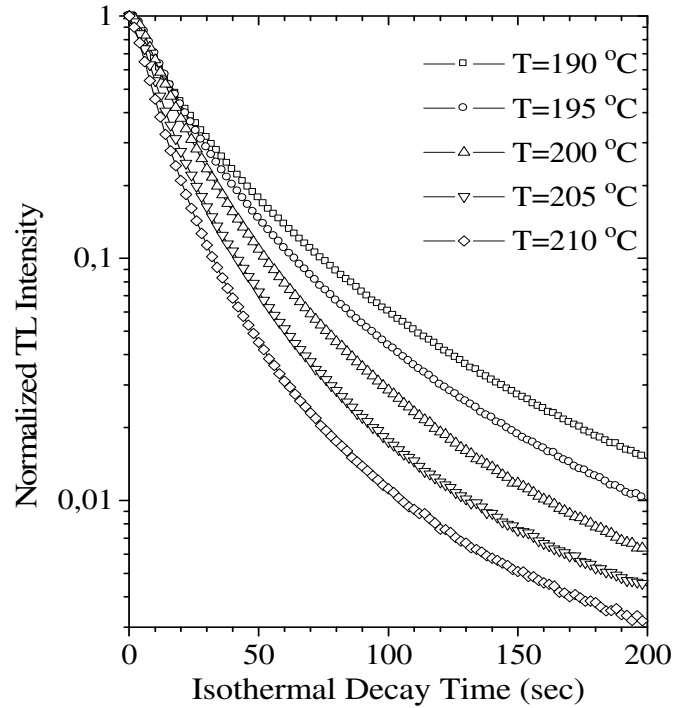


Figure 5.44 Normalized isothermal decay curves of peak 3 at 190, 195, 200, 205,  $210 \pm 1$  °C for the radiation dose of 12 Gy

Another method that was used to determine the kinetic parameters in this study is the VHR method. This method is based on the shift position of the temperature ( $T_m$ ) at the maximum point of intensity ( $I_m$ ) to higher temperatures when the heating rate is increased. In the absence of a distribution of activation energies, a plotting of  $\ln(T_m^2 / \beta)$  against  $1/(kT_m)$  should give a straight line of slope  $E_a/k$  and intercept  $\ln(sk/E_a)$ . The major advantage of this method is that the required data is to be taken at a peak maximum ( $I_m$ ,  $T_m$ ) which, in the case of a large peak surrounded by smaller satellites, can be reasonably accurately determined from the glow curve. For the VHR method, the three heating rates of  $1$  °C $s^{-1}$ ,  $3$  °C $s^{-1}$  and  $5$  °C $s^{-1}$  were applied.

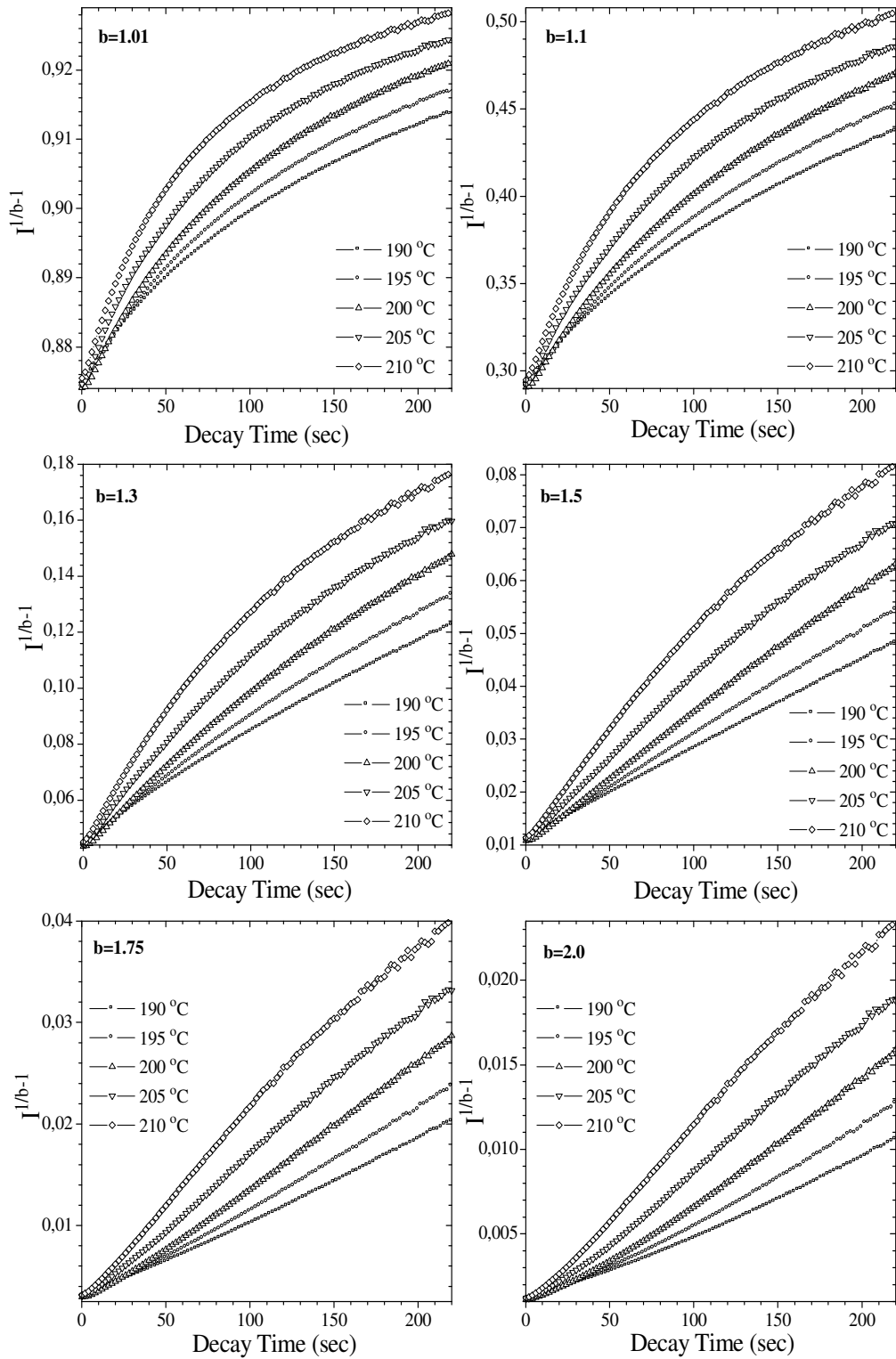


Figure 5.45 Plots of  $I^{\frac{1}{b}-1}$  versus decay time for peak 3

The measured glow curves after these three heating rates are shown in figure 5.46. It can be seen from this figure that the peak maximum temperatures increase with heating rate, but in addition there is a slight decrease in the intensities of all glow peaks. The decreasing luminescence intensity of glow peaks of  $\text{Li}_3\text{B}_5\text{O}_7:\text{Al}$  phosphor as a function of the increasing heating rate is a phenomenon frequently observed in the practice of TSL. It has been suggested that it is due to thermal quenching effect in which the luminescence efficiency decreases as the temperature increases due to the increased probability of non-radiative transitions [96]. As a result, the calculated kinetic parameters from the slopes and intercepts are given in table 5.5.

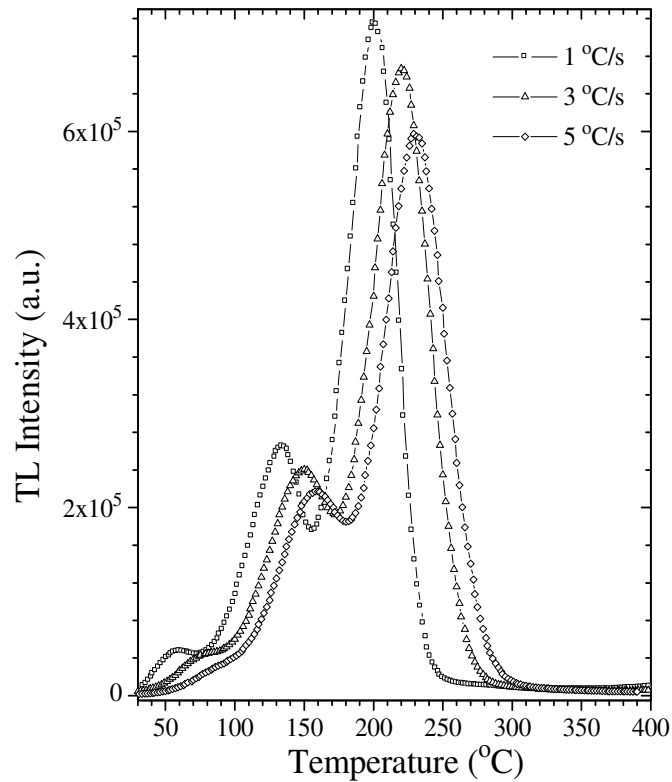


Figure 5.46 Some of the selected glow curves of Al-doped  $\text{Li}_3\text{B}_5\text{O}_7$  measured at various heating rates for 1, 3, and 5 °C/s. All glow curves were measured after  $\beta$  irradiation of 12 Gy

The kinetic parameters of main dosimetric peak 3 were also tested using the RIR method. A strong overlapping of TL peaks makes this method the most suitable procedure for the determination of number of glow peaks and their related kinetic parameters. Here, an irradiated sample is heated at a linear heating rate up to a temperature  $T_{stop}$  corresponding to a point on the low temperature tail of the first peak. The sample is then cooled down quickly to room temperature and then reheated at the same rate to record the entire remaining glow curve and the value of activation energy  $E_a$  is calculated. The process is repeated several times on the same annealed/irradiated sample at a different  $T_{stop}$  values, and two measurements were taken within each 10 °C region. According to this method, at the beginning of the TL glow peak, the concentration of trapped electrons  $n_o$  changes by only a small amount with temperature and thus it can be regarded as constant, so that the first- and general-order TL equations are simplified as  $I(T) \propto A \exp(-E_a/kT)$ , where  $A$  is a constant and the TL intensity is independent of the  $b$ . Therefore, a plot of  $\ln(I)$  versus  $1/T$  would yield a straight line with a slope of  $-E_a/k$  and a y-intercept of  $\ln(s/\beta)$ , from which  $E_a$  and  $s$  can readily be calculated. This method can be used only in the initial region of the TL signal up to ~10% of its peak maximum ( $I_m$ ). However, if the intensity at the beginning of each peak is very low and especially when the glow curve is composed of several glow peaks, the obtained values of  $E_a$  may not reflect the actual values. Therefore, in this case, the values of  $E_a$  obtained by the RIR method often need corrections. Christodoulides [97] and S.C.Singh *et al.* [98] have proposed to use the high-level of glow peaks to reduce the inaccuracies in  $E_a$  due to high levels of the used signal, which was also used in the present work. Another matter during the evaluation of  $E_a$  by RIR is the effect of thermal quenching on the evaluated  $E_a$ . This effect leads to underestimations of the activation energies obtained by RIR method. Since, the experimental glow curve shape is highly distributed by thermal quenching effect; it can't give reliable information about the values of  $E_a$ .

However, the RIR method analyzes only that the leading part of the glow peak and as such is yielding data appropriate to only that component of the TL signal comprising the full peak. Therefore, even if the RIR method gives erroneous values of  $E_a$  when the thermal quenching is present in the material, it should be expected that the plot of  $E_a$  against  $T_{stop}$  still gives plateau regions with a gradual decrease at

the end of each plateau after RIR method even if the glow curve is the superposition of overlapping glow peaks. If a plot of  $E_a$  against  $T_{stop}$  shows a stepwise curve after the RIR method, it allows one to estimate the number of peaks. Each plateau region in this plot indicates the existence of an individual glow peak. If a gradual rise of  $E_a$  exists at the end of the plateau region, it is an indication that the glow curve has overlapping glow peaks. Figure 5.47 shows some of the selected glow curves after the  $T_m(E_a)$ - $T_{stop}$  procedure following the irradiation of samples to a dose level  $D=12$  Gy. As seen from this figure, the  $T_m$  of all glow peaks is continuously shifted to high temperature side with increasing  $T_{stop}$ . The result of calculated activation energies is shown in figure 5.48. As shown from this figure, there are four plateau regions, so the RIR studies have identified four peaks in aluminum activated lithium triborate, designated P1-P4, in the temperature range from ~50-300 °C. The first plateau region is around 60 °C, after the disappearance of peak 1 above  $T_{stop}>120$  °C another plateau region was obtained. After the complete depletion of peak 2, another flat region between 160 °C and 240 °C becomes constant around  $1.26\pm 0.02$  eV which corresponds to peak 3. At the end of this region, another flat region was again obtained above  $T_{stop}>240$  °C which belongs to peak 4.

In this thesis, it has also examined the effect of  $T_{stop}$  on the  $T_1$ ,  $T_2$ ,  $T_m$ ,  $\mu_g$  and  $I_m$  of peak 3. Figure 5.49 shows the changes in them as a function of  $T_{stop}$ . As seen from this figure the maximum peak intensity of peak 3 is constant up to  $T_{stop}=100$  °C, as  $T_{stop}$  increases  $I_m$  starts to decrease because the  $T_{stop}$  reaches the maximum peak temperature of about 200 °C. In figure 5.50a it can be seen that the shape parameter  $\mu_g$  is between 0.42 and 0.45 up to  $T_{stop}=120$  °C, its value increases slowly with a small up down changes, until maximum peak temperature, above  $T_{stop}>200$  °C the shape parameter increases continuously reaching the value of about 0.6. Figure 5.50b also shows the variation of activation energy  $E_a$ , vs  $T_{stop}$  obtained by PS method. It can be concluded from this figure that  $E_a$  is constant about 1.12 eV with a small changes until  $T_{stop}=100$  °C, then increases continuously, and gets the value of 1.36 eV about its maximum peak temperature.

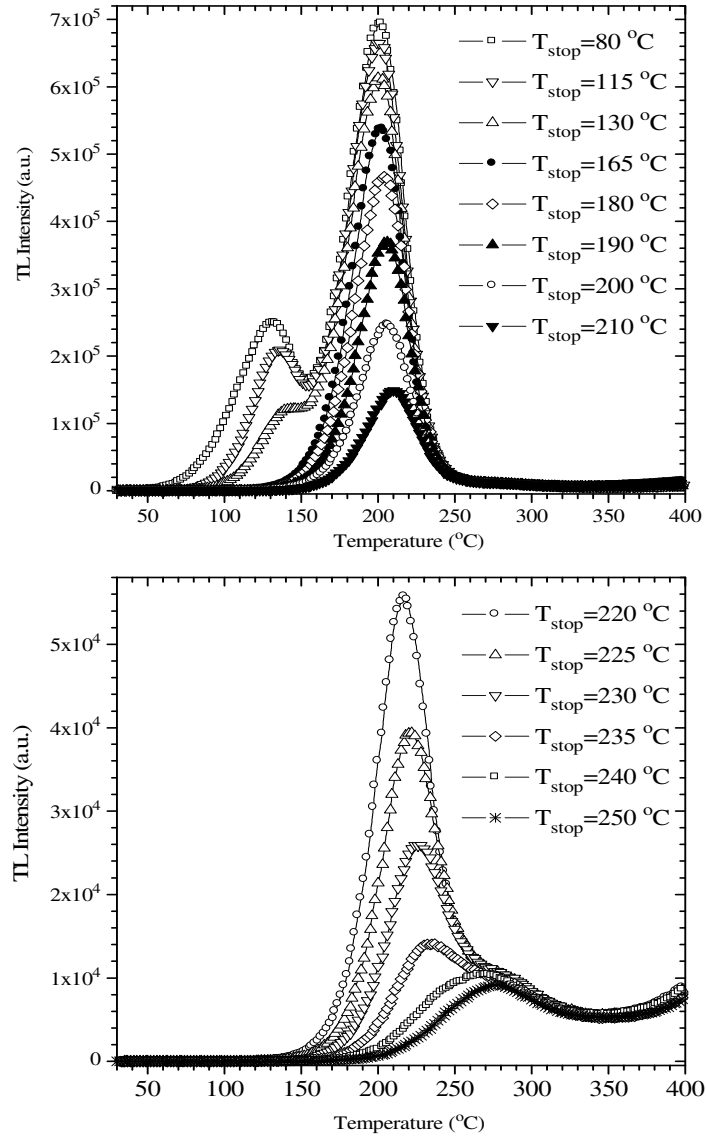


Figure 5.47 Some of the selected glow curves of Al-doped LiB<sub>3</sub>O<sub>5</sub> after different  $T_{\text{stop}}$  temperatures at a linear heating rate  $\beta = 1 \text{ }^\circ\text{C/s}$ . Dose levels are always adjusted to 12 Gy.

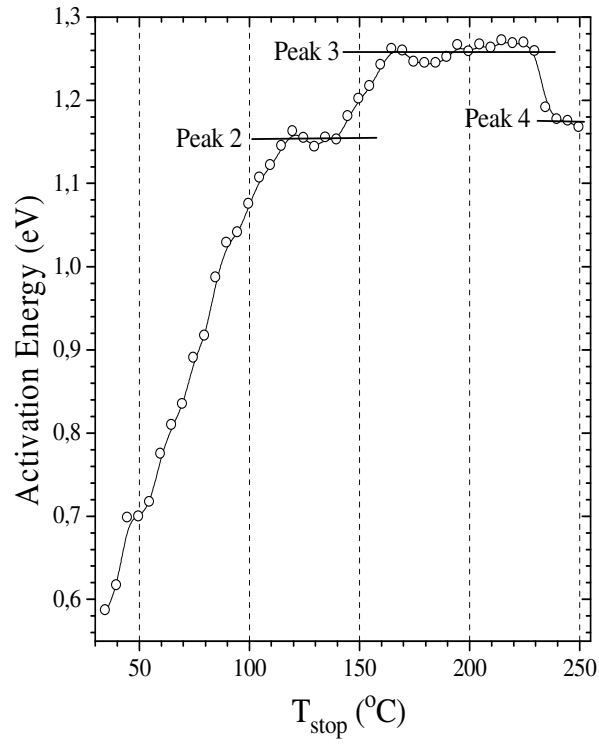


Figure 5.48 The activation energy ( $E_a$ ) resulting from the RIR method after  $T_m(E_a)$ - $T_{stop}$  procedure

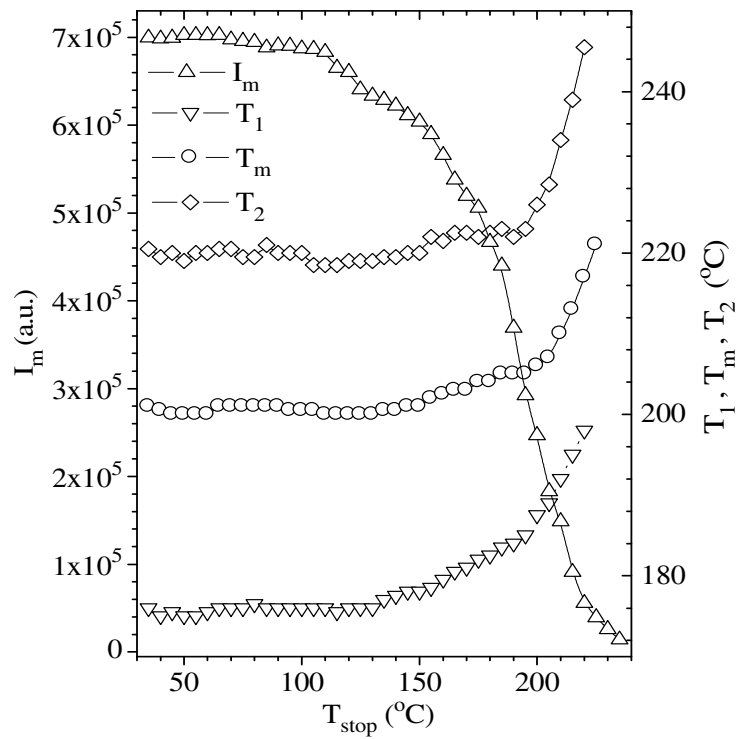


Figure 5.49  $T_1$ - $T_{stop}$ ,  $T_m$ - $T_{stop}$ ,  $T_2$ - $T_{stop}$ , and  $I_m$ - $T_{stop}$  plot for the thermoluminescent dosimetric glow peak of Al-doped  $\text{LiB}_3\text{O}_5$

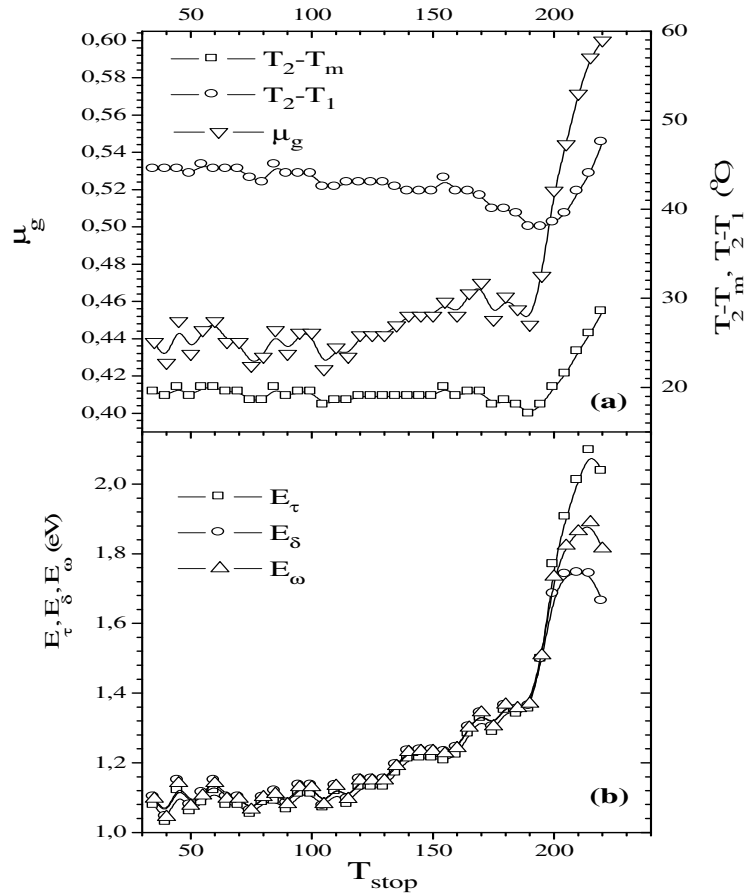


Figure 5.50 (a) The geometric factor  $\mu_g$ ,  $T_2 - T_1$  and  $T_2 - T_m$  as a result of  $T_{stop}$  determined from the  $T_m - T_{stop}$  procedure. (b) The activation energy ( $E_a$ ) resulting from the PS method after the  $T_m - T_{stop}$  procedure

Table 5.5 The values of the activation energy  $E_a$  (eV) and frequency factor  $s$  of main dosimetric peak of Al- doped  $LiB_3O_5$  determined by the Chen's PS, RIR, VHR, and TP methods

	IR Method	VHR Method	PS Method (Chen)			TP method
			$E_\tau$	$E_\delta$	$E_\omega$	
$E_a$ (eV)	1.26	1.12	0.99	0.98	1.0	1.019
$\ln(s)$ ( $s^{-1}$ )	34.3	20.11	21.32	21.06	21.57	22.17



The glow curve of this sample was also analyzed by the CGCD method. This method has become very popular to obtain kinetic parameters for the last two decades [99]. It has great advantages over the experimental methods (i.e. IR, PS, ID, VHR, TP etc.) owing to simultaneous determination of kinetic parameters of all peaks without additional thermal treatments and experimental repetitions. Also, this method uses all data points in the whole glow curve rather than just a few points during the curve fitting procedures. It is apparent that if the number of data points used in the analysis increases, the potential for accurate determination of the kinetic parameters gets better. However, it must be noted that different models, approximations and minimization procedures are used for the glow curve analysis in the CGCD program. As a consequence, one may wonder whether the results of CGCD method reflect the accurate kinetic parameters of the TL peaks. According to many experienced researchers, the results obtained by the CGCD method, in some cases, seem to be unreliable. Especially, the advantages of the CGCD method may be undermined in complex TL glow curves. One may get a local minimum of the least square function which may yield erroneous kinetic parameters as the computerized fitting routine attempts to define the “best-fit” to the numerical data. As a result, many possible sets of kinetic parameters could be assigned to the same glow curve. The used CGCD program, which is based on the least square minimization procedure, was developed at the Reactor Institute at Delft, The Netherlands. The detail results of these models were given in an IRI-CIMAT Report [100]. In this PhD thesis, the first-order and general-order kinetics were approximated for all CGCD evaluations by the expressions 2.53 and 2.54 respectively. The goodness of fit for all the measured glow curves was tested using the figure of merit (FOM) [101]. From many experiences, it can be said that, if the values of FOM are between 0.0% and 2.5% the fit is good, 2.5% and 3.5% is fair fit, and >3.5% is bad fit. In the analyses of the complex glow curves by CGCD method, it is very important to decide correctly how many glow peaks there are in the glow curve and which of them have first or general-order kinetics to obtain correct results. In some cases, the best-fits can be obtained when different number of peaks is used in the CGCD analyses instead of real number of glow peaks to be in the glow curve. However, the values of kinetic parameters do not reflect their correct values when an incorrect number of glow peaks are assumed in the glow curve even if the best-fits were obtained. Therefore, firstly one must decide the number of glow peaks and their kinetic orders in the glow

curve of  $\text{LiB}_3\text{O}_5: \text{Al}$ . In this thesis it was observed that the glow curve structure of this sample is well described by four first-order glow peaks. Because, the results of kinetic parameters are also highly dependent upon the input parameters such as the location of the individual peaks. The parameters finally so selected were the values that yielded the best overall fit to the designated high priority features of the TL results. Figure 5.51 shows the results of CGCD fitting on the assumption of three peaks and table 5.6 summarizes the  $E_a$  and  $s$  values.

Table 5.6 The values of the activation energy  $E_a$  (eV) and frequency factor  $s$  ( $\text{s}^{-1}$ ) of main dosimetric peak 3 of-Al doped  $\text{LiB}_3\text{O}_5$  determined by CGCD method

Peak no	$T_m$ ( $^{\circ}\text{C}$ ) ( $\beta=1$ $^{\circ}\text{C}\cdot\text{s}^{-1}$ )	$E_a$ (eV)	$\ln(s)$ ( $\text{s}^{-1}$ )
1	$50\pm 2$	0.34	7.51
2	$130\pm 2$	0.68	16.91
3	$200\pm 2$	0.99	21.28

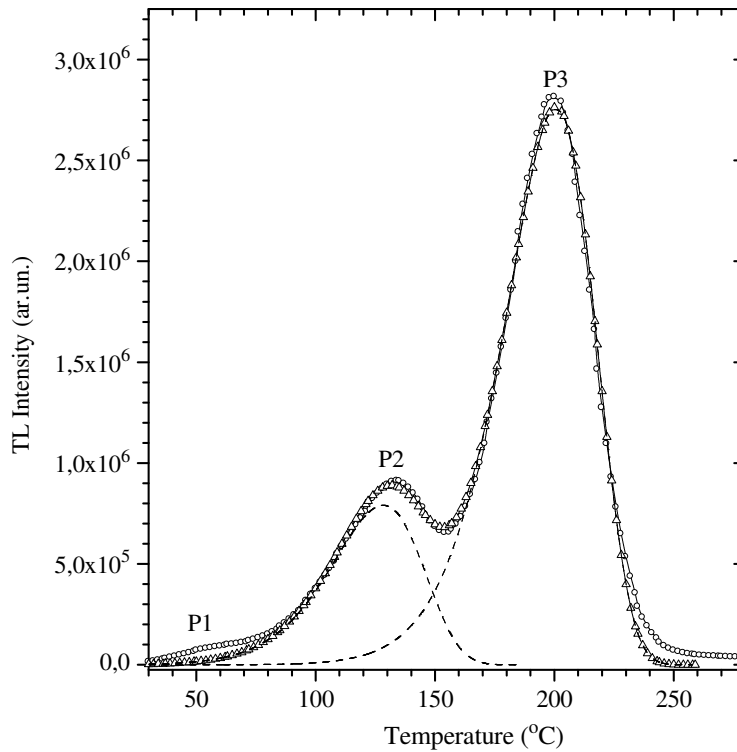


Figure 5.51 The CGCD analyzed glow curves of Al-doped  $\text{LiB}_3\text{O}_5$  measured after 0.6 Gy irradiation by beta ray at room temperature

## CHAPTER 6

### CONCLUSION

This thesis was planned to investigate the effect of various experimental techniques on the glow peaks and trapping parameters of some dosimetric materials. So,  $\text{CaF}_2\text{:Dy}$  (TLD-200),  $\text{CaF}_2\text{:Tm}$  (TLD-300),  $\text{CaF}_2\text{:Mn}$  (TLD-400) and Al doped  $\text{LiB}_3\text{O}_5$  (lithium triborate) crystals were selected as the experimental materials. The dose response characteristics and the behaviour of the glow curves of TLD-200, TLD-300 and TLD-400 crystals were investigated at two linear heating rates of 1 °C/s and 10 °C/s by using the dose response functions,  $f(D)$  and  $g(D)$ . Also the fading characteristics of the glow curves of the studied materials were investigated at two different environmental conditions; both in the dark and under the tungsten filament to understand the effect of light on the fading of the glow curves. The effect of thermal quenching was also investigated by calculating the total peak area under the glow curves for different heating rates from 1 °C/s to 30 °C/s for the  $\text{CaF}_2$  based crystals. The synthesis of Al doped lithium triborate (LBO) crystal was made in Middle East Technical University (METU), and the trapping parameters, namely the order of kinetics ( $b$ ), activation energy ( $E_a$ ) and the frequency factor ( $s$ ) associated with the dosimetric thermoluminescent (TL) glow peak (P3) of this material were evaluated by using different experimental techniques such as, the additive dose (AD), initial rise with partial cleaning (IR), variable heating rate (VHR), peak shape (PS), three points method (TPM), and computerized glow deconvolution (CGCD).

Nonlinearities often occur in the dose dependence of thermoluminescence (TL). These include sublinearity, usually when there is an approach to saturation in the dose dependence, as well as supralinearity, also termed superlinearity in the literature. The term supralinearity index,  $f(D)$ , is used in cases where the feature of interest is the deviation from linearity, namely, when the correction in the extrapolation is the main issue. The term superlinearity index,  $g(D)$ , in the dose ranges where the growth is more than linear and when extrapolation is not the main issue [6].

The results of the experiments in this study have shown that the linearity of the LTPs and HTPs of TLD-200 crystal continue up to  $\approx 1$  Gy at a linear heating rate of  $1\text{ }^{\circ}\text{C/s}$ . However, when the heating rate is increased to  $10\text{ }^{\circ}\text{C/s}$ , the LTPs show linear behaviour up to 10 Gy and the HTPs show linear behaviour up to 5 Gy. Moreover, the saturation dose level of glow peaks of this sample was affected from the heating rate. For example, the LTPs saturate after  $10^4$  Gy and HTPs saturate  $10^3$  Gy at a linear heating rate of  $1\text{ }^{\circ}\text{C/s}$ . On the other hand, the LTPs saturate after  $10^3$  Gy and the HTPs saturate  $10^4$  Gy at a linear heating rate of  $10\text{ }^{\circ}\text{C/s}$ . For the TLD-300; the main glow peaks 3 and 5 show linear behaviour up to 5 Gy for both heating rates at  $1\text{ }^{\circ}\text{C/s}$  and  $10\text{ }^{\circ}\text{C/s}$ . Also the saturation dose levels of these peaks are not affected from the heating rate. At both heating rates, the peak 3 saturates after 5 Gy and peak 5 saturates after  $10^4$  Gy. The linear behaviours of glow peaks of TLD-400 continue up to 10 Gy at a linear heating rate of  $1\text{ }^{\circ}\text{C/s}$ . On the other hand, they show linear behaviour up to  $10^2$  Gy at  $\beta=10\text{ }^{\circ}\text{C/s}$ . Even the heating rate affects the linearity of these peaks, their saturation dose levels are not affected from the heating rate, such that the peak 1 saturates after  $10^4$  Gy, peak 2 and peak 3 saturate after  $10^3$  Gy at both heating rates. It can be concluded from these results that the linearities of glow peaks of TLD-200 and TLD-400 increases when high heating rate was used, but the linearity of glow peaks of TLD-300 is not affected from the heating rates. Therefore, this crystal is the most suitable one for the dosimetric investigations from the TLD-200 and TLD-400 due to its high linear behaviour at both heating rates.

Different researchers in the field have viewed the effect of supralinearity/superlinearity from two somewhat different points of view. One point of view has to do with the rate of change with dose of the  $f(D)$  and  $g(D)$ . The other approach is related more to the applications of TL in dosimetry and archaeological and geological dating, and basically has to do with the correction to be made in extrapolation in cases where supra (super) linearity occurs following an initial linear dose range or prior to such a linear range [6]. Several models are discussed in the literature which aims at explaining the nonlinearity of the dose dependence. Many theories have been forwarded to explain the cause of the supralinearity in TLD materials. Conveniently, they can be classified as models in which the critical processes occur during the absorption of radiation, and models in which the critical processes occur during heating (i.e. during TL readout). The evidence, at least for

LiF-based materials, clearly shows that the critical mechanism is that of competition during the heating stage of TL readout. During heating, electrons released from traps, may either recombine with trapped holes to produce TL or be retrapped in deeper traps, which act as competing centers. If the material did not have any competing traps (no competition) the TL-sensitivity would be higher at low doses and linearity would be observed up to saturation [3]. The competition-during heating process was first suggested by Rodine and Land [88] and was later analyzed mathematically by Kristianpoller *et al* [89] (using a kinetic analysis of retrapping and recombination) and by Mische and McKeever [29] (using probability analysis).

It is well known that the peak temperature of a TL peak depends on the heating rate. It also influences the TL sensitivity and, hence, the trends of the dose-response curve [90]. Therefore, the controlled heating during the TL readouts is an important requirement to avoid the effects of heating rate. Influence of heating rate on the response of TLDs was first correlated with thermal quenching of luminescence by Gorbics *et al* [91] in six TLD phosphors. Thermal quenching was understood to be due to the increased probability of nonradiative transitions competing with the radiative transitions. Since the increase in the heating rates resulted in an increase in the temperature of occurrence of the TL glow peak, this shift in the temperature was held responsible for the increase in the contribution of nonradiative transitions due to the presence of the competing traps. It was inferred that the glow peaks occurring at higher temperatures must exhibit higher thermal quenching.

The experimental results in this study showed that the linearity of glow peaks of TLD-300 crystal is not affected with the change of heating rate. This result clearly proves that there are no thermal quenching effect and competing deep trap in this material. But the linearity of glow peaks of TLD-200 and TLD-400 are affected from the change of heating rate because of the presence of deep competing traps which can initially trap electrons during irradiation. It is already known that the TLD-200 and TLD-400 are highly affected from the thermal quenching. So, if the materials have thermally disconnected deep traps, it will be necessary to reset the occupancy of these more stable traps by appropriate annealing after each reading, especially after high dose applications.

For the storage time experiment TLD-200 sample was annealed at  $500 \pm 1$  °C for 1 hour than, 12 Gy dose exposed each time and left fading. The storage time experiments were performed for different time periods from 1 day to 4 weeks for dark fading, and from 1 week to 3 weeks for light fading, under the tungsten filament lamp of 55 lux which is located at a distance of 20 cm from the sample. The measured glow curves of CaF<sub>2</sub>: Dy at the end of the planned storage periods are shown in figure 5.13. As seen from this figure, peak 1 was neglected after 1 week storage time due to its fast fading. The low temperature peaks 1-5 are quickly decreased while high temperature peaks 6-8 are not sufficiently influenced from storage periods at room temperature in the dark. As seen from figure 5.14, P1-P5 reduced to typically 40 % of their original value after 4 weeks. The storage time experiment performed in the light, the situation is different; both low and high temperature peaks were highly affected from the storage times such as P1-P5 reduced to nearly 75% and P6-P8 reduced to 25% of their original value. For the storage time experiments TLD- 300 crystal was annealed at  $400 \pm 1$  °C for 1 hour and irradiated up to 72 Gy. The storage time experiments were performed for different time periods. It has also been investigated the optical fading at room temperature. The measured glow curves of CaF<sub>2</sub>: Tm at the end of the planned storage periods are shown in figure 5.27. As seen from this figure, P1 reduced to 95 %, P2 70 % of their original values. P3, P4 and P5 are reduced to nearly 5 % of their original values but P6 is not affected from the planned storage time period of 4 weeks, performed in the dark. In the optical fading experiment, P1 reduced to 98 % and P2 reduced to 85 % of their original values. P3 reduced to 10 % and P4 reduced to 3 % of their original value. P5 and P6 are almost not affected from the storage time period of 3 weeks. . For the storage time experiments TLD- 400 crystal was annealed at  $400 \pm 1$  °C for 30 min and irradiated up to 36 Gy. The measured glow curves of CaF<sub>2</sub>: Mn at the end of the planned storage periods are shown in figure 5.40. As seen from this figure, the peaks are not highly affected from the storage time periods performed in the dark. According to figure 5.41, P1 reduced to typically 15 %, P2 and P3 reduced to 5% of their original value after 6 weeks. In the optical fading experiment, the situation is different; P1 reduced to 95%, P2 reduced to 90% and P3 reduced to nearly 85 % of their original values after 3 weeks. This illustrates that the peaks are highly affected from the optical condition.

The experimental results indicated for the glow curve of Al-doped LiB<sub>3</sub>O<sub>5</sub> after beta-irradiation between 0.04 Gy and ≈5 Gy in the temperature range from room temperature to 400 °C is the superposition of at least three glow peaks. On the other hand, when the dose level is increased above ≈5 Gy, a new peak (peak 4) starts to generate at the high temperature side of main dosimetric peak. The kinetic order ( $b$ ), activation energy ( $E_a$ ), and the frequency factor ( $s$ ) of main dosimetric peak were calculated by applying different experimental methods. In order to determine the kinetic order from the glow curve the AD method was firstly used and it indicates that all of the glow peaks have first-order kinetics. Also Chen's peak shape method showed that the symmetry factor  $\{\mu_g = (T_2 - T_m)/(T_2 - T_1)\}$  of the isolated glow peak 3 of Al-doped LiB<sub>3</sub>O<sub>5</sub> has been found to be 0.42±1 which gives a kinetic order of about 1.05±0.05. The similar result was also obtained by the CGCD method.

The values of the activation energy were calculated by using Gartia, Singh & Mazumdar's PS method for different  $x$ -values, the TP method developed by Rasheedy, the IR, VHR, CGCD and Chen's PS methods. The results are tabulated in table 5.5 and 5.6. As can be seen from these tables, the average values of the  $E_a$  values of P3 obtained by the TP, CGCD, VHR and PS methods of Chen and Gartia, Singh & Mazumdar gives very close results. As seen, the value of the activation energy obtained by these methods is about 1.05±0.05 eV. On the other hand, the value of  $E_a$  obtained by the IR method gives slightly higher values as compared with those methods. One possible explanation for the reason of these differences is that the P3 is not originated from a discrete energy level but instead it is a distribution of traps. In reality, when the  $T_m - T_{stop}$  procedure was checked it is seen that the position of peak slightly shifts toward the high temperature side with increasing  $T_{stop}$  (Fig.5.46). This result indicates that it has a distribution of traps and a heat treatment after irradiation may cause a variation in the activation energies of this peak.

## REFERENCES

- [1] Aitken, M.J. (1985). *Thermoluminescence Dating*. Academic Pres; London, ISBN 0-12-0446380-6.
- [2] Daniels, F., Boyd, C.A. and Saunders, D.F. (1953). *Science*, **117**, 343.
- [3] McKeever, S.W.S., Moscovitch, M. and Townsend, P.D. (1995). *Thermoluminescence Dosimetry Materials: Properties and Uses*, Nuclear Technology Publishing, Ashford, Kent TN23 1YW England.
- [4] Kortov, V. (2007). Materials for thermoluminescent dosimetry: Current status and future trends. *Radiation Measurements*,**42**, 576-581.
- [5] Chen,R. and McKeever, S.W.S. (1997). *Theory of Thermoluminescence and Related Phenomena*, World Scientific, Singapore.
- [6] Yazıcı, A.N. (2005). The influence of heating rate on the TL response of glow peaks of beta-irradiated CaF<sub>2</sub>: Dy (TLD- 200). *Journal of Physics D: Applied Physics*, **38**, 3860–3864.
- [7] Chen, R., McKeever, S.W.S. (1994). Characterization of nonlinearities in the dose dependence of thermoluminescence. *Radiation Measurements*, **23**, 667-673.
- [8] Furetta, C.(1989). *Review Models in Thermoluminescence*. Kluwer Academic Publiher; ISBN 0022-2461.
- [9] Randall, J.T. and Wilkins, M.H. F. (1945). Phosphorescence and electron traps: I. The study of trap distribution. *Proceedings of the Royal Society A*, **184**, 366-389.
- [10] Randall, J.T. and Wilkins, M.H. F. (1945). Phosphorescence and electron traps: II. The interpretation of long-period phosphorescence. *Proceedings of the Royal Society A*, **184**, 390-407.
- [11] Chen, R. in: Horowitz, Y.S. (Ed.) (1984). *Thermoluminescent and Thermoluminescent Dosimetry, Vol. 1*, CRC Press, Boca Raton, FL.
- [12] Kitis, G., Gomez-Ros J.M. and Tuyn, J.W.N. (1998). Thermoluminescence glow curve deconvolution functions for first, second and general orders of kinetics. *Journal of Physics D:Applied Physics*, **31**, 2636-2641.
- [13] Garlick, G.F.J and Gibson, A.F. (1948). The electron trap mechanism of



luminescence in sulphide and silicate phosphors. *Proceedings of the Physics Society*, **60**, 574-589.

- [14] Bos, A.J.J. and Dielhof, J.B. (1991). The analysis of thermoluminescent glow curves in CaF<sub>2</sub>:Tm (TLD-300). *Radiation Protection Dosimetry*, **36**, 231-239.
- [15] May, C.E. and Partridge, J.A.(1964). Thermoluminescence kinetics of alpha irradiated alkali halides. *Journal of Chemical Physics*, **40**, 1401-1415.
- [16] Chen, R. and Winer, A.A. (1970). Effects of various heating rates on glow curves. *Journal of Applied Physics*, **41**, 5227-5232.
- [17] Piters, T.M. and Bos, A.J.J. (1993). Thermoluminescence Emission Spectra of LiF (TLD-100) after different Thermal Treatments. *Journal of Physics D:Applied Physics*, **47**, 91-94.
- [18] McKeever, S.W.S., (1983). *Thermoluminescence of solids*. Oklahoma State University Press.
- [19] Chen, R. (1969). On the Calculation of Activation Energies and Frequency Factors from Glow Curves. *Journal of Applied Physics*, **40**, 570-575.
- [20] Azerin, J. (1986). *Nuclear Tracks*, **11**, 159.
- [21] Kitis, G. and Tuyn, J.W.N. (1998). A simple method to correct for the temperature lag in TL glow-curve measurements. *Journal of Physics D:Applied Physics*, **31**, 2065-2073.
- [22] Kitis, G. and Pagonis, V. (2007). Peak shape methods for general order thermoluminescence glow-peaks: a Reappraisal. *Nuclear Instrumentation and Methods B.*, **262**, 313-322.
- [23] Grossweiner, L.I. (1953). A note on the Analysis of First-Order Glow curves. *Journal of Applied Physics*, **24**, 1306-1308.
- [24] Halperin, A. and Braner, A. (1960). Evaluation of thermal activation energies from glow curves. *Physical Review Letters*, **117**, 408-415.
- [25] Gartia, R.K., Singh S.J., and Mazumdar, P.S. (1989). *Physica Status Solidi (a)*, **11**, 407.
- [26] Bos, A. J. J., Piters, J.M., Gomez Ros, J. M. and Delgado, A. (1993). (GLACANIN, and Intercomparison of Glow Curve Analysis Computer Programs) IRI-CIEMAT Report 131-93-005 IRI Delft.
- [27] Mahesh, K. Weng, P. S. and Furetta, C. (1989). *Thermoluminescence in Solids and its Applications*, (Nuclear Technology Publishing Ashford).
- [28] Hsu, P. C. and Wang, T. K. (1986). On the annealing procedure of CaF<sub>2</sub>:Dy.

*Radiation Protection Dosimetry*, **16**, 253-256.

- [29] Kathuria, S. P. and Sunta, C. M. (1979). Kinetics and trapping parameters of thermoluminescence in LiF TLD-100-dependence on dose. *Journal of Physics D:Applied Physics*, **12**, 1573-1587.
- [30] Rasheedy, M.S.(2005). A new evaluation technique for analyzing the thermoluminescence glow curve and calculating the trap parameters. *Thermochimica Acta*, **429**, 143-147.
- [31] Horowitz, Y. S. (1981). The theoretical and microdosimetric basis of thermoluminescence and applications to dosimetry. *Physics in Medicine and Biology*, **26**, 765-824.
- [32] Mische, E. F., McKeever, S.W.S. (1989). Mechanism of supralinearity in LiF thermoluminescence dosimeters. *Radiation Protection Dosimetry*, **29**, 159-175.
- [33] Cameron, J.R., Suntharalingam, N., Kenney, G.N. (1968). *Thermoluminescence dosimetry*, Univ. Wisconsin Press, Madison.
- [34] Zimmerman, D.W. and Cameron, J.R. (1968). In *Thermoluminescence of geological materials* (ed. McDougall, D.J.), p. 485 Acad Press, London.
- [35] Durrani, S.A., Khazal, K.A.R., McKeever, S.W.S., Riley, R.J.(1977). Studies of changes in the thermoluminescence sensitivity in quartz induced by proton and gamma irradiations. *Radiation Effects and Defects in Solids*, **33**, 237-244.
- [36] Horowitz, Y.S., Kalef-Ezra, J. (1981). Relative thermoluminescent response of LiF-TLD to <sup>252</sup>Cf fission fragments. *Nuclear Instruments and Methods*, **187**, 519-525.
- [37] Chandra, B., Lakshmanan, A.R., Bhatt, R.C. (1981). Effect of deep traps on sensitization in LiF (TLD-100) phosphor a correlation study between peak 7 and 10 centres. *Physica Status Solidi (a)*, **66**, 335-340.
- [38] Lakshmanan, A.R., Chandra, B., Bhatt, R.C. (1982). On the role of Z centres and competing nonluminescent centres in the sensitisation and supralinearity mechanism of LiF TLD-100 phosphor. *Journal of Physics D:Applied Physics*, **15**, 1501-1517.
- [39] Nink, R., Kos, H.J. (1976). *Physica Status Solidi (a)*, **35**, 121-129.
- [40] Jain, V.K. (1980). Radiation-induced sensitization and UV effects in lithium fluoride TLD phosphor. *Physica Status Solidi (a)*, **60**, 351-356.
- [41] Jain, V.K. (1981). *Physica Status Solidi (a)*, **60**, 341.

- [42] Sagastibelza, F., Alveraz Rivas, J.L. (1981). Thermoluminescence in LiF (TLD-100) and LiF crystals irradiated at room temperature. *Journal of Physics C: Solid State Physics*, **14**, 1873-1889.
- [43] Muccillo, R., Rolfe, J. (1974). Effect of Irradiation on Impurity-Vacancy Dipoles in KBr Crystals Doped with Strontium. *Physica Status Solidi (b)*, **61**, 579-587.
- [44] Ogundare, F.O., Balogun, F.A., and Hussain, L.A. (2005). Heating rate effects on the thermoluminescence of fluorite. *Radiation Measurements*, **40**, 60-64.
- [45] Kitis, G., Spiropulu, M., Papadopoulos, J. And Charalambous, S. (1993). Heating rate effects on the TL glow-peaks of three thermoluminescent phosphors. *Nuclear Instruments and Methods*, **73**, 367-372.
- [46] Betts, D.S., Couturier, L., Khayrat, A.H., Luff, B.J. and Townsend, P.D. (1993). Temperature distribution in thermoluminescence experiments. *Journal of Physics D: Applied Physics*, **26**, 843-848.
- [47] Taylor, G.C. and Lilley, E. (1982). Rapid readout rate studies of thermoluminescence in LiF (TLD-100) crystals. *Journal of Physics D: Applied Physics*, **15**, 2053-2065.
- [48] Nakajima, T. (1976). On the competing trap model for the nonlinear thermoluminescence response. *Japan Journal of Applied Physics*, **15(6)**, 1179-1180.
- [49] Jain, V.K. (1978). The dependence of TL intensity on heating rate and deep trap in LiF. *Journal of Applied Physics*, **17**, 949-950.
- [50] Spooner, N.A. and Franklin, A.D. (2002). Effect of the heating rate on the red TL quartz. *Radiation Measurements*, **35**, 59-66.
- [51] Nanjundaswamy, R., Lepper, K. And McKeever, S.W.S. (2002). Thermal quenching of TL in natural quartz. *Radiation Protection Dosimetry*, **100**, 305-308.
- [52] Berkane- Krachi, A., Iacconi, P., Bindi, R. and Vinceller, S. (2002). Analysis with a multilayer model of heating rate effect on TL. *Journal of Physics D: Applied Physics*, **35**, 1895-1902.
- [53] Kıyak, N.G. and Buluş, E. (2002). Effect of annealing temperature on determining trap depths of quartz by various heating rates method. *Radiation Measurements*, **33**, 879-882.
- [54] Kelly P., Braunlich P., Abtani A., Jones S.C. and deMurcia M., (1984). Heating of Continuous Thermoluminescent Layers with Localised Laser

Beams. *Radiation Protection Dosimetry*, **6**, 83-86.

- [55] Gorbics S.G., Nash A.E. and Attix F.H., Proc. 2nd Int. Conf on Lum. Dos., (1968). Gatlinburg, TN, USA, 587.
- [56] Kitis G., Spiropulu M., Papadopoulos J. and Charalambous S., (1993). Heating rate effects on the TL glow-peaks of three thermoluminescent phosphors. *Nuclear Instruments and Methods B*, **73**, 367-372.
- [57] Kitis G., Papadopoulos J., Charalambous S. and Tuyn J.W.N., (1994). The Influence of Heating Rate on the Response and Trapping Parameters of Alpha-Al<sub>2</sub>O<sub>3</sub>:C. *Radiation Protection Dosimetry*, **55(3)**, 183-190.
- [58] Driscoll C.M.H., National Radiological Protection Board, Tech. Mem. **5(82)**.
- [59] Busuoli G. (1981). *Applied Thermoluminescence Dosimetry, ISPRA Courses*, Edited by M. Oberhofer and A. Scharmann, Adam Hilger Publisher.
- [60] Furetta, C. (2003). *Hanbook of TL*. Word Scientific Publshing Co. ISBN 9812382402.
- [61] 9010 Optical Dating system User Manuel, Dec. 1993.
- [62] Özdemir, Z., Özbayoğlu, G., Kızılyallı, M. and Yılmaz, A. (2004). Synthesis and characterization Of lithium triborate. *Physicochemical Problems of Mineral Processing*, **38**, 321-327.
- [63] Özdemir, Z., Özbayoglu, G., Yılmaz, A. (2007). Investigation of thermoluminescence properties of metal oxide doped lithium triborate *Journal of Material and Science*, **42**, 8501-8508.
- [64] Merz, J.L. and Pershan, P.S. (1967). *Physical Review Letters*, **162**, 217-235.
- [65] Fong, F.K. (1964). *Chemical Physics*, **41**, 245.
- [66] Binder, W. and Cameron, J. R. (1969). Dosimetric Properties of CaF<sub>2</sub>: Dy *Health Physics*, **17**, 613-618.
- [67] Sunta, C. M. (1970). Thermoluminescence spectrum of gamma-irradiated natural calcium fluoride. *Journal of Physics C: Solid State Physics*, **3**, 1978-1983.
- [68] Binder, W., Disterhoft, S. and Cameron, J. R. (1968). *Proc. 2nd. Int. Conf. on Luminescence Dosimetry, Gatlinburg*.
- [69] Sukis, D. R. (1971). Thermoluminescent Properties of CaF<sub>2</sub>: Dy TLD's *Transactions on Nuclear Science*, **18**, 185-189.

- [70] Hasan, F. and Charalambous, S. (1983). *Journal of Physics C: Solid State Physics*, **16**, 259-262.
- [71] Yazici, A. N. and Oztürk, Z. (2001). Analysis of the isolated glow peak 6 in CaF<sub>2</sub>:Dy (TLD-200) following post-irradiation annealing at 145°C. *Nuclear Instrumentation and Methods B*, **174**, 499-506.
- [72] Yazici, A.N., Chen, R., Solak, S. and Yegingil, Z. (2002). The analysis of thermoluminescent glow peaks of CaF<sub>2</sub> : Dy (TLD-200) after β-irradiation. *Journal of Physics D: Applied Physics*, **35**, 2526-2530.
- [73] Furetta, C., Kuo, C.H. and Weng, P.S. (1999). Fading prediction in thermoluminescent materials using computerised glow curve deconvolution (CGCD). *Nuclear Instruments & Methods In Physics Research*, **423**, 183-189.
- [74] Lucas, A. and Kapsar, B. (1977). In: Proc. 5th Conf. on Luminescence Dosimetry, Sao Paulo, Barsil (Phys. Inst., Giessen) pp.131.
- [75] Marczewska, B., Bilski, P., Budzanowski, M., Olko, P., Chernov, V. (2001). Dosimetry properties of Tm-doped single CaF<sub>2</sub> crystals, *Radiation Measurements*, **33**, 571–576.
- [76] Bos, A.J.J. and Dielhof, J.B. (1991). The analysis of thermoluminescence dosimetry materials. *Radiation Protection Dosimetry*, **37**, 231-239.
- [77] Hayes, W. and Stoneham, A.M. (1974). In: *Crystals with the Fluorite Structure*, ed. W. Hayes (Clarendon Press, Oxford) p.185.
- [78] Jacob, M., Meissner, P. And Rassow, J. (1990). Infrared Thermoluminescence Signals of TLD-300 (CaF<sub>2</sub>:Tm) Detectors. *Radiation Protection Dosimetry*, **33**, 291-294.
- [79] Lakshman, A.R. and Tiwari, S.S. (1993). Optical Absorption and Thermoluminescence Studies in CaF<sub>2</sub>:Tm Crystals Irradiated at Room Temperature. *Radiation Protection Dosimetry*, **47**, 243-246.
- [80] Danilkin, M., Lust, A., Kerikmäe, M., Seeman, V., Mändar, H., Must, M. (2006). CaF<sub>2</sub>:Mn extreme dosimeter: Effects of Mn concentration on thermoluminescence mechanisms and properties. *Radiation Measurements*, **41**, 677 – 681.
- [81] Zarate-Morales, A., Buenfil, A.E. (1996). Environmental gamma dose measurements in Mexico City using TLD, *Health Physics*, **71** (3), 358.
- [82] Kalchgruber, R., Goksu, H.Y., Hochhauser, E. Wagner, G.A. (2002). Monitoring environmental dose rate using Risø TL/OSL readers with built-in sources: recommendations for users, *Radiation Measurements*, **35**, 585.

- [83] Chakrabarti, K., Sharma, J., Mathur, V.K. (1993). Laser bleaching of deep traps and reduction of zero dose problem in CaF<sub>2</sub>:Mn dosimeters, *Radiation Protection Dosimetry*, **47**, 155.
- [84] Jiang, Y., Jia, C.L., Wang, L., Wang X.L., Chen F., Wang, K.M., Lu, Q.M., Ma, H.J., Shen, D.Y. (2006). The optical properties of planar waveguides in LiB<sub>3</sub>O<sub>5</sub> crystals formed by Cu<sup>+</sup> implantation, *Applied Surface Science*, **253**, 2674-2677.
- [85] Shepeleva, Y.F., Bubnovaa, R.S., Filatovb, S.K., Sennovab, N.A., Pilnevac N.A. (2005). LiB<sub>3</sub>O<sub>5</sub> crystal structure at 20, 227 and 377 °C, *Journal of Solid State Chemistry*, **178**, 2987-2997.
- [86] Schulman, J.H., Kirk, R.D. and West, E.J. (1967). *Proceedings of the International Conference on Luminescence Dosimetry*, Stanford University, CONF-650637, p.113.
- [87] Prokic, M. (1993). MgB<sub>4</sub>O<sub>7</sub>:Mn as a New TL Dosemeter. *Radiation Protection Dosimetry*, **47**, 191-193.
- [88] Furetta, C., Prokic, M., Salamon, R., Prokic, V. and Kitis, G.(2001) *Nuclear Instruments and Methods A*, **456**, 411.
- [89] Li, J., Hao, J.Q., Li, C.Y., Zhang, C.X., Tang, Q., Zhang, Y.L., Su, Q., and Wang, S.B. (2005). *Radiation Measurements*, **39**, 229.
- [90] Karali, T., Rowlands, A.P., Prokic, M., Townsend, P.D. and Halmagean, E. (2002). Thermoluminescent Spectra of Rare Earth Doped MgB<sub>4</sub>O<sub>7</sub> Dosimeters. *Radiation Measurements*, **100**, 333-336.
- [91] Depci, T., Özbayoğlu, G., Yilmaz, A. and Yazıcı, A.N. (2008). The thermoluminescence Properties of Lithium Triborate (LiB<sub>3</sub>O<sub>5</sub>) Activated by Aluminium. *Nuclear Instruments and Methods B*, **266**, 755-762.
- [92] Topkasu M. and Yazıcı, A.N. (2007). The thermoluminescence properties of natural CaF<sub>2</sub> after β-irradiation. *Nuclear Instruments and Methods B*, **264**, 293-301.
- [93] Gartia R.K., Singh S.J., and Mazumdar P.S. (1989). Determination of the Activation Energy of Thermally Stimulated Luminescence Peaks Obeying General-Order Kinetics. *Physica Status Solidi (a)*, **114**, 407-411.
- [94] Rasheedy, M.S. (2005). A new evaluation technique for analyzing the thermoluminescence glow curve and calculating the trap parameters. *Thermochimica Acta*, **429**, 143-147.
- [95] Kathuria, S. P. and Sunta, C. M. (1979). Kinetics and trapping parameters of

thermoluminescence in LiF TLD-100-dependence on dose. *Journal of Physics D: Applied Physics*, **12**, 1573-1588.

- [96] Wintle, A. G., *Geophys. J. R.* (1975). *American Astronomical Society*, **41**, 107.
- [97] Christodoulides, C. (1985). Errors involved in the determination of activation energies in TL and TSDC by the initial rise method. *Journal of Physics D: Applied Physics*, **18**, 1665-1672.
- [98] Singh, T.S.C., Mazumdar, P. S. and Gartia, R. K. (1988). On the determination of activation energy in thermoluminescence by the initial rise method. *Journal of Physics D: Applied Physics*, **21**, 1312-1314.
- [99] Horowitz, Y. S. and Yossian, D. (1995). Computerised Glow Curve Deconvolution: Application to Thermoluminescence Dosimetry. *Radiation Protection Dosimetry*, **60 (1)**, 5-12.
- [100] Bos, A.J.J., Pijpers, J. M., Gomez Ros, J. M. and Delgado, A. (1993). (GLACANIN, and Intercomparison of Glow Curve Analysis Computer Programs) IRI-CIEMAT Report 131-93-005 IRI Delft.
- [101] Misra, S. K. and Eddy, N. W. (1979). *Nuclear Instruments and Methods*, **166**, 537.

## **CURRICULUM VITAE**

### **PERSONAL INFORMATION**

Surname, Name: KAFADAR, VURAL EMİR

Nationality: Turkish (TC)

Date and Place of Birth: 24 June 1978, İskenderun- HATAY

Marital Status: Married

Phone: +90 505 576 8570

e-mail: kafadar@gantep.edu.tr

### **EDUCATION**

<b>Degree</b>	<b>Institution</b>	<b>Year of Graduation</b>
MS	Gaziantep University, Physics Eng.	2004
BS	Gaziantep University, Physics Eng.	2001
High School	Dörtyol Lisesi	1995

### **WORK EXPERIENCE**

<b>Year</b>	<b>Place</b>	<b>Enrollment</b>
2004- Present	Gaziantep University	Research Assistant

### **FOREIGN LANGUAGES**

English



## PUBLICATIONS

1. Kafadar, V.E., Yazıcı, A.N., Yıldırım, R.G. (2009). Determination of trapping parameters of dosimetric thermoluminescent glow peak of Lithium TriBorate ( $\text{LiB}_3\text{O}_5$ ) activated by Aluminum. *Journal of Luminescence*, **129**, 710-714
2. Kafadar, V.E., Yazıcı, A.N., Yıldırım, R.G. (2009). The effects of heating rate on the dose response characteristics of TLD-200, TLD-300 and TLD-400. *Nuclear Inst. and Methods in Physics Research, B*
3. Yazıcı, A.N., Doğan, M., Kafadar, V.E., Toktamış, H. (2006). Thermoluminescence of undoped and Ce-doped  $\text{BaB}_4\text{O}_7$ . *Nuclear Inst. and Methods in Physics Research, B*, **246**, 402-408
4. Yazıcı, A.N., Kafadar, V.E., Toktamış, H. (2006). Thermoluminescent dosimetric characteristics of  $\beta$ -ray irradiated RbCl single crystal doped with Eu- and OH-ions. *Nuclear Inst. and Methods in Physics Research, B*, **246**, 387-392
5. Yazıcı, A.N., Kurt, K., Kafadar, V.E., Gürler, S., Topaksu, M. (2006). The analysis of thermoluminescent glow peaks of natural zircon after  $\beta$  irradiation. *Nuclear Inst. and Methods in Physics Research* **248**, 133-141
6. Bedir, M., Öztaş, M., Yazıcı, A.N., Kafadar, V.E. (2006). Characterization of Undoped and Cu-doped ZnO thin films deposited on glass substrates by spray pyrolysis. *Chin. Phys. Lett*, **23**, 939
7. Öztaş, M., Bedir, M., Yazıcı, A.N., Kafadar, V.E., Toktamış, H. (2006). Characterization of copper-doped sprayed ZnS thin films. *Physica B.*, **381**, 40-46
8. Yazıcı, A.N., Öztaş, M., Kafadar, V.E., Bedir, M., Toktamış, H. (2006). The analysis of thermoluminescent glow peaks of copper doped ZnS thin films after  $\beta$ -irradiation. *Journal of Luminescence*, **124**, 58-66